

Univerzita Karlova
Přírodovědecká fakulta

Studijní program: Biochemie



Mgr. Lucie Vaňková

Nové vazebné proteiny odvozené od malých proteinových domén cílené na diagnosticky využitelné terče

Novel binding proteins derived from small protein domains targeting diagnostically important molecules

Disertační práce

Školitel: RNDr. Petr Malý, CSc.

Praha, 2018

**Charles University
Faculty of Science**

Study programme: Biochemistry



Mgr. Lucie Vaňková

Novel binding proteins derived from small protein domains targeting diagnostically important molecules

Nové vazebné proteiny odvozené od malých proteinových domén cílené na diagnosticky využitelné terče

Doctoral thesis

Supervisor: RNDr. Petr Malý, CSc.

Prague, 2018

Prohlašuji, že jsem tuto disertační práci vypracovala samostatně pod vedením školitele RNDr. Petra Malého, CSc., a všechny použité prameny jsem řádně citovala. Tato práce ani její podstatná část nebyla předložena k získání jiného nebo stejného akademického titulu.

V Praze, dne

.....

Lucie Vaňková

Acknowledgment

First of all, I would like to thank my supervisor Petr Malý, without whose guidance and support I would never finish this work. I appreciate his ability to encourage me to work, even if not everything was going well. His scientific enthusiasm and optimism was a source of incredible driving force for me. Thanks also belong to all my colleagues in the lab, who helped me with experiments and created a pleasant working environment full of willingness and understanding. Next, I would like to thank our colleagues from partner universities in Ljubljana and Ústí nad Labem, and members of the Dyntec company for pleasant collaboration on projects and valuable advice and suggestions. Great thanks belong to Radim Osička from the Institute of Microbiology, who introduced me to the flow cytometry measurements. He was also the kind of person I could come to for advice at any time. Another important person I would like to thank is Jiří Černý from the Laboratory of Structural Bioinformatics of Proteins, who cooperated on the rational design of the Myomedin scaffold.

Special thanks belong to my parents, who brought me to diligence and responsibility and indirectly led me to science. Finally, I would like to express my greatest thanks to my husband Lukáš, who always supported me in all my decisions. I am glad to have someone at my side who understands that my work is important to me and allows me to work on myself, educate myself and become better in what I do. The infinite power for summarizing my scientific results was given to me by a new life emerging inside of me. This little man was closest to me during writing my PhD thesis and gave me a sense of peace and satisfaction.

Abstract

The rapid development of the gene engineering techniques, especially methods for *in vitro* directed evolution and combinatorial mutagenesis, has triggered the generation of new binding agents to almost any antigen of interest as an alternative to broadly used antibodies. These so-called non-Ig scaffolds are often derived from proteins with useful biophysical properties. While the therapeutic market is still dominated by monoclonal antibodies, the easy option of desired customization of non-Ig binders by conventional methods of gene engineering predestine them largely for the use in the diagnostic area.

The ABD scaffold, derived from a three-helix bundle of albumin-binding domain of streptococcal protein G, represents one of the small non-Ig scaffolds. In our laboratory, we have established a highly complex combinatorial library developed on the ABD scaffold. This ABD scaffold-derived library was used to generate unique binders of human prostate cancer (PCa) biomarkers PSP94, KLK2, KLK11 for the more precise diagnosis of PCa.

The second part of the thesis describes the generation of ABD-derived binders selectively recognizing different phenotypes of circulating tumor cells as a binding component of the cell capture zone of microfluidic chip for lung adenocarcinoma diagnosis. Beside this already proven model, the newly developed libraries derived from the Myomedin scaffold were used to yield a novel type of binders that would recognize other cell-surface epitopes on target molecules.

In the third part of the thesis, a collection of unique protein binders targeted to the Shiga toxin (Stx) B-subunit was generated with the use of ABD-derived combinatorial library. They were optimized for the surface display in *Lactococcus lactis* and functionally characterized. After subsequent improvement of the binding properties of particular S1B variants, Lactic acid bacteria with surface-displayed S1B binders would be useful for antagonizing pathogenic bacteria strains by the removal of Stx from the human gastrointestinal tract.

The last part of the thesis is devoted to the development of unique polyvalent vaccines for immunization of piglets and calves against enteric diseases. Current vaccines offer only a limited number of valences and do not offer protection against some serious diarrheal diseases. For successful introduction of the vaccines to the market, precise and reliable ELISA kits and protocols for verification and validation of their quality were developed. This assay is able to detect serum antibodies against 10 factors of the pathogenicity and is currently being used as a crucial part of the validation process before these highly innovative vaccines enter the market in 12 European countries.

Abstrakt

Rychlý vývoj technik genového inženýrství, zejména metod pro *in vitro* řízenou evoluci a kombinatorickou mutagenezi, umožnil rychlý rozvoj nových vazebných proteinů pro téměř jakýkoli požadovaný antigen jako alternativu k dnes široce používaným protilátkám. Tyto tzv. scaffolds jsou často odvozeny od malých proteinových domén s užitečnými biofyzikálními vlastnostmi. Zatímco na biofarmaceutickém trhu stále dominují monoklonální protilátky, možnost snadné cílené modifikace vazebných proteinů je předurčuje především pro použití v diagnostice.

ABD scaffold, odvozený od albumin vázící domény streptokokového proteinu G tvořené třemi spojenými alfa-šroubovicemi, patří do rodiny malých vazebných domén. V naší laboratoři byla na základě ABD scaffoldu vyvinuta vysoce komplexní kombinatorická knihovna vazebných proteinů. Tato knihovna byla použita k selekci nových vazebných proteinů pro lidské sérové biomarkery rakoviny prostaty PSP94, KLK2, KLK11, jež mohou být použity k vývoji nových multifaktoriálních biosenzorů pro přesnější diagnostiku rakoviny prostaty.

V druhé části dizertace je popsán vývoj vazebných proteinů odvozených od ABD scaffoldu určených pro selektivní rozpoznání různých fenotypů cirkulujících nádorových buněk jako součást mikrofluidního čipu vyvíjeného pro diagnostiku plicního adenokarcinomu. Vedle tohoto již osvědčeného modelu byly k selekci vazebných proteinů použity nově vyvinuté kombinatorické knihovny odvozené od Myomedinového scaffoldu, jehož odlišná struktura vazebného povrchu by mohla sloužit k rozpoznání jiných epitopů na cílových molekulách.

Ve třetí části práce byla vytvořena sbírka unikátních vazebných proteinů odvozených od ABD scaffoldu a cílených na podjednotku B Shiga toxinu (Stx). Tyto varianty byly optimalizovány pro orientované vystavení na povrchu buněk *Lactococcus lactis* a funkčně charakterizovány. Po následném vylepšení vazebných vlastností některých vybraných variant by mohly takto upravené bakterie *L. lactis* sloužit k odstranění Stx z lidského gastrointestinálního traktu, a tím ke snížení účinku patogenních bakterií.

Poslední část práce je zaměřena na vývoj unikátních polyvalentních vakcín pro imunizaci selat a telat proti střevním onemocněním. Současné vakcíny nabízejí jen omezený počet valencí a nenavozují ochranu proti některým závažným průjmovým onemocněním. Pro úspěšné uvedení vakcín na trh byly vyvinuty spolehlivé ELISA soupravy a protokoly pro ověření a validaci jejich kvality. Tyto ELISA sety jsou schopny detekovat sérové protilátky proti 10 faktorům patogenity a v současné době jsou používány v procesu validace před vstupem vakcín na trh ve 12 evropských zemích.

Table of Contents

Acknowledgment	- 1 -
Abstract	- 2 -
Abstrakt	- 3 -
Table of Contents	- 4 -
1. Introduction	- 6 -
1.1. Small protein domains - “protein scaffolds”	- 6 -
1.1.2. Scaffolds based on hypervariable loops	- 7 -
1.1.3. Scaffolds based on secondary structures	- 10 -
1.2. Combinatorial libraries	- 14 -
1.3. <i>In vitro</i> selection techniques	- 16 -
1.3.1. Introduction to selection techniques	- 16 -
1.3.2. Ribosome display	- 17 -
1.4. Utilization of protein scaffolds	- 19 -
1.4.1. Binding proteins promising for therapy	- 19 -
1.4.2. Diagnostic direction	- 21 -
1.5. Detection systems in diagnostics	- 28 -
2. Aims of the thesis	- 31 -
2.1. Binding proteins targeted to prostate cancer biomarkers	- 31 -
2.1.1. Generation of binders specific for human PSP94	- 31 -
2.1.2. Development of binders of human kallikrein 2 and kallikrein 11	- 31 -
2.2. Binding proteins targeted to surface markers of epithelial and mesenchymal cells for sorting circulating tumor cells	- 33 -
2.2.1. Binders derived from the ABD scaffold	- 33 -
2.2.2. Binders derived from Myomedin scaffold	- 33 -
2.3. Binding proteins specific for Shiga toxin 1 B Subunit	- 35 -
2.4. Development of procedures and tools for the validation of polyvalent vaccines against bacterial enteral diseases	- 37 -
3. Results	- 39 -
3.1. Binding proteins targeted to prostate cancer biomarkers	- 39 -
3.1.1. Binders specific for human PSP94	- 39 -
3.1.2. Binders of human kallikrein 2 and kallikrein 11	- 48 -
3.2. Binding proteins targeted to surface markers of epithelial and mesenchymal cells for sorting circulating tumor cells	- 55 -
3.2.1. Binders derived from the ABD scaffold	- 56 -
3.2.2. Binders derived from the Myomedin scaffold	- 65 -
3.3. Binding proteins specific for Shiga toxin 1 B Subunit	- 72 -

3.4. Development of procedures and tools for validation of the polyvalent vaccines against bacterial enteral diseases	- 84 -
4. Discussion	- 94 -
5. Materials and Methods	- 101 -
6. References	- 116 -
7. Enclosed publications	- 121 -
8. Supplementary data	I.

1. Introduction

1.1. Small protein domains - “protein scaffolds”

The explanation of the concept of protein scaffolds is closely associated with the discovery of antibodies. The variable antigen-binding site of antibodies has evolved in the immune system of higher vertebrates to bind almost all kinds of foreign substances to provide an effective humoral response. The natural mechanism of antigen recognition was the initial impulse to use a similar principle for targeted purposes. Although fabricated monoclonal antibodies are currently the most widely used structures for detecting different molecules, they possess many limitations. As large high-molecular-weight compounds, they are very unstable and have difficulties to penetrate into the tissue. They contain post-translational modifications making their recombinant production complicated and expensive. The multi-domain architecture with disulfide bonds complicates their recombinant production in reducing the environment of bacterial expression systems, requiring special conditions such as expression in the periplasm to guarantee the correct disulfide bond formation. The Fc region often causes undesired interactions in the human body. Furthermore, non-humanized antibodies are usually immunogenic. Despite the above-mentioned disadvantages, monoclonal antibodies or their recombinant fragments (Fab and Fv fragments, single-chain antibody domains such as camelid VHH fragments or scFvs) are now the most common biopharmaceuticals. After application of antibody engineering methods along with the library techniques, the first *in vitro* engineered antibodies and antibody fragments were successfully brought to the market [1, 2].

The rapid development of the gene engineering techniques, especially methods for *in vitro* directed evolution and combinatorial mutagenesis, has prompted the idea to use other structures as binding agents. These so-called non-Ig scaffolds are often derived from proteins with useful biophysical properties that are in nature able to bind to another partner molecule or molecules. Protein-protein interactions are an inseparable property of all living organisms. They promote essential biological processes such as cell adhesion, immune recognition, signal transduction, and molecular transport. Several laboratories have started to test different protein architectures for the construction of practically useful binding proteins. The most preferred are human proteins, minimizing their immunogenicity in the therapeutic use. As a scaffold, the whole parental protein structure can be used, or it can be composed of a single structural domain or repeated modules. They are usually very small, mostly between 40 and 180 amino acids, of which around 10-20 are involved in the binding. They can be easily produced by solid-phase

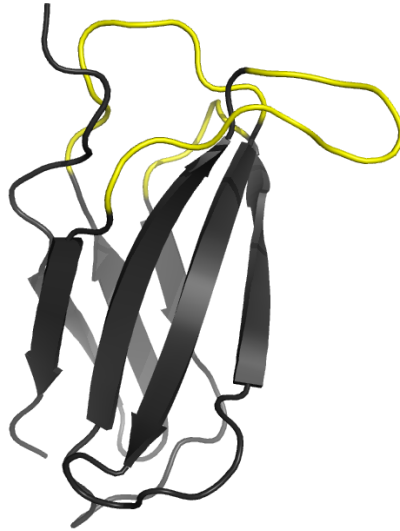
peptide synthesis, enabling site-specific conjugation of other compounds. Their great benefit is the easy option of desired customization of such small molecules. Using conventional methods of gene engineering, their multivalency and multispecificity can be achieved [2, 3].

Any chosen protein domain scaffold must fulfil several criteria due to its potential future application. The main parameter is the stable core structure that can tolerate side chain replacements in the exposed surface region without disrupting its overall stability. Another important feature is the absence of cysteine residues that are usually important for forming a rigid secondary structure, and this might complicate production of stable proteins derived from the parental scaffold in prokaryotic host cells. The small size of the protein domain is beneficial for fast tissue penetration during *in vivo* imaging, but for a possible therapy, further *in silico* optimization of the scaffold structure is inevitable, involving suppression of immunogenicity by elimination of T- and B-cell epitopes by mutagenesis or by additional masking. Before the scaffold is chosen as a master structure for generation of a high complex combinatorial library, a test of production of the wild-type structure in the host cells must be performed. Typically, *in silico* optimization of the master parental domain structure is performed to support the protein solubility and stability and prevent formation of aggregates. When the domain structure has been selected and further optimized, calculation of free energy for all residues is made to identify positions for mutable amino acid residues to avoid disruption of the core protein structure. The identified positions for randomization form a base for generation of a highly complex combinatorial library as a tool for *in vitro* directed evolution. This process comprises custom setting of the selection conditions to obtain binders with the desired properties.

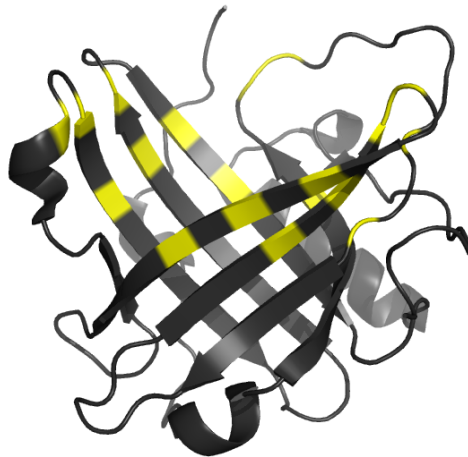
1.1.2. Scaffolds based on hypervariable loops

Currently, many of protein scaffolds have been designed based on different displaying geometries. One of the concepts for non-Ig scaffolds relies on randomization of **hypervariable loops**, imitating the pattern of antibodies. The most important examples are:

Adnectins, which share very similar folding with antibodies. They are based on the 10th fibronectin type III domain, beta-sheet sandwich fold with diversified loops. In contrast to antibodies, they have a simpler, single-domain structure without disulfide bonds. As a consequence, Adnectins are easier to manipulate and compatible with bacterial expression systems [4, 5].



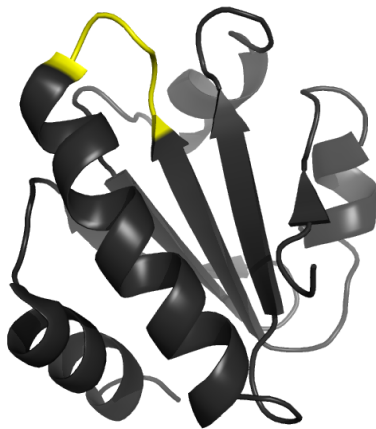
Anticalins are derived from lipocalins, a biologically widespread family of transport and storage proteins for vitamins, hormones, and secondary metabolites. They share a central beta-barrel comprising eight antiparallel strands. At the open end of the barrel, there are four structurally variable loops connecting each pair of β -strands. This loop region can be subjected to targeted randomization [6, 7].



Kunitz-domains, derived from inhibitors of serine proteases, are robust and stable protein scaffolds containing a single randomized peptide loop. Different developed Kunitz-domain variants preferably serve as protease targets [2].



Peptide aptamers share the similar principle of variable loops on a structurally robust protein derived from TrxA, a highly soluble and structurally robust enzyme involved in the cytosolic thiol/disulfide equilibrium of *Escherichia coli*. This scaffold is also mostly used as inhibitor of different enzymes [2].



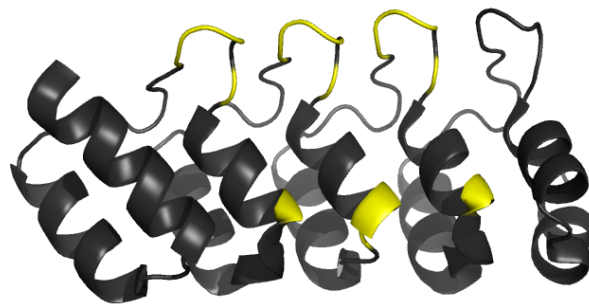
Microbodies represent an example of the functional scaffold containing disulfide bridges. They are small triple-stranded antiparallel beta-sheet structures with a cystine-knot motif that arises from three connecting disulfide bridges [8].



1.1.3. Scaffolds based on secondary structures

Another group of scaffolds are based on beta-sheet or helical geometry. The examples are:

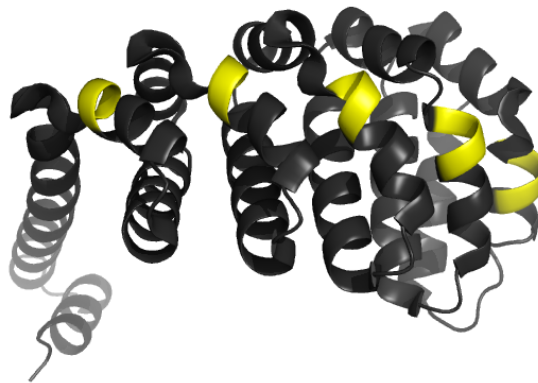
Designed Ankyrin Repeat Proteins (DARPs) are derived from an ankyrin repeat motif present in numerous naturally occurring proteins involved in a variety of biological activities. Ankyrin repeat protein fold contains a beta-turn, followed by a pair of antiparallel alpha-helices and a loop that forms the connection to the next repeat. DARPs consist of different numbers of ankyrin modules. The randomized positions are located in the spike of the beta-turn and along the exposed surface of the first alpha-helix [2, 9, 10].



The architecture of **Affilins** is based on the repeated beta-sheet fold. Modified are the surface-exposed amino acids within the beta-sheet structure. This group of binders includes two different protein scaffolds: human gamma-crystallin, protein from the eye lens, and human ubiquitin, small protein involved in intracellular protein degradation [11, 12].



Natural **Armadillo repeat proteins** are alpha-solenoid proteins that bind to unstructured regions of proteins in the processes of signal transduction or nuclear transport. Each armadillo repeat is composed of three helices folded in a triangular arrangement with extended peptide-binding groove. Designed armadillo repeat proteins have been developed for the binding of unstructured proteins [13, 14].



Affibodies are derived from the Z domain of protein A from *Staphylococcus aureus*. This bacterial three-helix bundle module serves in nature for binding to IgG. Using randomization of exposed amino acids on the surface of two of the alpha-helices, the binding preferences to other molecules have been achieved [15-17].



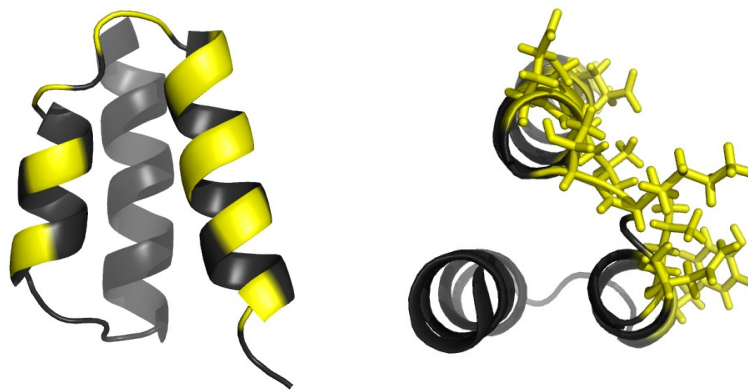
A very similar concept of three-helix motif comprises the **Albumin-Binding Domain (ABD)**. Because ABD is a master scaffold used in our laboratory, and it is the keystone of the

majority of my results given in the thesis, I will describe its structure in more detail. In nature, ABD can be found in various surface proteins expressed by gram-positive bacteria. In the blood stream, the bacteria bind to host serum proteins to evade the immune system and to collect nutrients. As serum albumin is the most abundant protein in the plasma, the occurrence of albumin-binding domains in different surface proteins is very common. Various ABDs differ in species specificity and binding affinity. The most studied and so far best characterized ABDs are from evolutionarily very close streptococcal protein G and protein PAB (peptostreptococcal albumin-binding) from *Finnegoldia magna*. Albumin-binding domains from other Streptococcus strains have also been explored, with a high potential for future therapeutic applications [18, 19].

Protein G of streptococcus groups C and G has separate binding domains for IgG and human serum albumin (HSA). Protein G from strain G148 contains three ABD modules (ABD1-3). The last C-terminal module ABD3 has been extensively studied and used for a wide range of protein engineering approaches. It is composed of 46 amino acid residues forming a left-handed three-helix bundle, where helices 2 and 3 represent the albumin-binding site and contain most conserved regions. The structure is very similar to the above-mentioned Affibodies derived from staphylococcal protein A. From the crystallization studies it is known that the HSA-binding region occupies only a single face of the molecule. The key spots, contributing to the albumin binding, are mainly the residues 26–33 in the end of helix 2 (especially Val-32) and the beginning of helix 3. Tyr-21 was found to be the cause of a broad specificity of ABD3, because it can potentially interact with various polar or charged amino acids on albumins from different species. In contrast, non-polar Phe-21 from the PAB protein is responsible for the strong binding to HSA [20, 21].

Using directed mutagenesis, the natural broad albumin-binding specificity has been changed to achieve various desired properties, such as improved binding affinity to HSA, increased stability, or even novel binding sites for other molecules. The motivation for the use of ABD for different biotechnological purposes is in its ideal biophysical properties. The most important features are the absence of disulfide bonds and the broad capacity of high-fidelity refolding after thermal or chemical denaturation, high water solubility, sufficient temperature stability, and tolerance to high and low pH changes, probably caused by a stable core formed by hydrophobic residues, and its small size (5 kDa) [21]. Besides improved stability of some engineered mutants, the ABD3 domain has been subjected to de-immunization strategy. The bacterial origin of ABD is the biggest obstacle for its routine use in the therapeutic area. In an effort to achieve a non-immunogenic ABD molecule, candidate ABD094 has been developed.

ABD094 was demonstrated to have no immunogenic potential in T-cell proliferation assays [19]. The step forward was the idea of replacing the existing albumin-binding surface with a novel binding site to achieve the desired binding properties while retaining the favorable biophysical properties of the scaffold protein. Both rational and combinatorial approaches have been used for directed randomization of the albumin-binding surface or a surface situated on the opposite face of the molecule. The subsequent screening of generated mutants using *in vitro* selection methods has provided affinity proteins for various applications [22].



In our laboratory, we have established a model of a three-helix bundle derived from ABD3 as a scaffold protein. To generate a high-complex combinatorial library we used the *in silico* design of residues suitable for randomization. As appropriate mutable residues, altogether 11 amino acids: Tyr-20, Leu-24, Asn-27, Lys-29, Thr-30, Glu-32, Gly-33, Ala-36, Leu-37, Glu-40, and Ala-44, distributed over the last two helices and their interconnecting loop, were proposed for randomization. Computational analysis revealed that randomization of helices 2 and 3 (see figure above) would not only yield loss of HSA binding, but could also have little or no impact on the stability of the ABD scaffold. The randomization of 11 codons of the ABD-encoding sequence is expected to give rise to 2×10^{14} (i.e., 20^{11}) ABD variants [23-26].

Table 1. Overview of the scaffolds

Scaffold	Parental molecule	Geometry	PDB	MW (kDa)
Anticalins	Lipocalins	loops	4GH7	20
Adnectins	Fibronectin type III	loops	1FNF	10
Kunitz-domains	Inhibitor of serine proteases	loops	4BQD	7
Peptide aptamers	TrxA	loops	1ZCP	13-15
Microbodies	Cystine-knot motif	loops	1HYK	4
DARPinS	Ankyrin repeats	alpha-helices and loops	1SVX	14-21
Affilins	Gamma-crystallin	beta-sheets	2JDF	20
	Ubiquitin	beta-sheets	2W9N	10
Armadillo repeats	Armadillo repeats	alpha-helices	4DB8	5
Affibodies	Protein A	alpha-helices	2KZI	6
ABD	Protein G, PAB	alpha-helices	1GJT	5

1.2. Combinatorial libraries

A combinatorial protein library is a set of a large number of new protein variants generated from the scaffold parental molecule by simultaneous randomization of several residues. The directed mutagenesis of protein interfaces is a powerful tool how to alter the binding specificity of the existing binding interface. To create a combinatorial library and select desired variants from large protein libraries is more effective than testing individual mutants one by one. Most early directed evolution studies applied random mutagenesis methods, such as error-prone PCR or DNA shuffling, to generate large and diverse libraries. Currently, the development of combinatorial libraries has moved from random to semi-rational approaches in order to incorporate a novel binding site while retaining the favorable fold and stability of the original domain.

In silico design is usually done before selecting residues for randomization to identify the optimal binding interface and harmless sequence modifications, the structurally not important residues that can be easily modified without disruption of a major fold. This is more important when randomizing the regular secondary structure, which is more prone to changes in the regular fold than variable loops [27]. A great advantage is the well-known structure of the parental scaffold with characterized evolutionarily close variants with different binding characteristics allowing comparison of these variants sequentially to evaluate the relevance of the particular amino acids. A very nice example of sophisticated design for identification of the best mutable residues to create highly stable ABD is given in [28]. The development of an

improved DARPIn combinatorial library using structural investigations of the natural diversity of several known proteins containing ankyrin repeats is described in [9].

Besides searching in sequence and structural databases to find the proper consensus sequence for randomization, the computational guided mutagenesis approaches are another possibility how to design the input library. To identify the key stabilizing residues in the structure, the interaction energy map can be used. The method evaluates the importance of each residue in the protein structure based on the amount of stabilization energy the residue brings to the stability of the fold [23]. A novel computational method named SOCoM (Structure-based Optimization of Combinatorial Mutagenesis) has been developed. SOCoM allows the structure-based protein library design that enables optimization of large combinatorial libraries based on structural energies of their constituents [29].

In vitro methods give the user not only the option to decide where the mutations should occur, but also which residues are to be introduced. Because diversity is created at the codon level, codon redundancy is a crucial factor determining the effort for library screening. The goal is the balanced distribution of codons with respect to the expression system that will be used. The codon distribution suited for *E. coli* is not optimal for eukaryotic expression systems and vice versa. Furthermore, stop codons are undesirable. Even some amino acids, such as cysteine or proline, can be disadvantageous for some applications. The possibility to use defined nucleotide mixtures for the sequence synthesis give the user the opportunity to modify the diversity of the inherent DNA library. The most common strategies for chemical synthesis of randomized positions are NNK synthesis and the so-called TRIM technology. The NNK synthesis uses degenerate codons to eliminate incorporation of two of the three stop codons (N states for any nucleotide, K means T or G). The TRIM technology uses preassembled trinucleotide building blocks to achieve trinucleotide-defined mixtures. This technology allows complete customization of the amino acid composition at randomized sites and thus avoids the occurrence of unwanted stop codons or amino acids. In comparison to the NNK strategy, the TRIM technology is less prone to out-of-frame mutations [30, 31].

The size of the library can be maximized by choosing the number of amino acids for randomization. It is obvious that with the growing number of randomized residues grows the complexity of the library. Theoretically, by randomization of 12 amino acid residues, using 20 standard amino acids, we can get 20^{12} ($\sim 4 \times 10^{15}$) different protein variants. However, the absolute functional library size is different from the predicted one. For example, in ribosome

display (discussed below), it is given by the number of available ribosomes (about 10^{14}), the number of translated mRNA molecules (about 10^{13}), and thus the ternary complexes that are formed. In phage display, the number of available variants is mainly limited by transformation efficiency. The final size is also affected by the quality of the input PCR fragment or plasmid [32].

After assembly of the library, sequential and biophysical characterization of randomly chosen unselected library members is recommended. The possibility to use next-generation sequencing for the new combinatorial DNA library makes the process of the quality control really fast.

1.3. *In vitro* selection techniques

From combinatorial libraries containing tens of billions of varieties, a specific binder can be selected using *in vitro* selection methods. Phage, bacterial, ribosome, or yeast display are the most used approaches [32-35]. Other similar approaches or modifications of the above-mentioned examples have also been tested using a wide range of different target molecules [36]. In comparison to traditional *in vivo* immunization approaches, the *in vitro* systems do not have to struggle with problems such as inherent toxicity of the target molecule (e.g., toxins) or poorly immunogenic non-protein targets (e.g., carbohydrates, lipids). Furthermore, binders can be produced to a vast range of different epitopes on a single protein. The *in vitro* nature of selection methods allows manipulation of selection conditions to direct specificity. The general goal of the selection is to find a variant that will recognize the new target with sufficient affinity and will not have any residual binding to other unrelated control proteins. The strategies of individual approaches can be varied depending on what properties of the binder are required.

1.3.1. Introduction to selection techniques

All selection techniques must somehow couple the synthesized protein variant (phenotype) with its coding genetic information (genotype). One possible approach is to separate individual variants into compartments. The nature's example are cells, which represent appropriate units that can secure the expression of a particular variant while preserving its genetic information. The most frequently used is the expression of the protein binder on the surface of a cell (bacterial, yeast display). A similar example is a widely used display technology – phage display, where the bacterial cells are covered by phages producing the particular peptide variant.

The drawback of these techniques is the necessity to use transformation for incorporating the library into the cells, reducing its initial diversity.

The second principle is direct physical coupling of genetic material to the protein product. This approach can use cell-free systems, thus avoiding the transformation step. The advantage of *in vitro* translation is not only the possibility to use more complex libraries, but without any barrier, the genetic information is fully available for additional PCR-based randomization techniques. Examples of selection approaches based on physical connection are ribosome and mRNA display [32, 37].

1.3.2. Ribosome display

One of the most studied selection method, and also a technique established in our laboratory, is the ribosome display (RD). The physical connection in RD is between the synthesized protein and its mRNA. In nature, during translation, the protein chain is covalently connected via ester bond to the peptidyl-tRNA within the P-site, and thereby tightly maintained within the ribosome. After reaching the stop codon, the ester bond is hydrolyzed with the help of release factors, and the protein and then mRNA are released from the ribosome [32].

The principle of ribosome display is to prevent dissociation of the newly synthesized protein and mRNA encoding it from the ribosome. The resulting ternary complex (mRNA-ribosome-protein) in RD is the consequence of stalled translation caused by a missing stop codon. Besides removal of the stop codon, the experimental conditions are designed to prevent spontaneous hydrolysis of the ester bond and falling apart of the ternary complex. The reaction mix contains high concentrations of Mg²⁺ and other components, preventing natural mechanisms to rescue the stalled translation. Furthermore, the reaction takes place very shortly and is cooled thoroughly. The detailed procedure of RD is displayed in Figure 1.

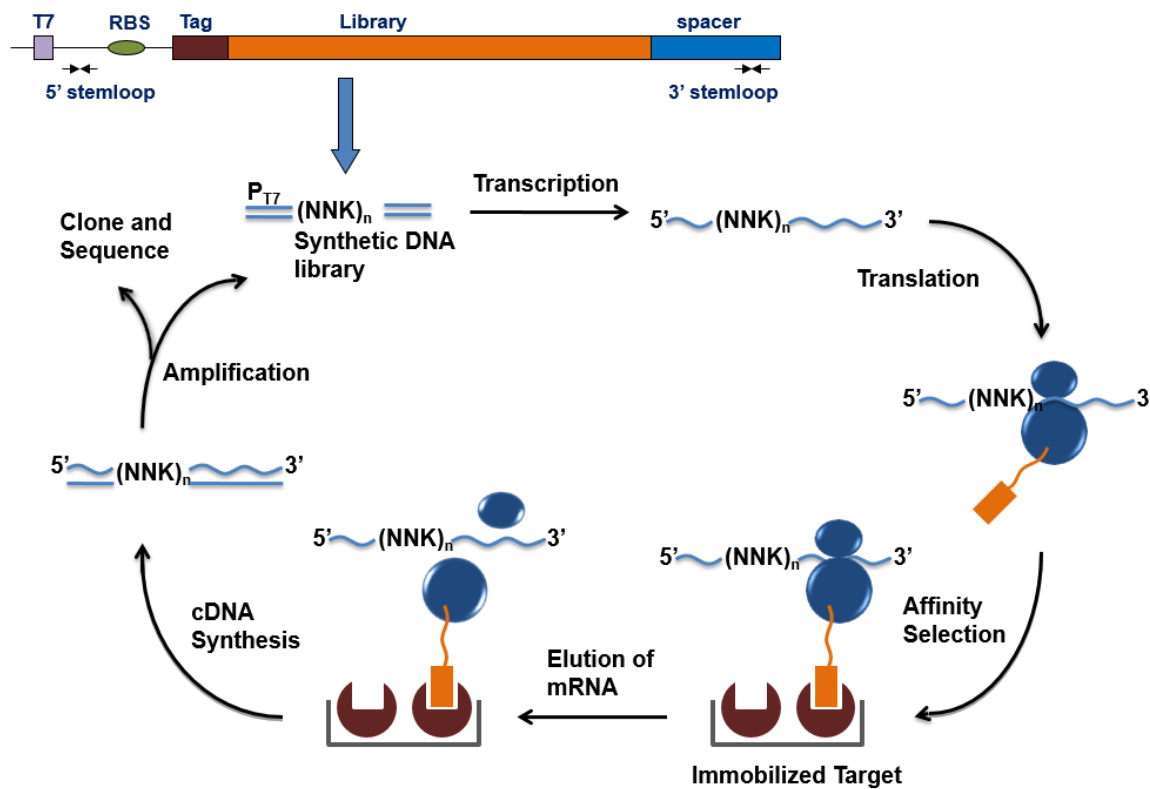


Figure 1. The ribosome display selection cycle

The process starts by the assembly of a DNA cassette containing a strong promoter and ribosome binding site (RBS) followed by ORF, encoding a combinatorial library, terminated by a spacer sequence without stop codon. The spacer should be long enough to allow the final protein variant to fold into a functional binding domain and stick it further out from the ribosome. Using a cocktail of enzymes comprising the transcription and translation machinery of *E. coli*, the DNA is transcribed into mRNA and then translated. In addition, molecular chaperones and small heat-shock proteins are present in the *E. coli* extract, facilitating the proper folding of the protein. The construct comprises 5' and 3' stemloops at the mRNA level, protecting the mRNA against RNases.

The formed ternary complexes are exposed to immobilized target molecules. The protocol can be modified by replacing direct immobilization of the target molecule on the plate by magnetic beads. This alternative has the advantage that all molecules are free in solution and the binding is not influenced by steric restrictions or by the charge of the modified surface of the plate. It is obvious that the way how the target molecule is exposed to the library is crucial for the final selection outcome; the construction and subsequent use of the recombinant target protein for the use in RD should be addressed. The non-binding complexes are washed away. mRNA is

then released from the bound complexes by addition of chelating agents and isolated. Purified mRNA is reverse transcribed and the cDNA is PCR amplified. The resulting PCR product, now enriched by target-binding variants, proceeds to the next round of the selection [38]. The number of RD cycles typically varies between three to five, depending on the affinity requirements of the selected binders. Each round usually differs in the stringency of applied selection conditions. After the final round, the selected DNA library is ligated into a suitable vector and individual binding molecules are identified by picking individual colonies. Positive clones are identified using binding assays such as enzyme-linked immunosorbent assay (ELISA).

Ribosome display is a broadly used *in vitro* evolution technology, which has been successfully used for selection of binders against many target molecules both for academic and commercial purposes [32]. The supposed disadvantage of RD based on *E. coli* expression system is that some proteins of eukaryotic origin are prone to aggregation during the translation. However, this case does not occur as often as one would expect. It was experimentally proved that some proteins that could not be expressed in functional form in *E. coli* can still fold attached to the ribosome. It is supposed that the ribosome can enhance the solubility of the ternary complex and sterically block aggregation [32]. Another possible alternative is to use a eukaryotic translation system. Nevertheless, the design of the input DNA library must be changed and corresponding eukaryotic enzymes must be added to the reaction mixture.

1.4. Utilization of protein scaffolds

Many proteins have been specifically targeted by different non-Ig scaffold binders. The most frequent applications are treatment and diagnosis of cancer and inflammatory diseases, or a combination of both therapy and diagnosis (theranostics). Despite the fact that some individual binding proteins from the above-mentioned groups of scaffolds are already pursued for medical applications (biopharmaceuticals), drugs derived from protein scaffolds are still rare. The biopharmaceutical market is still dominated by therapeutic antibodies [1, 39].

1.4.1. Binding proteins promising for therapy

The prerequisite for a protein binder to be successful in therapeutic applications is the absence of immunogenic effects, and the binding proteins derived from human scaffolds, for example Adnectins and Anticalins, therefore appear more attractive than bacterial protein scaffolds such

as peptide aptamers or Affibodies. However, scaffolds derived from prokaryotic proteins can be subjected to so-called deimmunization and successfully used [15, 16, 19]. Also, they should not interfere with other endogenous molecules, but the residual interaction with other targets is difficult to predict. The small size of non-Ig scaffolds is rather a disadvantage. Rapid penetration and elimination of small particles are desired in diagnostic molecular imaging, while for therapeutic use, slow clearance and longer half-life are more preferred. On the other hand, the small molecule can be easily modified by conjugation with half-life prolonging agents such as polyethylene glycol, Fc fragment, albumin, or albumin-binding proteins [16, 40, 41].

The common molecular targets are usually relevant disease-related molecules such as signaling molecules, surface receptors, or soluble mediators. Selected binders then serve as functional inhibitors or antagonists interfering with particular signaling pathways. Inflammatory diseases are often characterized by increased concentrations of pro-inflammatory mediators. The decrease in their concentration can be achieved by preventing interaction of a particular cytokine with its cognate receptor. This principle is used for the development of biopharmaceuticals for the treatment of psoriasis. Psoriasis is an autoimmune disease associated with IL-23-mediated signaling. IL-23 is a heterodimer comprised of p40 and p19 subunits. Only the p19 subunit is specific for the IL-23 signaling pathway. The goal is to prevent the interaction of IL-23 with its cognate receptor either by inhibitory binding to IL-23 or IL-23R (receptor). The inhibitory ABD variants targeting the p19 subunit of human IL-23 (ILP binders) and IL-23R (REX binders) have already been generated [25, 26]. A collection of REX variants, with sub- to nanomolar KD values for the binding to IL-23R and with a promising therapeutic potential, was identified. To reduce the immune activity, Anticalin antagonists against T-cell receptor CTLA-4 (cytotoxic T-lymphocyte antigen 4) have been developed [42].

Regarding cancer, VEGF-R2, a receptor involved in tumor angiogenesis, has been targeted by Adnectins [5]. Anticalins possessing subnanomolar affinities to soluble angiogenic factor VEGF have been characterized [7]. Many surface structural molecules specific for cancer cells have been described. Binders targeting these specific surface structures can be used for the delivery of cytotoxic compounds and thus destroying the cancer cells. Affibodies are the first type of scaffold protein that has been applied for toxin delivery. Truncated exotoxin A from *Pseudomonas aeruginosa* provides highly selective toxicity to HER2-expressing cancer cells. Fusion of the HER2-recognizing Affibody with this toxin and with an ABD domain for prolonged residence in circulation has gained a prospective anticancer agent [15]. Similarly, the

anti-HER3 therapeutic Affibody construct flanking ABD with low picomolar affinity to HER3 was designed [16]. Other Affibodies generated for cancer treatment include binders to EGFR, IGF-1R, and PDGFR β (www.affibody.com [43]).

Another possible therapeutic application is utilization of probiotic lactic acid bacteria in the delivery of therapeutic binding proteins to the human intestine. Lactic acid bacteria prepared in the study of Zadavec et al. were engineered to effectively display the ABD-derived binding proteins against Shiga toxin 1 B subunit (Stx1B) on their surface. ABD-derived S1B variants were biochemically, biophysically and functionally characterized, displayed on the surface of *L. lactis*, and their ability to bind Stx1B was confirmed. Engineered lactococcal cells capable of binding Stx1B could be a possible instrument for the treatment of infections caused by shiga toxin-producing bacteria, as there is currently no specific treatment [44].

Many other potential biopharmaceuticals are currently under preclinical development, and a few of the above-mentioned examples are about to enter the phase I or phase II clinical study [5][4, 45].

1.4.2. Diagnostic direction

An appropriate binder for *in vitro* diagnostic methods must be able to identify, quantify, or localize a particular disease marker with sufficient affinity and specificity. This requires minimal interference with the background compounds and compatibility with several detection methods. The complicated handling and expensive production of antibodies triggered the use of non-Ig protein binders in diagnostic applications in which antibodies are already well established and widely used. The disadvantage, in comparison to conventional antibodies, is their monomeric architecture, giving weaker signals in these applications. Most artificial binding proteins behave like monovalent Fab fragments, and thus must be engineered to exhibit high target affinity in order to yield sensitive detection. Sophisticated solution to this problem is functional dimerization of two effector domains in order to double the binding affinity [16].

Engineered scaffold proteins are promising components for the common use in diagnostic methods where antibodies have already been well established. The most common used diagnostic methods are reviewed in chapter 1.5. Another suitable application in diagnostics is development of *in vivo* imaging agents. Proteins with molecular weights over 45 kDa such as

antibodies have been shown to accumulate in tumors nonspecifically, causing the analysis unreliable. In contrast, small size Non-Ig binders have revealed very good imaging properties. They provide better tissue penetration and more rapid blood clearance. By introducing a cysteine residue for covalent coupling, they can be easily conjugated with radionuclides, fluorescent dyes, paramagnetic iron particles, or ultrasound contrast agents. ADAPT6, a variant of ABD-derived Affinity Proteins (ADAPT) binding to HER2, has been shown to be an appropriate particle for radionuclide labeling and *in vivo* imaging [41]. The ABD scaffold is sufficiently small, does not contain cysteines, allowing use of oxidizing and reducing conditions during the conjugation of the labeling agents without affecting the regular structure. Anticalins targeting human prostate-specific membrane antigen (PSMA), a disease-related target for imaging and therapy of prostate cancer, have been identified. The best candidate with improved dissociation rate was able to bind PSMA with the affinity in picomolar range [40]. Several other Non-Ig scaffold proteins, such as Affibodies, Microbodies, and DARPins, have been successfully used for imaging of therapeutic targets in preclinical studies [41].

Artificial protein binders can replace antibodies as capture agents for the detection and separation of diagnostically relevant target molecules. With both thermal and chemical stability as a prerequisite for repeated use, they may act as biomolecular sensors in the chip technology for diagnostics of plasma proteins. The most promising field is detection of cancer biomarkers.

1.4.2.1. Diagnosis of prostate cancer based on detection of prostate cancer biomarkers

Prostate cancer (PCa) is the most common lethal type of cancer among men over 50 years of age. The severity of the disease is evidenced by the annual increase in mortality rates. Clinical PCa can be successfully treated at its early stage, when the cancer is restricted to the prostate gland. The diagnosis of early stage is critical for the prevention and early treatment, but the initial stages of cancer are difficult to detect. Current clinical practice is based on ultrasonography, digital rectal inspection, computed tomography scan, magnetic resonance imaging, and cancer protein assay [46]. The latter relies on the detection of prostate-specific antigen (PSA) and is primarily based on the use of enzyme-linked immunosorbent assay (ELISA). PSA is a glycoprotein secreted by normal prostate epithelial cells and belongs to the human kallikrein gene family of serine-proteases (KLK3) [47, 48]. PSA is currently the most used serum marker available for the clinical detection of PCa. Increased PSA levels, exceeding 4 ng/ml in the blood, are considered as abnormal and are a stimulus for further investigation [49, 50]. The

definitive diagnosis is determined by histopathological verification of adenocarcinoma in prostate biopsy.

The wide availability of the PSA assay revolutionized PCa screening and resulted in reduction of the number of patients found to have metastatic disease at initial diagnosis [47]. While the massive onset of PSA screening has made great progress in early detection of PCa, the simple use of PSA for PCa diagnosis is insufficient because methods that rely only on the detection of the whole PSA are not sensitive enough in the so-called “grey zone” of 4-10 ng/ml, where the elevated PSA level could also be triggered by non-cancer causes such as benign prostatic hyperplasia (BPH), higher age, cystitis, catheterization, injury, or other disruption of the prostate basement membrane. This could lead to a high rate of false positives resulting in repeated biopsies and unnecessary surgeries. Furthermore, some aggressive prostate cancers do not produce PSA [47]. To overcome this drawback, alternative detection approaches have been proposed. Deeper study of PSA and advances in the development of new analytical tools have opened new possibilities for PSA detection. Different PSA isoforms have been revealed to improve PCa diagnosis. The total amount of serum PSA (tPSA) consists of PSA bound to protease inhibitors, mostly to alpha-1-antichymotrypsin (cPSA), or free unbound form (fPSA). This more complex assay increased the specificity by 20 % over total PSA alone. While the correlation between fPSA and total PSA is more informative, it still gives false positives [51]. Recently FDA-approved Prostate Health Index (PHI) in combination with sophisticated imaging systems have partially improved PCa diagnosis. The PHI method includes determination of (-2)pro-PSA in combination with free and total PSA levels. PSA is a serine protease, which is initially produced as an inactive pro-PSA form. It has been shown that cancer tissues contain higher levels of truncated forms of pro-PSA. This screening system improves the specificity and decreases the number of unnecessary biopsies; however, it has not shown significant improvement in the ability to distinguish between BPH and PCa and also between biologically mild and aggressive cancer [46]. The discovery of different PSA glycosylation patterns in PCa could improve diagnosis of the aggressive versus non-aggressive form of PCa. A decrease in the core fucose and an increase in the α 2,3-sialic acid percentage of PSA are more typical of high-risk PCa. The identification of glycosylation-specific changes could improve the decision making for patients. Unfortunately, the concentration of serum PSA is very low in the patients' sera, making this analysis very challenging [47].

Another possibility to improve the current PSA detection tools is the choice of **alternative biomarkers**. In recent years, various more or less suitable candidates have been proposed for enhancing the accuracy of PCa diagnosis [49, 52-54]. The studies of various biomarkers indicate that no single biomarker is likely to have the appropriate degree of certainty to predict the development of cancer. Parallel examination of two or more biomarkers potentially offers a more accurate and specific alternative than the current tests. While the analysis of urine biomarkers appears to be very interesting, there is much more interest in profiling blood proteins. The most useful clinical biomarkers will probably be those that can be assayed from blood samples.

1.4.2.1.1. Kallikreins

The human kallikrein family of proteases consists of 15 members (named KLK1-15). The human glandular kallikrein gene family comprises three members: tissue kallikrein (KLK1), human glandular kallikrein 2 (KLK2), and prostate-specific antigen (PSA or KLK3) [48, 55]. KLK2 is structurally very close to PSA (Fig. 2.). They share 78% amino acid sequence homology. The main difference between KLK2 and PSA is their substrate specificity. PSA has chymotrypsin-like substrate specificity and KLK2 has trypsin-like substrate specificity. Similarly as PSA, KLK2 is expressed in the highest level in the prostate. The main biological role of KLK2 in seminal plasma is to cleave the gel-forming proteins semenogelin I, semenogelin II and fibronectin. Moreover, KLK2 was found to activate the enzymatically inactive PSA by cleavage of their full length pro-PSA [56]. KLK2 has been shown to be a predictive marker for PCa progression. Similarly to PSA, KLK2 can also be found in the serum in different forms, including free KLK2. The levels of KLK2 were shown to be elevated in PCa. The secretion of KLK2 is stimulated by androgens, progestins, glucocorticoids, and mineralocorticoids. In some studies, the outcomes of KLK2 screening were more informative than those of serum PSA. Better results were observed especially when compared with higher Gleason score, suggesting that KLK2 could be a good marker for high-risk prostate tumors [57]. It was previously shown that the correlation between KLK2 and PSA is low. For example, the expression of PSA tends to decrease with increasing tumor grade, whereas that of KLK2 increases or remains constant [52]. Although KLK2 seems to be more specific, the protein levels in the serum are about 1 % of total PSA, making the assay less sensitive. In any case, it has been shown that KLK2 is able to enhance cancer detection in patients with a total PSA serum level of 2–10 ng/ml [52] and that measurement of KLK2 in addition to free and total

PSA in the serum allows better separation of men with BPH from those with PCa, suggesting that KLK2 is a good candidate that might complement the information obtained by PSA [58]. Due to its very close sequence and structural identity with PSA, some monoclonal anti-PSA antibodies cross-react with KLK2 [56]. Thus, it is very important to find a very specific antibody or binding protein to be used for KLK2 detection.

There is growing evidence that members of the kallikrein family could be useful as biomarkers of prostate cancer, especially when used in combination. Besides the above-mentioned KLK2, kallikrein 4, kallikrein 6, and kallikrein 11 have also been shown to have a predictive role in the detection of PCa. It has been demonstrated that the expression levels of KLK11 increased after the radiation therapy, in contrast to KLK2 and PSA levels. Similarly to KLK2, the concentration of KLK11 in seminal plasma and prostatic extracts is ~300 fold lower than PSA, requiring sensitive detection tools [59].

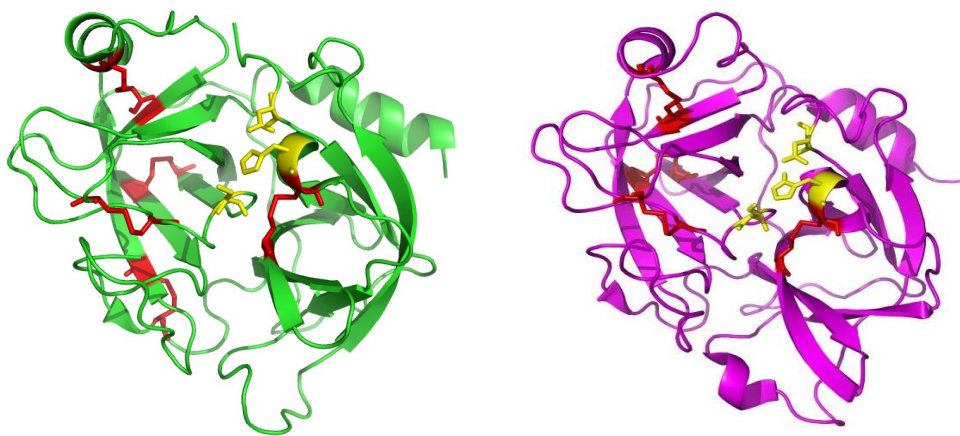


Figure 2. The crystal structure of human KLK2 and KLK3 (PSA). (PDB: 4NFE and 2ZCH). Kallikreins comprise the largest cluster of proteases in the human genome. It is a family of 15 sequentially related trypsin- or chymotrypsin-like serine proteases. KLK2 (in green) and KLK3 (in magenta) show ~80% identity in amino acid sequence. The overall structure is maintained by 10 cysteine residues (cysteine residues are labeled red). Proteolytic triad Ser, His, Asp within the catalytic pocket is depicted yellow. Interestingly, the crystal structure of KLK11 remains unknown.

1.4.2.1.2. PSP94

Since prostate cancer has been found to have hereditary predispositions, several genome-wide studies for PCa genetic risk factors have been made. One of the genetic risk factors linked to PCa is the single-nucleotide polymorphism (SNP) on chromosome 10q11, rs10993994, which is significantly associated with mRNA expression of the MSMB gene [60, 61]. Men with the risk allele have decreased expression of MSMB in both normal prostate and tumor tissue [62]. This finding has led to a greater interest in further study of this gene and its product. MSMB codes for Prostate Secretory Protein of 94 amino acids (PSP94), also known as seminal plasma inhibin (HSPI) or beta-microseminoprotein (b-MSP) [63]. PSP94 is present both in reproductive and some non-reproductive tissues, and is one of the most abundant proteins in human seminal plasma. It is a non-glycosylated, cysteine-rich protein whose exact biological function has not been clearly defined. Several functions have been postulated for this protein, including inhibition of sperm motility, prevention of spontaneous acrosome reaction in the sperm [64], calcium- and pH-dependent candidacidal activity, growth regulation, and apoptosis [65, 66].

At a physiological pH range, PSP94 acts as a dimer. At acidic pH, PSP94 can dissociate into monomers [67] and is then available for interaction with other proteins. Many PSP94-binding proteins have been identified in the plasma and seminal plasma using affinity chromatography and co-immunoprecipitation, suggesting other biologically important roles. PSP94 was shown to bind to human immunoglobulin, preventing an immune response to spermatozoa in the female reproductive tract. PSP94 bound to Prostatic Acid Phosphatase (PAP) prevents the proteolysis of semenogelins leading to the liquefaction of human semen [68]. Other binding partners are members of the Cysteine Rich Secretory Protein family PSPBP (PSP94-binding protein) and CRISP-3 (Cysteine Rich Secretory Protein-3). There is also evidence for the existence of PSP94-binding proteins on prostate cancer cells, which after binding of PSP94 initiate a signaling cascade that results in apoptosis of the tumor cell [65, 66]. Some *in vivo* and *in vitro* functional studies have been done proving that PSP94 has a tumor-suppressive role in PCa [69].

In addition to its interesting biological function, several studies have demonstrated the clinical potential of serum levels of PSP94 as a diagnostic marker for prostate cancer [52, 63, 68-70]. It has been shown that PSP94 expression decreases as PCa progresses, with complete lack of PSP94 production in highly advanced metastatic prostate cancer. The decrease in the expression is mainly caused by Enhancer of zeste homologue-2 (EZH2), a known epigenetic silencer of

gene expression. EZH2 has been suggested to silence MSMB expression in advanced PCa [70, 71]. This differential expression could allow the use of PSP94 as a prognostic marker of PCa with the ability to determine the stage, progression, and recurrence of the disease. Furthermore, another advantage of using PSP94 as a PCa biomarker is the fact that its expression is not affected by the loss of androgen receptor activation and is retained despite hormone manipulation. This suggests that PSP94 could be a particularly useful biomarker in patients that have been previously exposed to androgen-ablating agent therapy [63, 70].

1.4.2.2. Diagnosis of lung adenocarcinoma based on the detection of circulating tumor cells

Circulating tumor cells (CTCs) represent a heterogeneous population of cancer cells that has been identified in the blood of patients with diagnosed cancer. They enter the blood stream from the primary or metastatic site of the tumor by passive shedding or through the dynamic processes of stromal invasion. Within the circulation, most of the cells die. Some cells that survive the intervention of the immune system and the sheer stress of the blood stream remain dormant or undergo proliferation to form metastasis. The population of CTCs undergoes the epithelial-mesenchymal transition (EMT) process (Fig. 3.). During the EMT, CTCs gradually lose their epithelial phenotype and gain mesenchymal properties. CTCs with more mesenchymal phenotype may have enhanced ability to intravasate and to participate in distal metastasis formation, and are considered more aggressive.

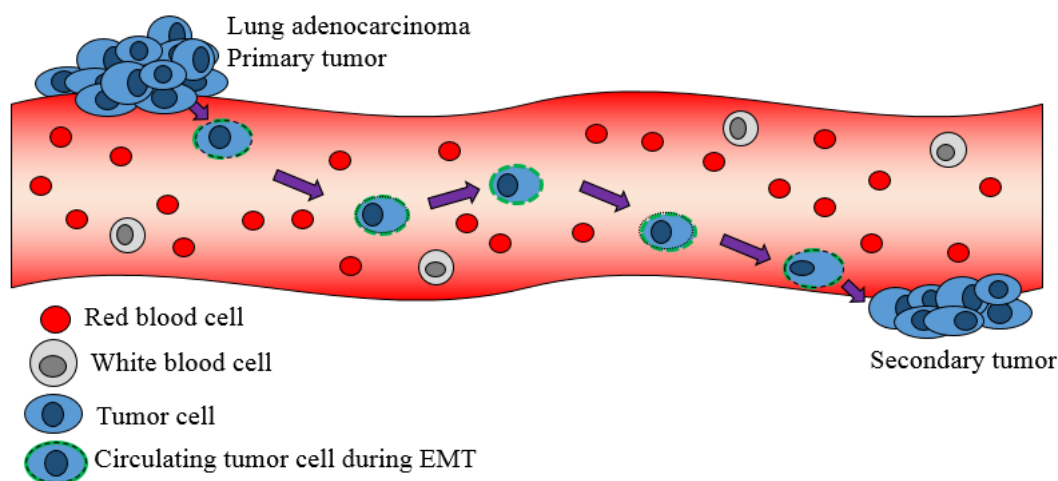


Figure 3. Epithelial-mesenchymal transition

CTCs have been studied as predictive biomarkers of a number of different malignancies, including breast cancer, melanoma, gastrointestinal cancer, lung cancer [72], and prostate cancer [73]. Lung cancer is the most frequent cause of cancer deaths worldwide. The high mortality is caused by the fact that 70 % of the diagnosed lung cancers are in advanced stage that has already spread locally or to distant organs [74]. New diagnostic approaches for early detection of lung adenocarcinomas as well as novel insights into the molecular mechanisms underlying lung adenocarcinoma pathogenesis are urgently needed [75]. Monitoring of CTCs in the peripheral blood of cancer patients provides a number of potential applications such as early cancer detection, disease staging, monitoring of recurrence, prognostication, and therapy selection. A major benefit of the blood-based approaches in comparison to solid tissue biopsy is that they can be performed repeatedly with low risk of side effects, allowing dynamic measurement of CTCs as an indicator of the disease stage and response to therapy.

After the discovery of CTCs in peripheral blood, some technical achievements to isolate them have been made. Although improvements in the molecular technology have partially enabled routine detection of the rare CTCs in blood samples, the cellular heterogeneity and low abundance of CTCs (<10 cells/ml) in blood still make their profiling a big analytical challenge. A big pitfall of common isolation strategies is the identification of CTCs using only epithelial biomarkers. This tool, which relies mostly only on the EpCAM (epithelial cell adhesion molecule) epithelial marker as a major capture structure, fails to identify CTCs of predominantly mesenchymal origin, thus misinterpreting the resulting data. Therefore, alternative approaches using specific markers are being explored [76-78].

1.5. Detection systems in diagnostics

The most common used diagnostic methods include immunoassays, biosensors, microarrays, as well as fluorescence microscopy and flow cytometry. Enzyme-linked immunosorbent assay (ELISA) is one of the most used immunoassays to date. ELISA permits highly sensitive and selective quantitative/qualitative analysis of antigens, including proteins, peptides, nucleic acids, hormones, and secondary metabolites [79, 80]. The routinely used ELISA based on antibodies possesses many advantages, making it one of the most universally used detection tools. The purity and specificity of the used antibody play an important role in the immunoassay. Monoclonal antibodies are preferred over polyclonal antibodies because of their monovalency. Utilization of polyclonal antibodies, reacting with multiple epitopes, can lead to

low specificity and sensitivity of the assay. There is also a higher risk of false-positive results. While the sensitivity and specificity of monoclonal antibodies belong to their major positive features, their production is an expensive and laborious process. To improve the sensitivity and specificity of the standard direct ELISA, sandwich ELISA is used as an alternative, in which two antibodies are used against one antigen. The modification of direct ELISA where the immobilized antigen is detected in the first step by primary antibody and then by secondary antibody is called indirect ELISA. Indirect ELISA has been successfully used for detecting toxins in the serum of cattle as well as humans [79]. While methodologies of ELISA are being improved to suit the new emerging experiments, the performance of standard ELISA is relatively time-consuming and it is not a suitable method for some applications such as detection within dynamic conditions.

The development of microfluidics technology during the last decade allowed demonstration of the new concepts of biosensors for the detection of diagnostic targets in the dynamic environment. The microfluidic devices have become a convenient tool mainly for the isolation of rare cells such as CTCs or stem cells from the blood for the diagnosis of different kinds of cancer. This technique enables not only detection of the cancer cells, but also their separation and sorting and single-cell handling. This highly innovative approach brings the possibility to perform phenotypic sorting followed by cell release for subsequent cultivation or lysis for further characterization such as RT-PCR. The majority of recently developed microfluidic devices usually applies commercially available antibodies immobilized in microfluidic channels of various geometries, in some cases combined with size-based filtration. Although excellent performance in the CTC capture was shown in some cases, devices using antibodies suffer from similar bottlenecks as standard antibody-based methods [81-83].

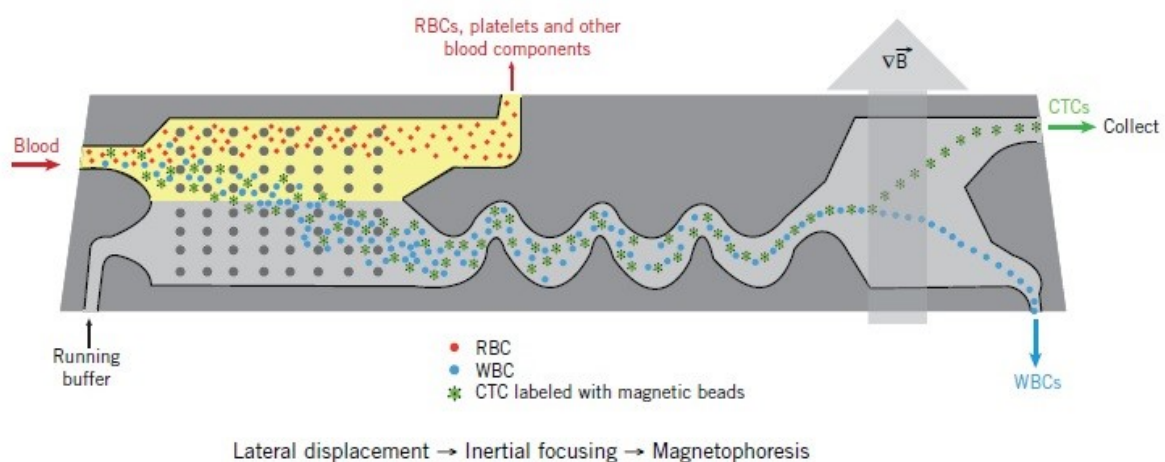


Figure 4. Example of a microfluidic chip (CTC – iChip [81])

Currently, binders derived from small protein scaffolds have appeared as a good option to overcome the limitations of antibodies. The advantages of these binders for their utilization as diagnostic tools are their small size, high stability over a wide range of pH and temperature, allowing repetitive use. They are more applicable for further modification increasing their potential utilization ability. As they are smaller, they are able to recognize hidden epitopes inaccessible for traditional antibodies. Moreover, the covalent immobilization of antibodies on microchip surfaces is not so straightforward and often can alter their binding sites or cause steric shielding [84, 85].

2. Aims of the thesis

2.1. Binding proteins targeted to prostate cancer biomarkers

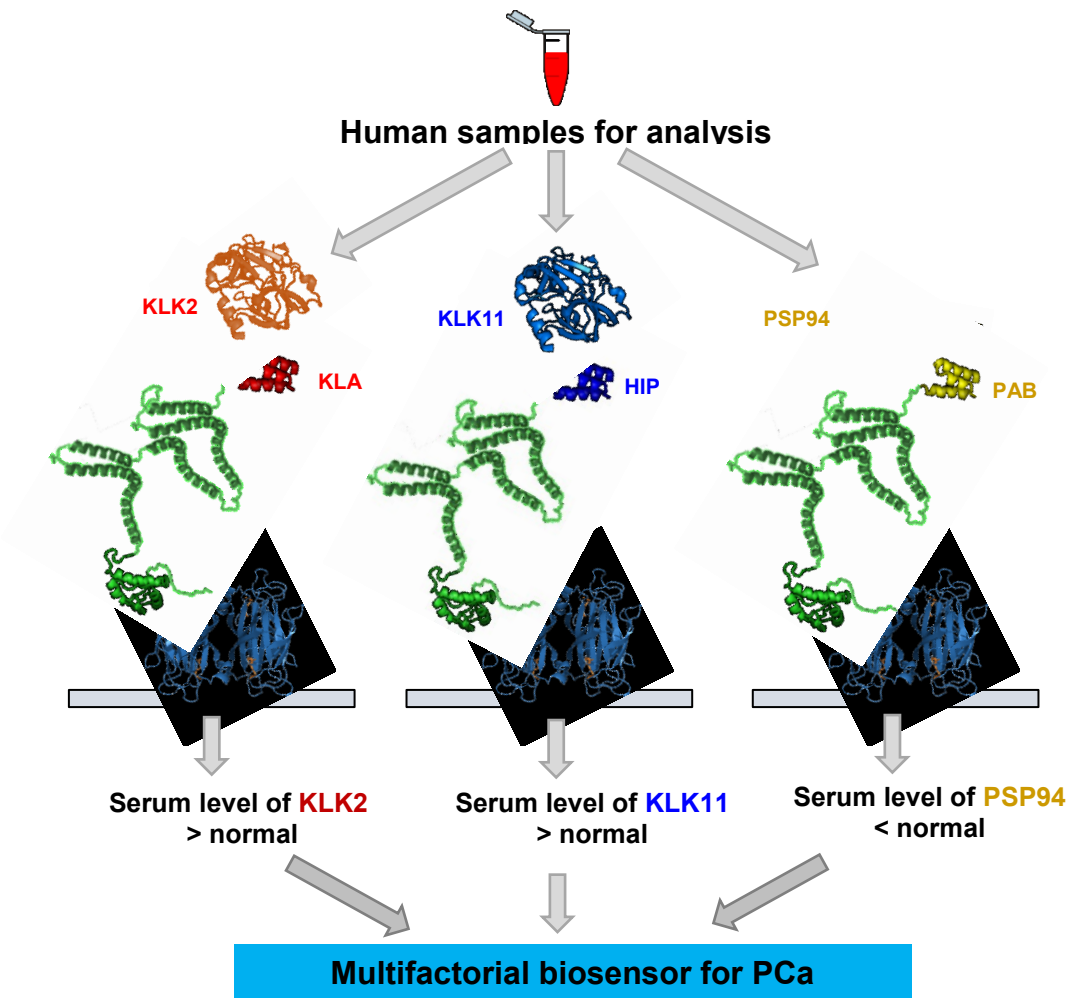
2.1.1. Generation of binders specific for human PSP94

2.1.2. Development of binders of human kallikrein 2 and kallikrein 11

Grant: *Novel binding biomolecule development for tumor in vitro diagnostics.* Ministry of Industry and Trade of the Czech Republic (programme TIP), reg.# FR-TI4/667, 2012-2014. Collaboration with EXBIO Praha, a.s., Czech Republic and Protean, s.r.o., Czech Republic.

Prostate cancer (PCa) is one of the most serious cancers in advanced countries. The treatment and diagnosis costs of the PCa are enormous. Due to the fact that preventive screening programs based on detection of the serum PSA level are insufficient, there is a growing pressure on the development of new diagnostics. Targeted diagnostics (and therapeutics) based on monoclonal antibodies have limited utility. The immune system responds poorly to tumor targets, making it difficult to develop specific reagents based on monoclonal antibodies. To overcome this obstacle, state-of-the-art technology based on alternative non-antibody binding agents has been proposed in this project. Their generation does not require limited immune system reactivity, as the whole process takes place *in vitro*, without the involvement of the living organism or individual cells. The major goal of the project is to develop a unique collection of binding biomolecules as alternatives to antibodies on the model of early detection of PCa, which might contribute to the development of more effective microfluidic chip-based multi-parametric serum diagnostics. The use of a suitable combination of particular binding proteins will increase the sensitivity and reliability of the assay. Currently, the clinically validated test for PCa diagnosis relies on detection of the serum level of prostate-specific antigen (PSA, KLK3) using a monoclonal antibody-based ELISA kit, but this examination, although widely used, fails to predict early stages of PCa development, and in addition does not distinguish precisely between the malign form of PCa and benign prostate hyperplasia. Due to the lack of this specificity, many patients have to undergo unnecessary prostate tissue biopsy [50, 86]. To overcome this drawback, a larger set of PCa biomarkers has been suggested to improve early prediction of PCa, to identify recurrent stages of the malignancy after prostatectomy and treatment, and to more precisely correlate serum-level oncomarkers with the histological Gleason scoring. Therefore, novel and more complex tools for improved PCa diagnosis, including multifactorial biosensors or ELISA sets, are being required.

The fundamental part of the project is devoted to the development of new binding proteins targeted to selected prostate cancer biomarkers PSP94, KLK2, KLK11. To generate novel binders targeting PSP94 (called PAB binders), KLK2 (called KLA binders) and KLK11 (called HIP binders), a high-complex combinatorial library derived from an albumin-binding domain (ABD) scaffold was used in combination with the ribosome display selection technique. The most promising candidates were functionally and biophysically characterized. These binders, after subsequent modification, could serve as a component of a biosensor with multiple biomarkers. It has been well documented that the expression of PSP94 is decreasing during the development of PCa, while for the KLK-family members, the increase in serum levels is an indicator of PCa progression. Therefore, the combination of these three oncomarkers can be more informative, significantly improving the accuracy and validity of this potential novel diagnostic tool.



2.2. Binding proteins targeted to surface markers of epithelial and mesenchymal cells for sorting circulating tumor cells

2.2.1. Binders derived from the ABD scaffold

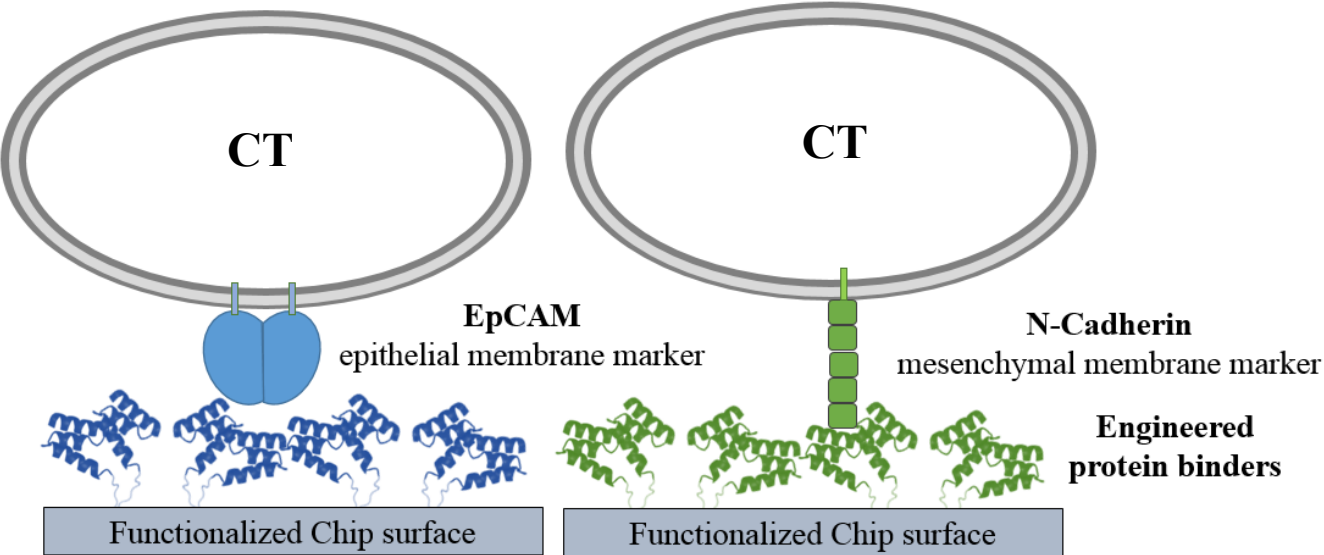
2.2.2. Binders derived from Myomedin scaffold

Grant: *Detection and evaluation of circulating tumor cells (CTCs) in patients with lung adenocarcinoma by microfluidic chip technology.* Czech Health Research Council, Ministry of Health of the Czech Republic, reg. # 16-29738A, 2016-2019. Partner Organizations: Department of Biology, Faculty of Science, University of J.E. Purkinje, Czech Republic; Krajská zdravotní a.s., Ústí nad Labem, Czech Republic.

Circulating tumor cells (CTCs) represent one of the promising diagnostic targets in monitoring lung adenocarcinoma progression and malignant transformation. Standard methods of CTC isolation from the blood are mostly based on isolation and counting of epithelial cell adhesion molecule (EpCAM) positive cells, so the other cell phenotypes that may be even more invasive are not taken into account. The running project “Detection and evaluation of CTCs in patients with lung adenocarcinoma by microfluidic chip technology” proposes development of a microfluidic chip that enables fast isolation and scoring of CTCs from a peripheral blood sample of the tested individual and to sort the particular CTC populations based on their respective epithelial/mesenchymal phenotype. The major advantage of this solution is a significant time reduction required for cell-type characterization (from three weeks of *in vitro* cultivation for cell enrichment to only one day) and the possibility of subsequent live cell release important for further cell cultivation and detailed characterization.

To construct the Cell Capture Zone of the microfluidic chip, it is necessary to develop a novel type of high-affinity binding proteins specific for epithelial and mesenchymal membrane markers that will be able to selectively capture lung adenocarcinoma CTCs under dynamic cell-sorting conditions. Such differentiation would enable more precise diagnosis of metastatic progression and adjusting the early therapy to individual patients. As target molecules for selection of the new binders, different recombinant forms of epithelial marker EpCAM and mesenchymal marker N-cadherin were designed and produced. To generate the binders, an assembled highly complex combinatorial library derived from ABD or Myomedin scaffold in combination with ribosome display selection were used. The most promising candidates selected by ELISA were characterized by measuring their binding properties using model cell lines of the particular phenotype. Five human cancer cell lines (MCF-7, DU-145, CCD1070Sk, HEK293T, PC-3) were analyzed for the expression of EpCAM and N-cadherin membrane markers using flow cytometry. The interaction of the binder with the cells was measured in the

real-time mode using LigandTracer® Green Line. The instrument is suited for monitoring the ligand binding to cell-surface receptors on living cells, allowing determination of the binding affinity and kinetics.

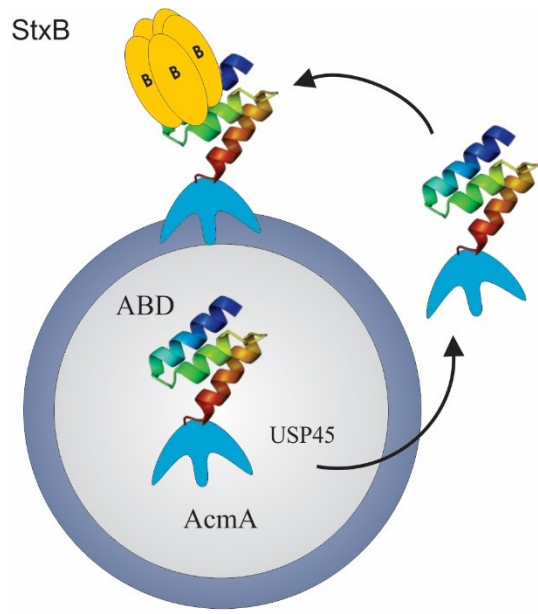


2.3. Binding proteins specific for Shiga toxin 1 B Subunit

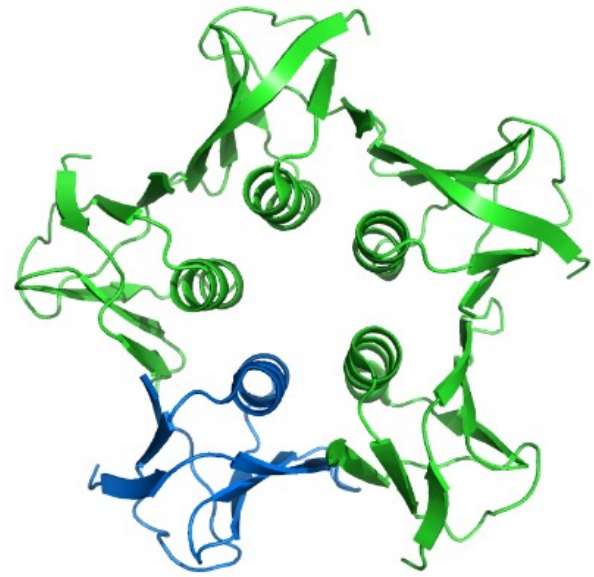
Grant: *Lactic acid bacteria-mediated intestinal delivery of novel therapeutic protein binders derived from scaffold of albumin-binding domain.* Czech Academy of Sciences, reg.# SAZU-16-01, 2016-2018. Partner Organization: Jozef Stefan Institute, Department of Biotechnology, SAZU, Slovenia.

Shiga toxin (Stx) is produced by enterohemorrhagic *Escherichia coli* and *Shigella dysenteriae*. It has been documented that Stx can cause diarrhea, dysentery and hemorrhagic colitis in human that may further develop into life-threatening hemolytic uremic syndrome, leading to acute renal failure. Stx is composed of the A subunit, responsible for intracellular toxic action, and non-toxic pentameric B subunit, responsible for binding to the host cell surface receptor globotriaosylceramide (Gb3). Because conventional anti-microbial treatment of infections by Stx-producing bacteria increases release of toxins from the killed bacteria, there is a need for the development of new therapies [87]. Engineered lactic acid bacteria with surface-displayed binding proteins targeting Stx from the human gastrointestinal tract have emerged as a potential solution. Lactic acid bacteria are part of the human intestinal flora. They have been demonstrated to have protective health effects in several diseases. Their proven safety to the human organism allows their utilization as vectors for the delivery of recombinant proteins to the gastrointestinal tract. Recently, they have been successfully engineered to display specific binders derived from various scaffolds against different targets on their surface [44, 88-90].

In this project, a collection of unique protein binders (S1B) targeted to Shiga toxin B-subunit has been generated using a complex combinatorial library derived from the ABD scaffold and ribosome display selection technique. The ABD scaffold, as a small, soluble and self-refolding molecule, is an appropriate structure for the surface display in *L. lactis*. The binding properties of the most promising S1B binders selected by ELISA were assessed using SPR measurement. After that, they were optimized for the surface display in *L. lactis* and functionally characterized. After subsequent improvement of the binding properties of particular S1B variants by the affinity-maturation approach, lactic acid bacteria with surface-displayed S1B binders would be useful for antagonizing pathogenic bacteria strains by the removal of Stx from the human gastrointestinal tract.



Lactococcus lactis cell



pentameric B subunit of Shiga toxin

2.4. Development of procedures and tools for the validation of polyvalent vaccines against bacterial enteral diseases

Grant: *Development of unique vaccines against serious diseases of animals.* Technological Agency of the Czech Republic (programme EPSILON), reg.# TH01010837 2015-2016 Collaboration with Dyntec spol., s.r.o., Czech Republic.

The demand for polyvalent vaccines against enteral diseases of pigs and cattle is associated with the increased demand for healthy food without excessive use of antibiotics. The use of antibiotics as growth stimulators has led to changes in the animal intestinal microflora and allowed the emergence of resistant strains of *Clostridium perfringens*, *difficile* and *Escherichia coli*. Current vaccines offer only a limited number of valences and do not offer protection against Beta2 toxin of *C. perfringens*, which is the main cause of serious diarrheal diseases in the offspring immediately after birth. One part of the project is devoted to the development of unique polyvalent vaccines for immunization of cattle before farrowing against enteric diseases of their offspring. A wide range of antigens contained in the vaccine will permit induction of an effective protection through one or two applications of the vaccine, reducing the negative impact on farrowing and vitality of the offspring caused by stress of repeated vaccinations of females before farrowing.

Successful introduction of the vaccine to the market requires development of precise and reliable diagnostic procedures for verification and validation of its quality. For this purpose, ELISA kits and particular protocols based on engineered recombinant variants of all used antigens in the developing vaccine have been developed, allowing determination of the titer of each of the particular preventative antibodies in the serum of immunized animals. The developed ELISA protocols and kits are able to detect serum antibodies against the following recombinant proteins: adhesin K99, adhesin K88, adhesin 987P, adhesin F41, toxoid LT of *E. coli*, and *C. perfringens* toxoid alpha, toxoid beta, toxoid beta2, toxoid epsilon, and *C. difficile* toxoid A. The presented technical solution is able to determine the amount of antibodies against up to 10 factors of the pathogenicity of bacteria causing diarrheal diseases of piglets and calves, thus determining their level of protection against disease. The developed technique is currently being used as a crucial part of testing aimed to determine the effectiveness and efficacy of the 10-valent vaccine by official authorities in the Czech Republic as a part of the validation process before entering the planned market in 12 European countries.



3. Results

3.1. Binding proteins targeted to prostate cancer biomarkers

Scientific outcomes:

Publication:

Marečková L., Petroková H., Osička R., Kuchař M., Malý P. Novel binders derived from an albumin-binding domain scaffold targeting human prostate secretory protein 94 (PSP94). *Protein & Cell*, 2015, vol. 6, s. 774-779. ISSN 1674-800X.

Utility models:

0445141-BTO-N 2016 RIV CZ, Prototype of recombinant binders targeted to human PSP94 oncomarker
0445152-BTO-N 2016 RIV CZ, Prototype of recombinant binders targeted to human KLK2 oncomarker
0445153-BTO-N 2016 RIV CZ, Prototype of recombinant binders targeted to human KLK11 oncomarker

Poster presentation:

Novel binders derived from an albumin-binding domain scaffold targeting Prostate Secretory Protein-94

L. Marečková, H. Petroková, M. Kuchař, J. Černý and P. Malý
XI. Discussions in Structural Molecular Biology, Nové Hrady, ČR, 2013

Modern drugs delivery systems and recombinant vaccines, The University Centre Telč, ČR, 2014

KLK2- and KLK11- binding proteins as novel class of recombinant capture ligands useful for improved Prostate Cancer diagnostics

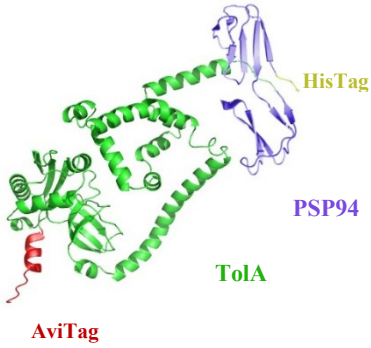
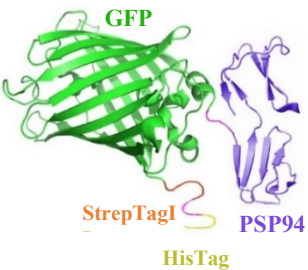


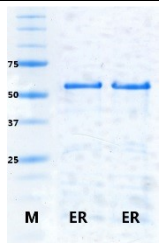
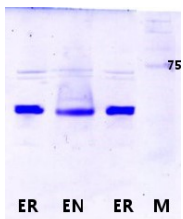
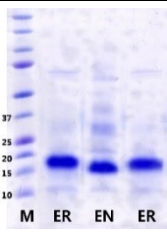
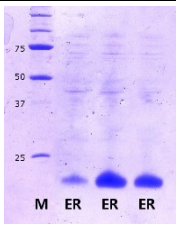
L. Marečková, H. Petroková and P. Malý
XII. Discussions in Structural Molecular Biology, Nové Hrady, ČR, 2014

3.1.1. Binders specific for human PSP94

Expression of recombinant variants of PSP94

To select binders raised against human PSP94, molecular assembly and production of PSP94 as a recombinant target molecule was performed. The secreted native PSP94 with a theoretical molecular mass of 10.7 kDa has been shown to have an apparent molecular mass of 17 kDa on SDS-PAGE [68]. Four different recombinant variants of human PSP94 were designed and produced in the soluble form: His-PSP94, Strep-PSP94, His-PSP94-TolA-Avi, and His-Strep-GFP-PSP94, comprising various purification and detection tags. A schematic overview of all the produced recombinant PSP94 variants with their structure drawings, molecular weights, purified elution fractions, and host expression cells is provided in Table 2.

Table 2. Overview of the designed recombinant PSP94 proteins. A panel scheme of the structure, expression and purification of the PSP94 proteins shown on the gels after SDS-PAGE. Drawings are based on PDB structures of human PSP94 (3IX0), GFP (4KW4), *E. coli* TolA C-terminal domain (1S62) and structure prediction of TolA sequence. M = molecular standard; ER = eluted fraction, reducing conditions; EN = eluted fraction, non-reducing conditions

His-PSP94-TolA-Avi		His-Strep-GFP-PSP94		His-PSP94		Strep-PSP94	
							
							
BL21 (DE3) BirA <i>E. coli</i>		SHuffle® T7 Express <i>E. coli</i>		ArcticExpress (DE3) <i>E. coli</i>		BL21 (DE3) <i>E. coli</i>	
Theoretical MW (KDa)	44	40		13		12	
SDS-PAGE MW (KDa)	55	40		18		17	

Selection of binders to PSP94

To select binders of the human PSP94 protein, a high-complex combinatorial library (theoretical complexity 2×10^{14} protein variants) derived from the albumin-binding domain (ABD) scaffold was used. In combination with five campaigns of ribosome display selection, a collection of PSP94-binding clones named **PAB binders** were generated. Sequence analysis of the PAB binders obtained by ribosome display revealed 29 unique sequence variants from overall 35 variants, indicating only a minimal redundancy among them (Fig. 5.A). All unique variants isolated after the final round of ribosome display selection were fused with 305 amino acid TolA spacer with C-terminal AviTag and expressed as bacterial soluble His-PAB-TolA-Avi fusion proteins (Fig. 5.B).

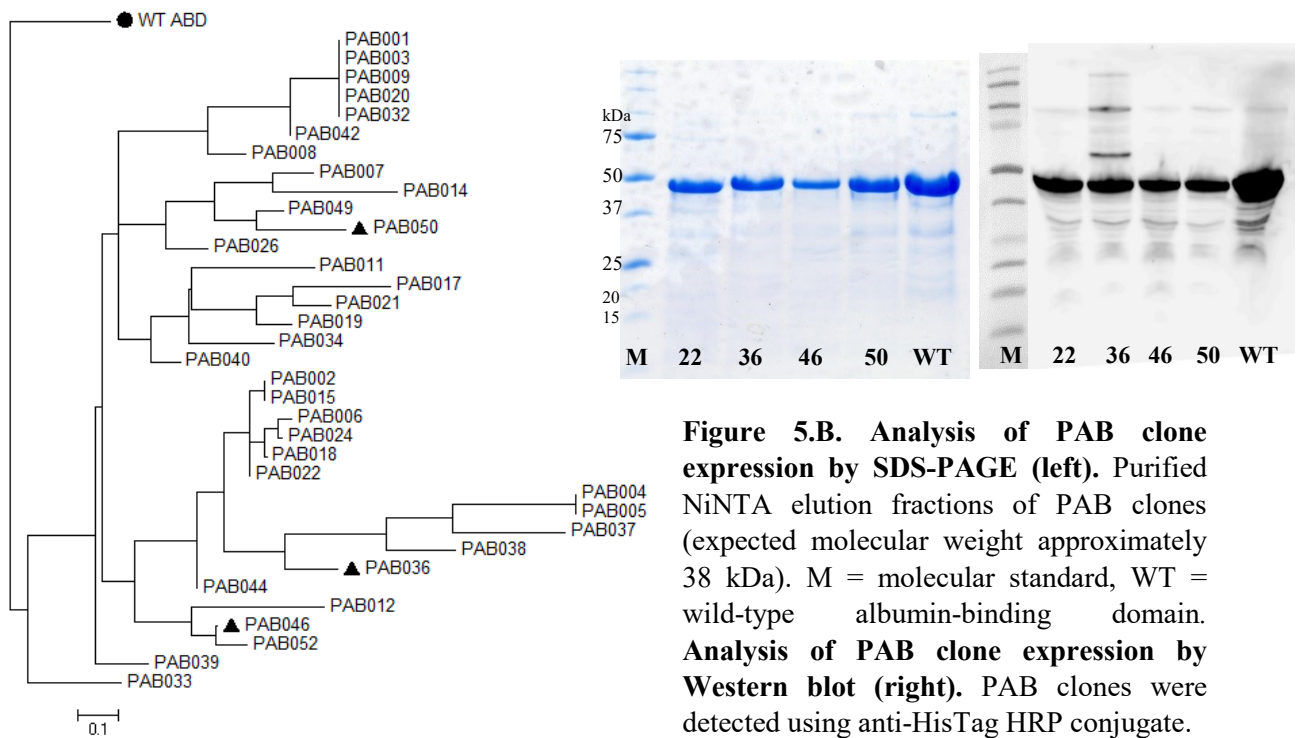


Figure 5.A. Similarity tree of polypeptide sequences of the obtained PAB binders. For similarity analysis, only the sequences between residues 20 and 46 were compared, as the N-terminal amino acid positions 1-19 were non-randomized. The sequence of non-randomized ABD-wild type (●) was used as a root of the tree. Four promising PAB variants, representing the highest affinity to PSP94, are highlighted as triangles.

Characterization of PAB binders

PAB binders were tested for the production in cell lysates of *E. coli* host cells. After verification of the binding function in ELISA in combination with Western blot analysis, several most promising candidates were selected for more detailed characterization. Purified recombinant proteins of these PAB variants confirmed the binding to the immobilized His-PSP94 and His-Strep-GFP-PSP94 bacterial proteins in ELISA using detection with streptavidin-HRP conjugate. We also verified that these selected protein variants do not substantially bind to a coated BSA protein (Fig. 6).

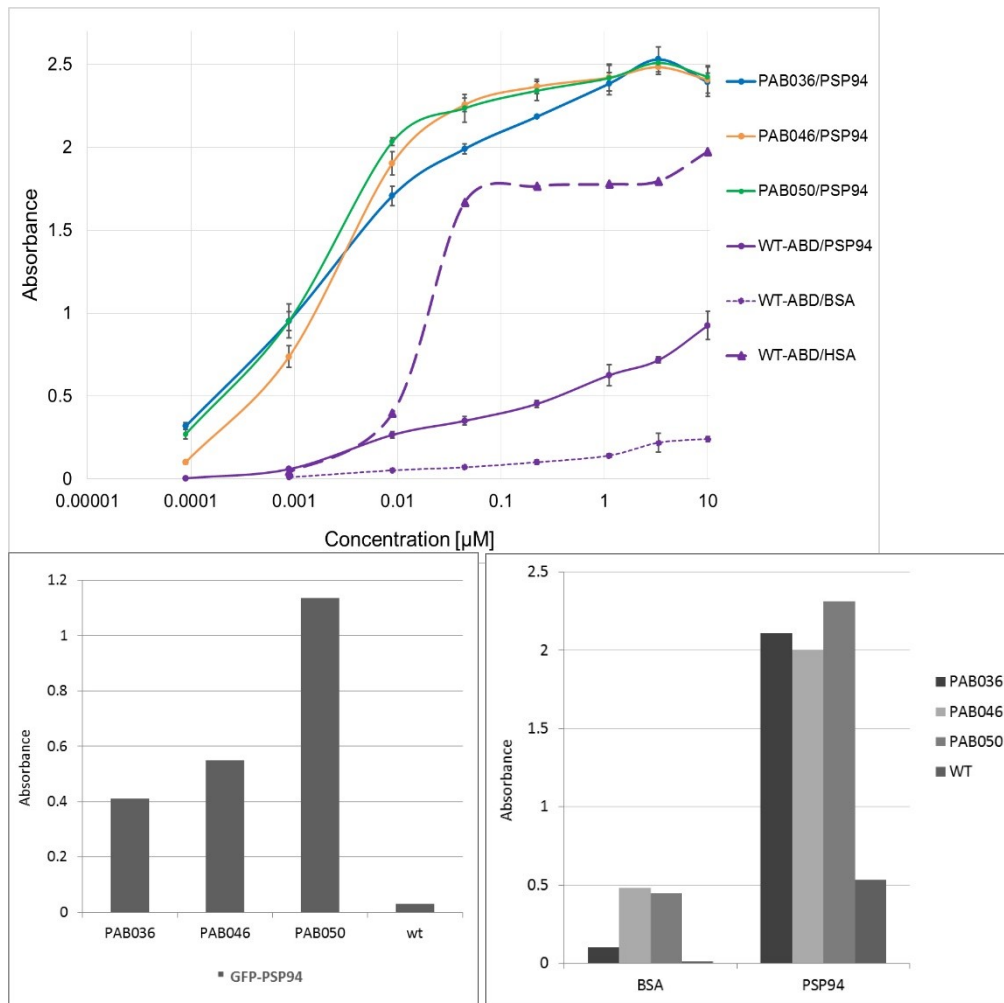


Figure 6. Soluble PAB clones bind to the recombinant PSP94 but not to the BSA control. Soluble PAB clones purified as biotinylated His-PAB-TolA-Avi fusion products were applied to a Polysorp microtiter plate coated with recombinant His-PSP94, His-Strep-GFP-PSP94, or BSA. Streptavidin HRP was used to detect the bound PAB clones. WT = wild-type ABD applied as a control.

To further verify that these PAB binders are capable of binding not only to prokaryotic products of human PSP94, but also to the native target, we used human prostate cancer LNCaP cells, which have been described to produce and secrete PSP94. It has also been shown that PSP94 is capable of binding to the surface of the LNCaP cells [63, 91, 92]. To verify this positivity, we used flow cytometry to assay the binding of two monoclonal and one polyclonal anti-PSP94 antibodies. As demonstrated in Figure 7, all three anti-PSP94 antibodies substantially bind to LNCaP cells, while the presence of only secondary Cy-5-conjugated IgGs remains to be negative. The results of binding of all three used anti-PSP94 antibodies to non-permeabilized cells are further supported by binding of these antibodies to the cells with permeabilized cell membranes, as demonstrated in Figure 7.B. In the next experiment, *in vivo* biotinylated PAB variants in the form of PAB-TolA-Avitag fusion proteins were tested by flow cytometry for the

ability to bind to the PSP94-expressing LNCaP cells. The ABD wild-type control variant, corresponding to the parental non-randomized ABD scaffold, was used as a control to exclude the possibility that non-randomized residues of the three-helical ABD bundle could mediate interactions with the prostate cancer cells. In addition, the presence of a ToIA fusion part, identical between PAB variants and the ABD wild-type control, should exclude that ABD-unrelated ToIA fusion protein moiety mediates, or substantially contributes, to the cell-surface binding. As demonstrated in Fig. 7, most of the tested PAB variants bind to non-permeabilized LNCaP cells, as detected by the streptavidin-PE conjugate as a secondary reagent. We also investigated the binding of PAB clones with permeabilized cells, and the results shown in Fig. 7 are in correlation with the intact cell staining.

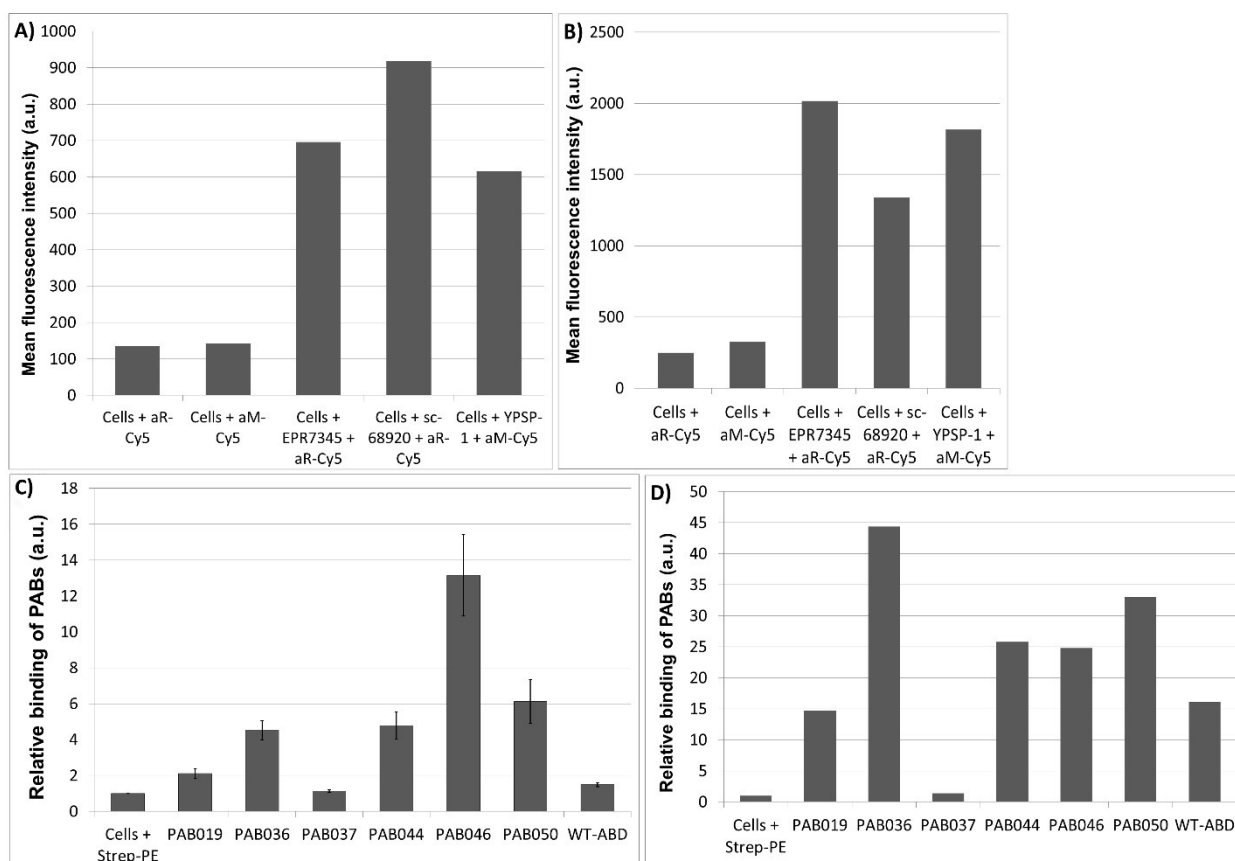


Fig. 7. Detection of PSP94 on non-permeabilized (A) and in permeabilized (B) LNCaP cells and binding of PAB clones to PSP94 on non-permeabilized (C) and in permeabilized LNCaP cells (D). Three kinds of primary antibodies against PSP94 were used for the PSP94 detection (EPR7345, sc-68920, YPSP-1). All three antibodies confirmed the presence of PSP94 both on non-permeabilized and in permeabilized LNCaP cells. Soluble PAB clones purified as biotinylated His-PAB-ToIA-Avi fusion products were added to non-permeabilized and permeabilized LNCaP cells and the binding was detected by streptavidin-PE conjugate. WT-ABD = wild-type ABD applied as a negative control.

Based on the result of this binding assay, we selected PAB036, PAB046, and PAB050 variants as the most promising candidates for further detailed characterization. The amino acid sequences of these three variants as well as the parental non-mutated wild-type ABD are presented in Table 3 with indicated positions of the randomized residues shown as grey boxes.

Table 3. Sequence similarity comparison of PAB binders. The non-randomized ABD wild-type sequence (ABD-WT) was aligned with the randomized sequenced PAB clones that were selected in ribosome display and belong to the best binders. Grey boxes indicate the 11 positions at which the residues of ABD (aa 20 to 46) were randomized. Multiple alignment was performed in ClustalW.

	20	21	22	23	24	25	26	27	28	29	30	31	32	33	34	35	36	37	38	39	40	41	42	43	44
ABD-WT	Y	Y	K	N	L	I	N	N	A	K	T	V	E	G	V	K	A	L	I	D	E	I	L	A	A
PAB036	W	Y	K	N	G	I	N	P	A	H	R	V	R	W	V	K	G	R	I	D	A	I	L	A	R
PAB046	R	Y	K	N	A	I	N	R	A	P	A	V	W	W	V	K	R	L	I	D	A	I	L	A	A
PAB050	L	Y	K	N	H	I	N	T	A	W	R	V	A	A	V	K	R	A	I	D	L	I	L	A	S

As an important proof of specificity of the PAB binders, cell-surface competition binding assays using LNCaP cells were performed. In the first experiment (Fig. 8.A), PAB binders competed with rabbit polyclonal antibody sc-68920 for binding to LNCaP cells. Cells were incubated with or without sc-68920 antibody for 15 min on ice, then PAB binders at concentration 10 µg/ml were added and left to incubate for 30 min. Binding of PAB variants was detected by a streptavidin-PE conjugate.

The data in Figure 8.A show that the dose of 4 micrograms of sc-68920 was able to suppress the binding of PAB046 and PAB050 by 30 % compared to the non-inhibited control (100 %) and this decrease was statistically significant as verified by ANOVA (indicated by asterisks). On the other hand, inhibition of PAB036 binding was only about by 15 %. WT-ABD protein was used as a negative control. In the second experiment (Fig. 8.B), PAB036, PAB046, and PAB050 variants were mixed with increasing concentrations of the recombinant PSP94 protein and left to bind to LNCaP cells for 30 minutes. The results of repeated experiments indicate that the increasing concentrations of the PSP94 protein inhibited binding of the PAB046 and PAB050 variants to the cells.

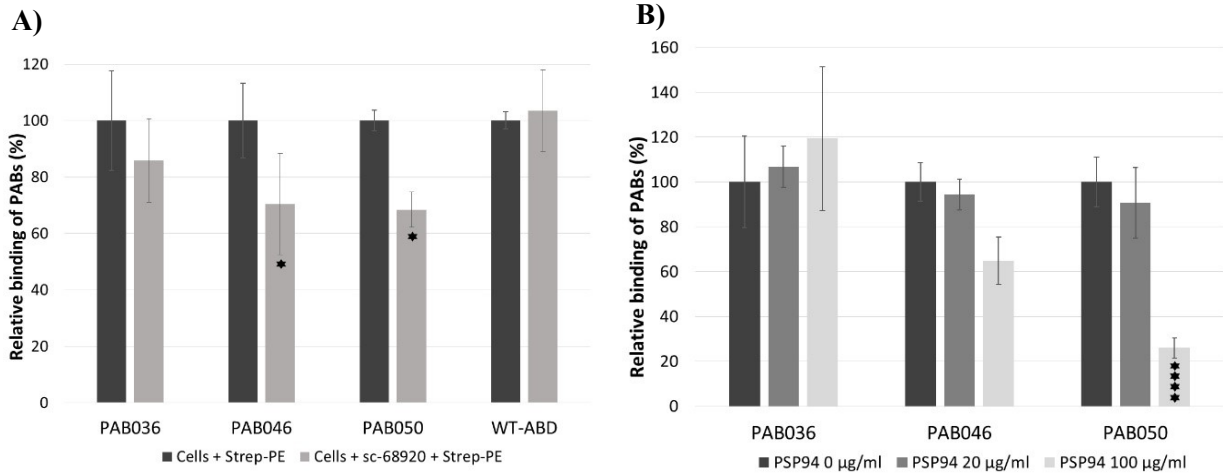


Figure 8. Competition of rabbit polyclonal antibody sc-68920 with PAB variants for binding to membrane-bound PSP94 on LNCaP cells (A). Competition of recombinant His-PSP94 with PSP94 on LNCaP cells for binding to PAB clones (B). The *in vivo* biotinylated PAB-TolA-Avi variants were detected by a streptavidin-PE conjugate. The fluorescent intensities of the PAB clones bound to LNCaP cells in the absence of recombinant PSP94 were taken as 100 % and the averaged values of the three experiments are shown with standard deviations. In all binding experiments, results are expressed as the arithmetic mean \pm standard deviation of the mean. Statistical analysis was done using one-way ANOVA followed by Dunnett's post-test, comparing all the samples with the control. GraphPad Prism 6.0 (GraphPad Software) was used to perform statistical analysis. Significant differences are indicated by asterisks (*, $P < 0.05$; **, $P < 0.01$; ***, $P < 0.001$; ****, $P < 0.0001$).

To estimate the binding affinity of the PAB variants to PSP94 in solution using microscale thermophoresis, we used a fluorescently-labelled HisTag-PSP94 protein and measured the interactions of the PAB036, PAB046, and PAB050 variants. Figure 9 shows the binding curves obtained for all selected PAB variants, representing one of the performed experiments. Using commercial software, K_d constants measured for all the three PAB variants were estimated to be 40 ± 6 nM and 72 ± 25 for PAB036, 49 ± 10 nM for PAB046, and 10 ± 3 , 12 ± 3 and 21 ± 8 nM for PAB050.

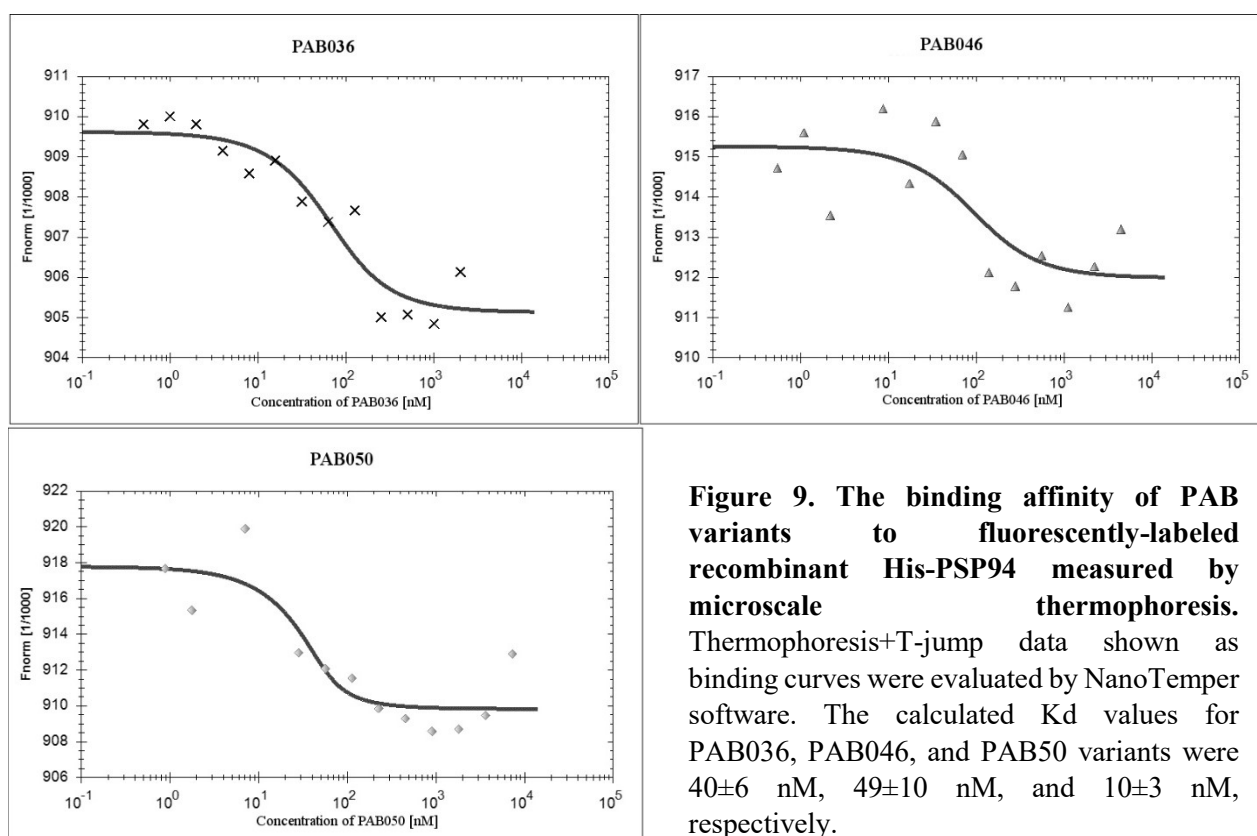


Figure 9. The binding affinity of PAB variants to fluorescently-labeled recombinant His-PSP94 measured by microscale thermophoresis. Thermophoresis+T-jump data shown as binding curves were evaluated by NanoTemper software. The calculated K_d values for PAB036, PAB046, and PAB050 variants were 40 ± 6 nM, 49 ± 10 nM, and 10 ± 3 nM, respectively.

To verify whether randomization of the ABD scaffold does not significantly decrease the PAB binders' stability, the thermal stability of PAB036, PAB046, PAB050, and WT-ABD control was measured using the thermal shift assay. Temperature melting points (T_m) measured in 300 mM NaCl, 50 mM Tris buffer, pH 8, were 59.6°C for PAB036, 48.5°C for PAB046, and 46.0°C for PAB050 (Fig. 10). The T_m value for the parental non-randomized wild-type ABD is 58.5°C . These data indicate that particular mutations in each of the variants can strongly affect the protein stability. While in case of the PAB036 variant the amino acid alterations slightly improved the original scaffold stability, the thermal stability of both PAB046 and PAB050 was significantly decreased.

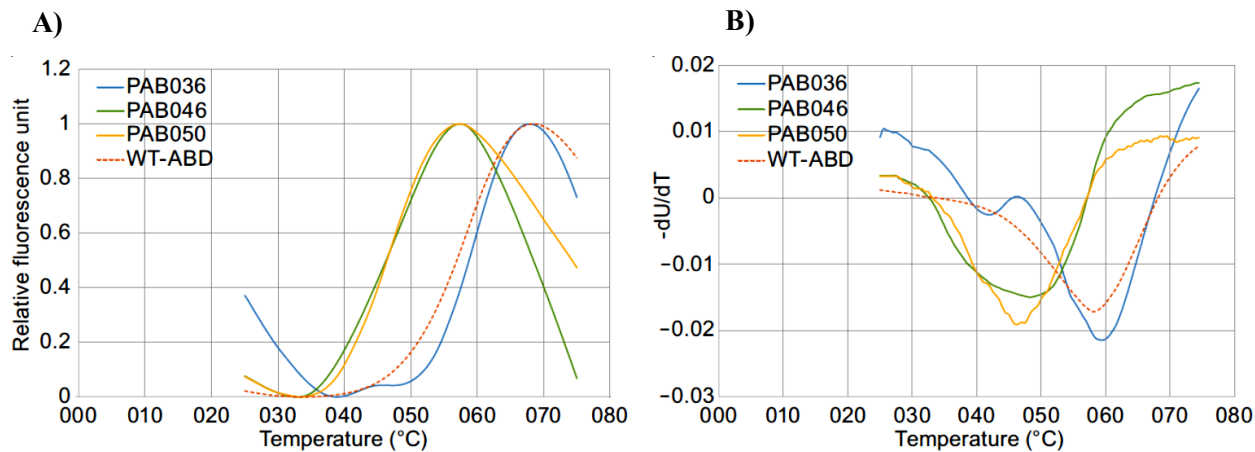


Figure 10. Thermal melting fluorescence curves of PAB binders and ABD wild-type control (A). First derivative of fluorescence versus temperature curves shown in panel (B). The melting point is given as the lowest point of the curve. All measurements were done in duplicate (PAB046) or in triplicates (PAB036, PAB050, WT-ABD) and averaged.

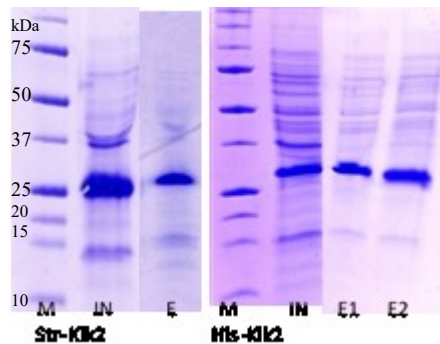
3.1.2. Binders of human kallikrein 2 and kallikrein 11

Production of recombinant KLK2 and KLK11

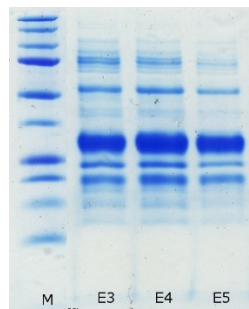
For selection of binders of human KLK2 and KLK11 and their following characterization, two different recombinant variants of KLK2 and one recombinant variant of KLK11 were designed and produced: His-KLK2, Strep-KLK2, and His-KLK11, composed of His or StrepII purification and detection tags at their N-terminus. Recombinant KLK2 and KLK11, both trypsin-like proteases, were produced without the inhibition pro-sequence. Different expression conditions (growth at 37°C, 30°C, 16°C, and 13°C) and different *E. coli* expression strains (Shuffle, Arctic Express, BL21 (DE3)) were tested (data not shown). Recombinant KLK2 was produced in *E. coli* BL21 (DE3) in the form of insoluble inclusion bodies. After refolding and purification (Fig. 11), their enzymatic activity was tested using cleavage of a chromogenic substrate (Fig. 12). As the substrate was gradually cleaved over time, we could assume that at least a part of the product was properly folded into the active form. Recombinant KLK11 was produced in the soluble form in the Shuffle strain within 16°C and purified using NiNTA affinity chromatography (Fig. 11).

SDS-PAGE

KLK2

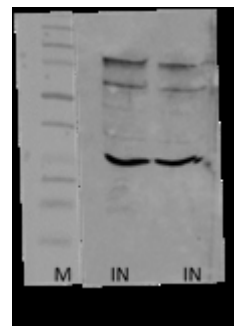


KLK11



Western blot

KLK2



KLK11

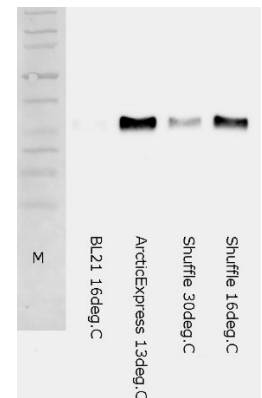


Figure 11. Analysis of KLK2 expression by SDS-PAGE (left) and Western blot (right). Recombinant KLK2 variants were detected using specific anti-KLK2 antibody (AP16632PU-N) and recombinant KLK11 was detected using anti-HisTag HRP conjugate. M = molecular standard; IN = inclusion bodies; E = purified elution fractions from affinity chromatography.

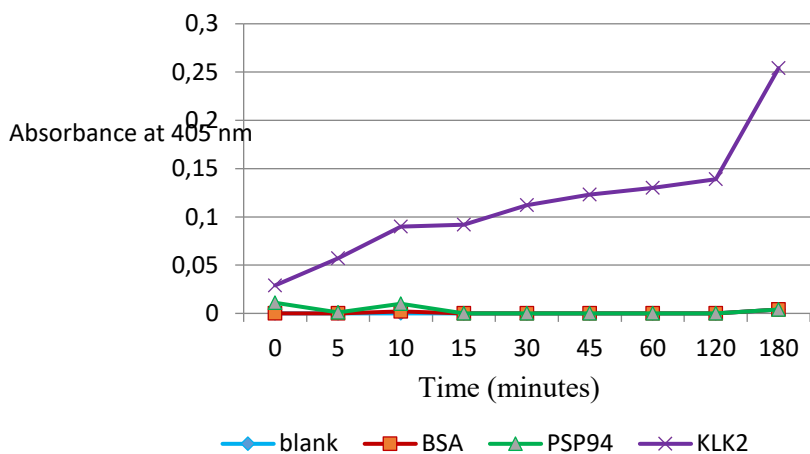


Figure 12. Cleavage of the chromogenic substrate. The process of the cleavage of N-Benzoyl-Pro-Phe-Arg-*p*-nitroanilide hydrochloride substrate by KLK2 and control proteins BSA and PSP94.

Selection of binders to KLK2 and KLK11

To select specific binders, a high-complex combinatorial library derived from the ABD scaffold was used in combination with five campaigns of the ribosome display selection technique. Two DNA collections of novel binders targeting KLK2 (**KLA binders**) and KLK11 (**HIP binders**) were inserted into the pET28b vector to produce the particular DNA libraries (Fig. 13). The sequence analysis revealed 16 unique KLA variants and 22 unique HIP variants, forming several separate clusters of clones relative to each other. The high sequence redundancy, evident especially among KLA binders, suggests a preference of these sequence in RD. All unique variants isolated after the final round of ribosome display selection were fused with the TolA sequence and AviTag-coding sequence using PCR, introduced into the pET28b plasmid, and expressed as bacterial soluble His-KLA(HIP)-TolA-Avi fusion products (Fig. 14).

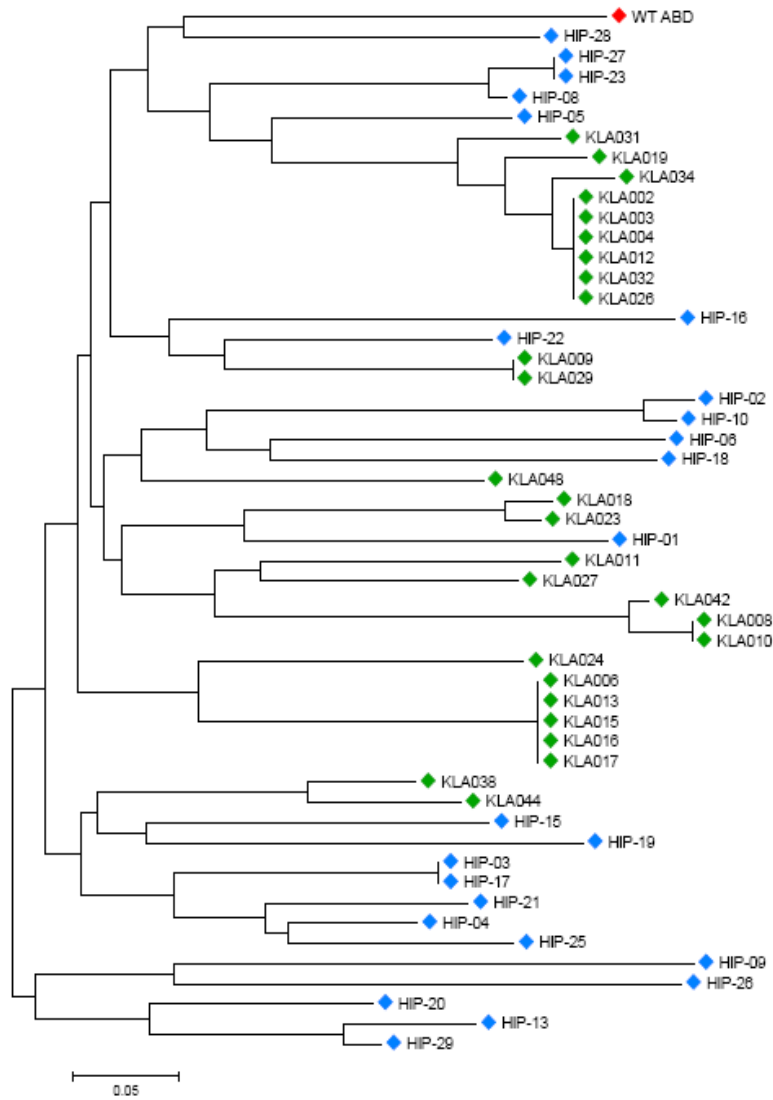


Figure 13. Similarity tree of polypeptide sequences of the obtained KLA and HIP binders. Sequence analysis of KLA binders (♦) and HIP binders (♦) obtained by ribosome display selection revealed 38 unique sequence variants. For similarity analysis, only the sequences between residues 20 and 46 were compared, as the N-terminal amino acid positions 1-19 were non-randomized. The sequence of wild-type ABD (♦) was used as a root of the tree.

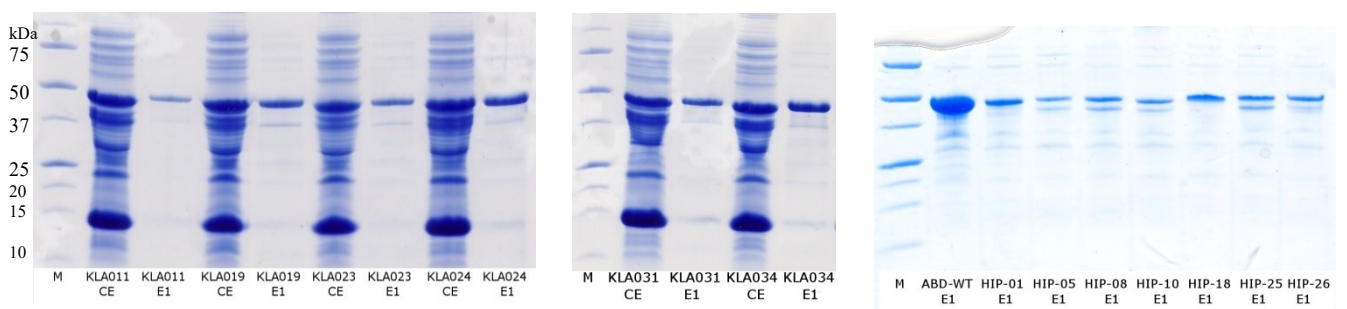


Figure 14. Analysis of purification of the selected KLA and HIP clones using SDS-PAGE. KLA and HIP clones were produced in *E. coli* BirA host strain in the form of *in vivo* biotinylated His-ABD-TolA-Avi fusion proteins and purified using Ni-NTA purification protocol. M = molecular standard, CE = non-purified cytosolic extract; E = purified eluted fractions; ABD-WT = albumin binding domain *wild type*.

Characterization of KLA and HIP binders

After verification of the binding function of crude cell lysates using ELISA in combination with Western blot analysis, several most promising candidates for more detailed characterization were selected. Purified recombinant proteins of these KLA and HIP variants (Fig. 14) were tested for their binding to recombinant KLK2 and KLK11 using ELISA. Figure 15 shows that these selected protein variants bind to their recombinant targets and do not substantially bind to a coated BSA protein.

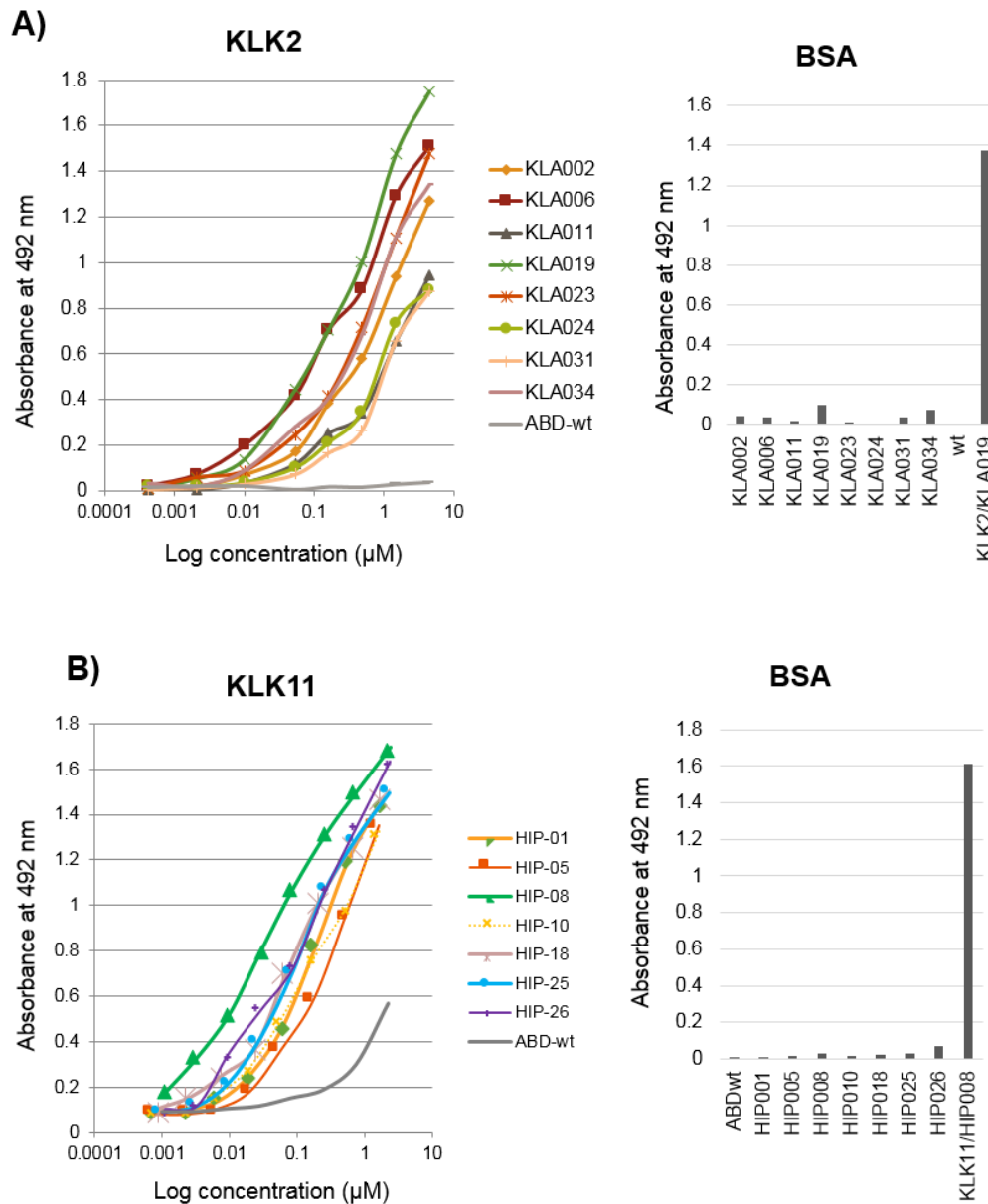


Figure 15. (A) Soluble KLA variants bind to recombinant KLK2. (B) Soluble HIP variants bind to recombinant KLK11. Purified soluble KLA (HIP) fusion proteins were applied to a Polysorp microtiter plate coated with recombinant KLK2 (KLK11) and BSA as a negative control. Streptavidin-HRP was used to detect the bound proteins. ABD-wt = parental wild-type ABD-TolA fusion protein applied as a negative control.

To determine the capability of selected binders to detect a native kallikrein product, human prostate carcinoma cell line LNCaP was selected as a suitable cell line for further flow cytometry assays, as the expression of KLK3 and KLK2 in the LNCaP cells was described in several publications [93, 94]. To confirm the presence of KLK2 and KLK3 in LNCaP cells, the primary rabbit polyclonal anti-KLK3 antibody with Cy5-conjugated secondary goat anti-rabbit antibody, and the KLK2 primary goat polyclonal antibody with FITC-conjugated secondary anti-goat antibody were used for the detection in permeabilized and non-permeabilized cells using flow cytometry (Fig. 16). Unfortunately, both permeabilized and non-permeabilized LNCaP cells were almost negative for KLK2 and KLK3 expression, thus making these cells inapplicable for further experiments.

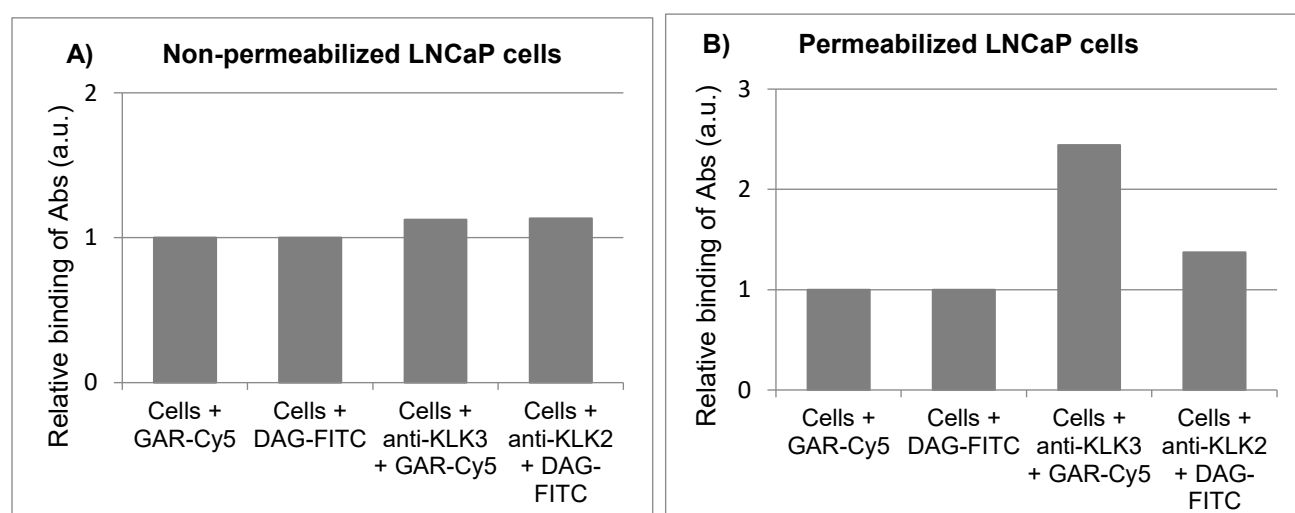


Figure 16. Detection of KLK2 and KLK3 on non-permeabilized (A) and in permeabilized (B) LNCaP cells. For the detection of KLK3 and KLK2, primary polyclonal rabbit anti-KLK3 antibody with Cy5-conjugated secondary goat anti-rabbit antibody, and KLK2 primary goat polyclonal antibody with FITC-conjugated secondary anti-goat antibody were used.

To determine how randomization of the ABD scaffold affected the overall stability of the selected clones, the thermal stability of KLA and HIP binders and WT-ABD control was measured using the thermal shift assay. Temperature melting points (T_m) of the selected KLA and HIP variants measured in three different buffers are given in Table 4. The T_m value for the parental non-randomized wild-type ABD is 58.5°C measured in TRIS buffers and 58°C measured in PBS buffer. The data indicate that mutations in KLA024, HIP26 and HIP18 variants strongly affected the protein stability (a decrease of at least 10°C). The higher concentration of NaCl and the presence of 500 mM imidazole caused better thermal stability of

the majority of KLA binders, with the most obvious difference measured for the KLA034 variant. The mutations in KLA006, KLA019, KLA023, and HIP001, HIP005, HIP008, HIP010, HIP025 only slightly decreased the original scaffold stability.

Table 4. The measured melting temperatures (T_m) of KLA and HIP variants using the thermal shift assay. T_m of the KLA clones were measured in buffers: 500 mM imidazole, 300 mM NaCl, 50 mM Tris, pH 8, and 300 mM NaCl, 50 mM Tris, pH 8. T_m of the HIP clones were measured in PBS buffer, pH 7.4. Wild-type ABD is the parental non-randomized molecule with the naturally highest T_m.

Name of the KLA clone	T _m in 50 mM TRIS, 100 mM NaCl buffer, pH 8 (°C)	T _m in 50 mM TRIS, 300 mM NaCl, 500 mM imidazol buffer, pH 8 (°C)	Name of the HIP clone	T _m in PBS buffer pH 7.4 (°C)
Wild-type ABD	58.5	58.5	Wild-type ABD	58.0
KLA006	52.0	57.0	HIP001	52.5
KLA019	51.0	58.0	HIP005	54.5
KLA023	50.5	51.5	HIP008	51.0
KLA024	48.5	42.5	HIP010	53.5
KLA034	47.0	57.0	HIP018	47.5
			HIP025	52.5
			HIP026	45.0

Summary

The generation and characterization of unique protein binders of human prostate cancer biomarkers PSP94 (PAB binders), human KLK2 (KLA binders), and human KLK11 (HIP binders) was presented. For selection of the binders, different recombinant variants of target proteins were expressed and characterized. All recombinant targets except for KLK2 were produced in soluble form in the *E. coli* host. Recombinant KLK2 was produced in the form of inclusion bodies and efficiently refolded. Its natural protease activity was tested by cleavage of a chromogenic substrate. Using a combinatorial library based on the ABD scaffold in combination with RD selection, DNA collections of PAB, KLA, and HIP binders, targeting prostate cancer biomarkers, were generated and cloned into a plasmid vector for production and screening of the best binding variants. The thermal stability of the particular clones was determined by the thermal shift assay. The most promising binders were demonstrated to bind to their recombinant protein targets and not to bind to BSA control. Furthermore, PAB046 and PAB050 variants were shown to recognize the PSP94 target protein in its native conformation. Several binding and competition experiments using flow cytometry of the LNCaP prostate

cancer cell line were performed. Based on these results, PAB046 and PAB050 were selected as the most promising binders of PSP94.

With further possible modifications using gene fusion or affinity maturation approaches, the presented binders appear attractive for the development of novel multi-factorial biosensors for more precise PCa and early stage diagnosis, as an improved alternative to the currently used ELISA-based standard PSA tests.

3.2. Binding proteins targeted to surface markers of epithelial and mesenchymal cells for sorting circulating tumor cells

Scientific outcomes:

Poster presentation:

Development of high-affinity protein binders for selective detection and separation of circulating tumor cells (CTCs) by microfluidic chip technology

L. Marečková and P. Malý

12th Euro Biotechnology Congress, Alicante, Spain, 2016

Protein binders as key components of microfluidic chip for selective detection and separation of circulating tumor cells (CTCs) in blood of patients with lung adenocarcinoma

L. Marečková, M. Štofík, J. Malý, H. Petroková, P. Malý

17th FEBS Young Scientists' Forum and 42nd FEBS Congress, Jerusalem, Israel, 2017

3.2.1. Binders derived from the ABD scaffold

Expression of recombinant targets EpCAM and N-cadherin

To identify and further separate epithelial and mesenchymal circulating tumor cells (CTCs), epithelial cell adhesion molecule (**EpCAM**) and mesenchymal cell marker **N-cadherin** were chosen as primary targets for novel protein binders. EpCAM is a transmembrane glycoprotein highly expressed in epithelial cancer cells and it has been considered as a dominant cell-surface antigen suitable for CTC detection. However, the lack of EpCAM expression on some CTCs supports the idea to use N-cadherin, a marker of mesenchymal phenotype, as a second additive biomarker. For the purpose of an oriented exposure of the target molecule during the selection steps of ribosome display, two recombinant variants of extracellular domain (24-265) of EpCAM, called His-EpCAM-Avi (HEP) and EpCAM-His-Avi (EPH) were assembled and expressed. Similarly, two recombinant variants coding for two distally exposed extracellular domains of N-cadherin called His-N-cadherin-Avi (HCA) and N-cadherin-His-Avi (CAH) were designed and produced in the form of *in vivo* biotinylated proteins in *E. coli* BL21 (DE3) BirA (Fig. 17). In addition to the purification 6xHis-Tag sequence, all variants contained the C-terminal AviTag sequence consensus as a target for biotin-ligase, ensuring proper orientation of *in vivo* biotinylated proteins immobilized via coated streptavidin in the well of the microtiter plate. For further biophysical and biochemical characterization of the binders, recombinant N-cadherin variant lacking the C-terminal AviTag (CAD) sequence was also constructed and expressed in *E. coli* BL21 (DE3) (Fig. 17). As both cell-surface markers are naturally glycosylated, commercial products of eukaryotic cells were used for testing the binding properties of the selected binders. All used variants of recombinant targets are shown in Table 5.

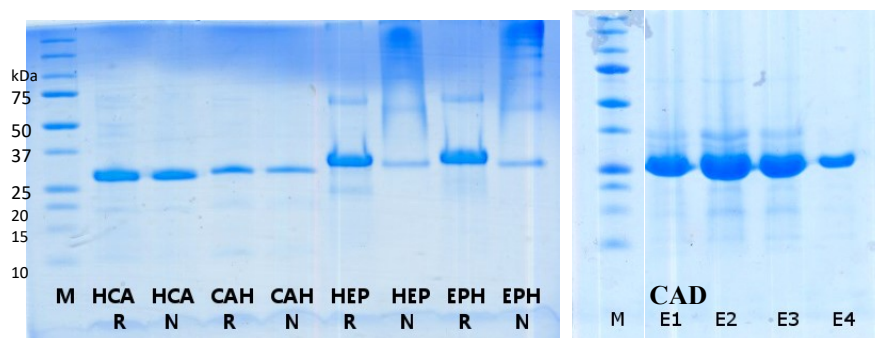




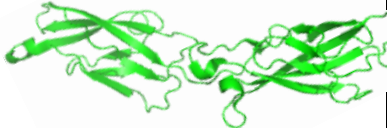






Figure 17. Analysis of the purification of recombinant EpCAM and N-cadherin using SDS-PAGE. M = molecular standard; E = purified elution fractions from affinity chromatography; R = eluted fraction, reducing conditions; N = eluted fraction, non-reducing conditions

Table 5. Scheme of the used recombinant protein variants of EpCAM and N-cadherin. Drawings of structures are based on PDB structures of human EpCAM (4MZV) and N-cadherin (5SZN).

Target	Structure	Recombinant variants – sequence scheme	Name
EpCAM	 <p>Extracellular domain</p>	  	<p>HEP</p> <p>EPH</p> <p>Commercial glycosylated product</p>
N-cadherin	 <p>Two out of five extracellular domains</p>	   	<p>HCA</p> <p>CAH</p> <p>CAD</p> <p>Commercial glycosylated complete extracellular moiety</p>

Selection of binders to EpCAM and N-cadherin

Using a series of ELISA binding assays, the binding conditions for both target proteins were optimized. The obtained parameters were subsequently used to optimize the established ribosomal display protocol. For selection of the binding molecules, a Medisorp microtiter plate was coated with recombinant EPH and CAH via streptavidin. In parallel, the plate was directly coated with both commercial glycosylated variants as an alternative. An irrelevant biotinylated protein containing HisTag or AviTag, respectively, bound via streptavidin or BSA was used for pre-selection. For RD selection, a DNA library derived from the ABD scaffold was used. Five rounds of RD were performed, and the final libraries were cloned into a vector for selection of particular clones named **EBA binders** (targeting EpCAM) and **CAB binders** (targeting N-cadherin). The plasmid DNA from the selected clones was sequenced and analyzed. Of the collection of EBA clones, 35 variants were sequentially correct, of which 22 had a unique

sequence (Fig. 18.A). Of the collection of CAB clones, 26 unique variants were identified (Fig. 18.B).

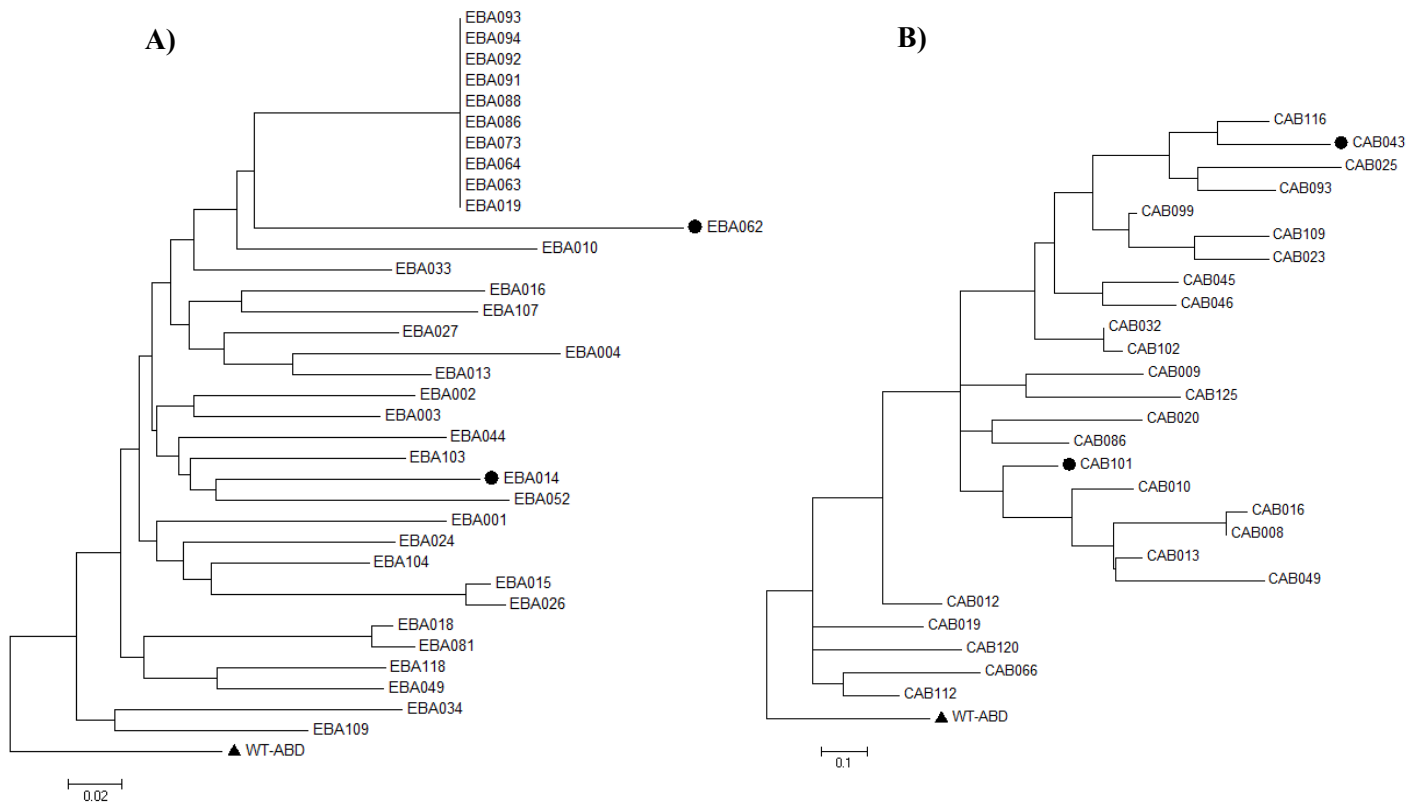


Figure 18. Comparison of sequence similarity of EBA variants (A) and CAB variants (B). The most promising variants EBA062, EBA014, CAB043, and CAB101, selected for further characterization, are marked with a black dot. The sequence of wild-type ABD (marked with a triangle) was used as a root of the tree. The analyses were conducted in MEGA7.

DNA of all unique variants was fused with the C-terminal sequence coding for TolA-AviTag protein and produced as *in vivo* biotinylated proteins in BL21 (DE3) BirA *E. coli* host cells. The diluted cell lysates were tested for the binding to recombinant EpCAM using ELISA. The EBA014 and EBA062 variants significantly bound to EpCAM and did not substantially bind to BSA and N-cadherin controls. Contrary to that, CAB043 and CAB101 variants bound to N-cadherin, with only negligible binding to BSA and EpCAM controls (Fig. 20). All these most promising binding proteins were purified (Fig. 19) and further characterized.

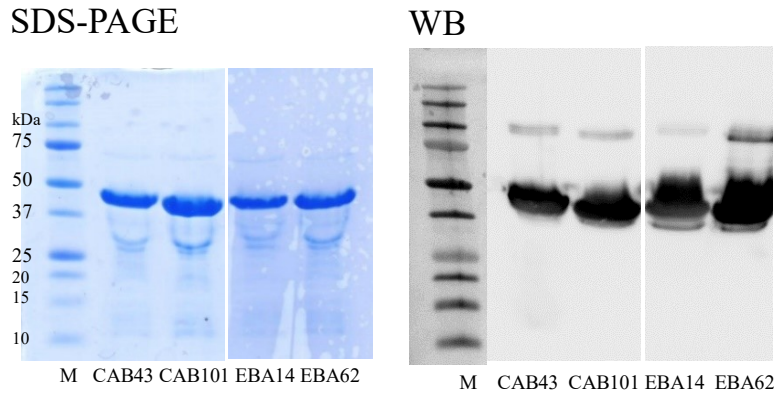


Figure 19. Expression of selected CAB and EBA binders analyzed by SDS-PAGE (left) and by Western blot (right). CAB and EBA clones were expressed and purified as *in vivo* biotinylated products and detected using a streptavidin-HRP conjugate. M = molecular standard.

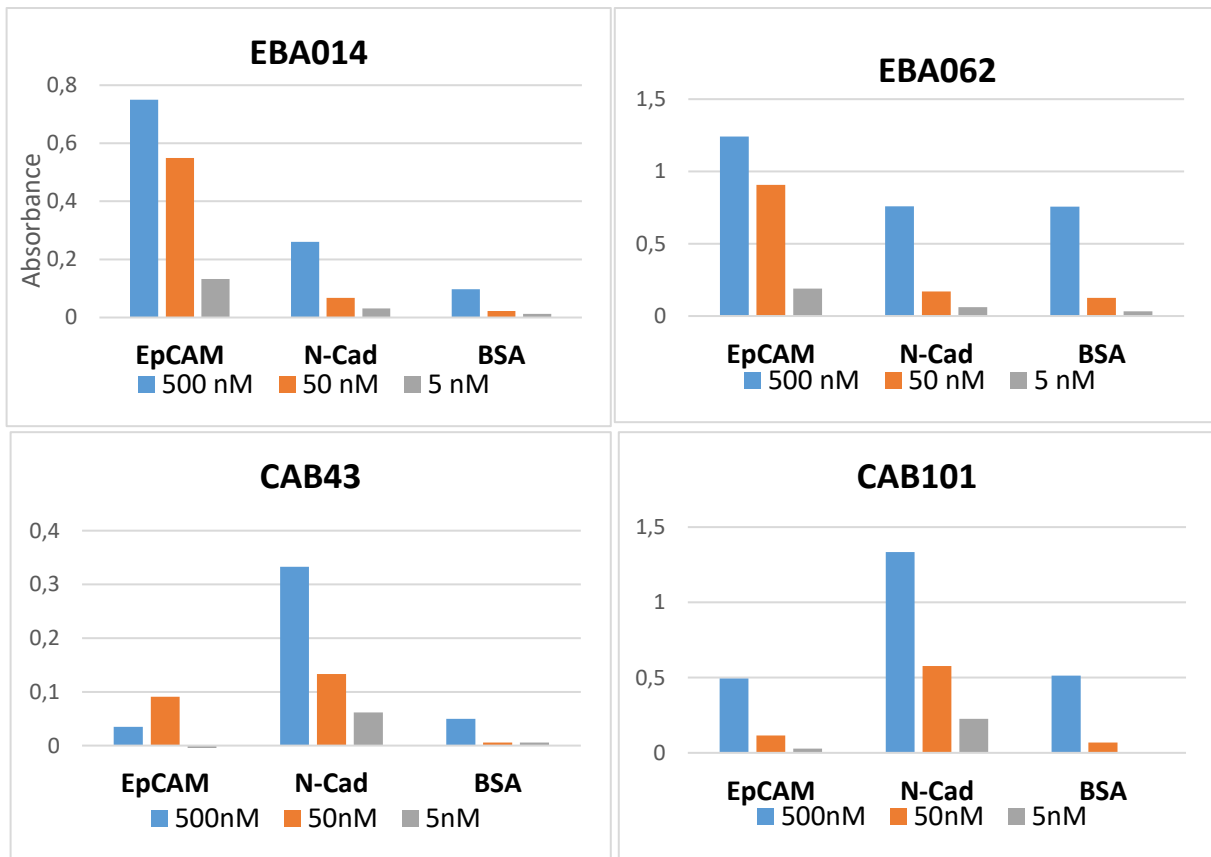


Figure 20. EBA and CAB variants bind to recombinant EpCAM and N-cadherin, respectively. Soluble EBA or CAB clones produced as *in vivo* biotinylated proteins were tested on a Medisorp microtiter plate coated with recombinant EpCAM, N-cadherin, and BSA. Streptavidin-HRP was used to detect the bound clones.

Because the EBA and CAB binders are supposed to be oriented on the surface of the chip in a way allowing capture of cells expressing EpCAM and N-cadherin, the reverse ELISA arrangement was performed, where EBA014, EBA062, CAB043, and CAB101 were bound via streptavidin on the surface of the microtiter plate. Bound EpCAM or N-cadherin were then detected using specific antibodies and secondary reagents (Fig. 21).

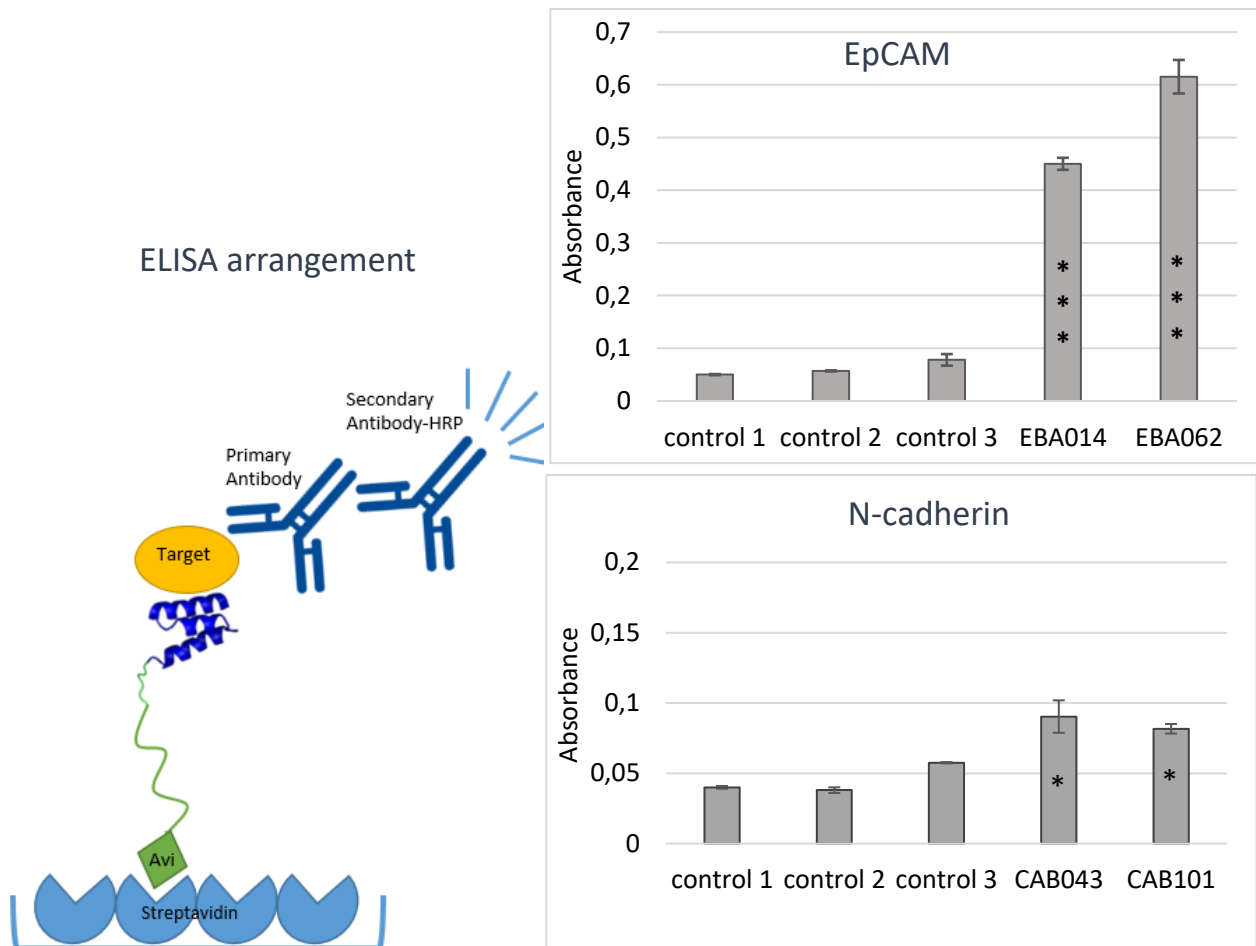


Figure 21. Scheme of the sandwich ELISA (left). Binding of recombinant EpCAM and N-cadherin to immobilized EBA and CAB binders, respectively (right). Purified *in vivo* biotinylated EBA or CAB clones were immobilized via streptavidin on the microtiter plate. Bound EpCAM or N-cadherin were detected using the particular antibodies. The averaged values of the experiment performed in triplicates are shown with standard deviations. Statistical analysis was done using one-way ANOVA. Significant differences are indicated by asterisks (*, $P < 0.05$; **, $P < 0.01$; ***, $P < 0.001$).

To verify the suitability of EBA and CAB binders to capture the cells, we decided to test their binding to living cells in real-time regime using a LigandTracer Green Line instrument suitable for monitoring the interactions of labeled proteins with living cells. First, five human cell lines, MCF-7, DU-145, CCD1070Sk, HEK293T, and PC-3, were analyzed for EpCAM and N-cadherin expression using flow cytometry (Fig. 22).

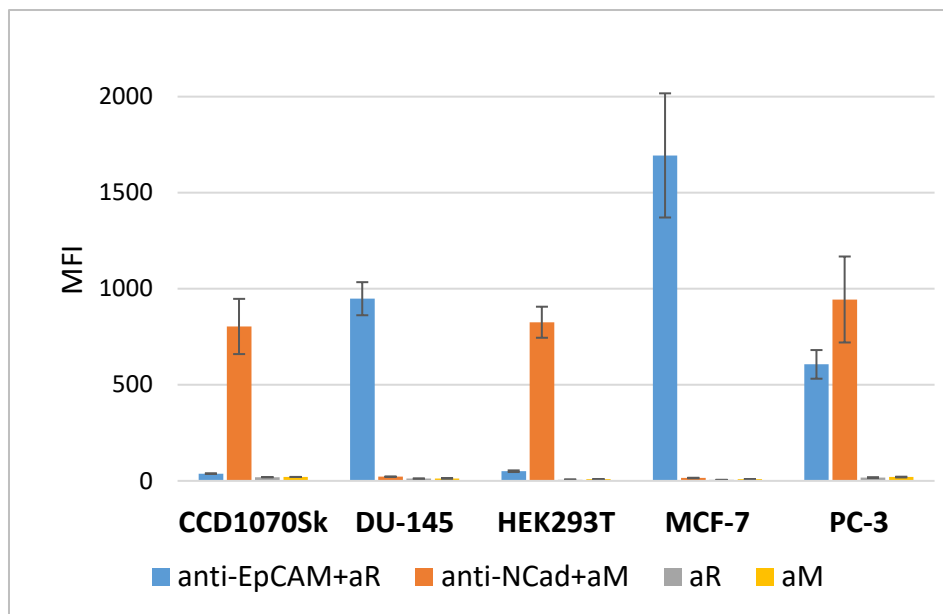


Figure 22. Detection of cell-surface expression of EpCAM and N-cadherin in human cell lines using flow cytometry. Five human cell lines, MCF-7, DU-145, CCD1070Sk, HEK293T, and PC-3, were analyzed for the expression of EpCAM and N-cadherin membrane markers using flow cytometry. Rabbit polyclonal anti-EpCAM (anti-EpCAM) and mouse monoclonal anti-N-cadherin (anti-NCad) were used as primary antibodies, anti-Rabbit AlexaFluor 647nm (aR) and anti-Mouse AlexaFluor 647nm (aM) were used as secondary antibodies. The averaged values of the two experiments performed in triplicates and duplicates are shown with standard deviations.

Of the all tested cell lines, MCF-7 as the EpCAM positive/N-cadherin negative, and CCD1070Sk as the EpCAM negative/N-cadherin positive cell lines were chosen as models for the LigandTracer binding experiment. On the cell dish, divided into the three zones, approximately one million of MCF-7 and CCD1070Sk cells were seeded. The last zone remained empty for measuring the protein binding to the plastic background (Fig. 23). The fluorescently labeled binders were then gradually added after defined time intervals to the culture medium and the change in fluorescence was observed.

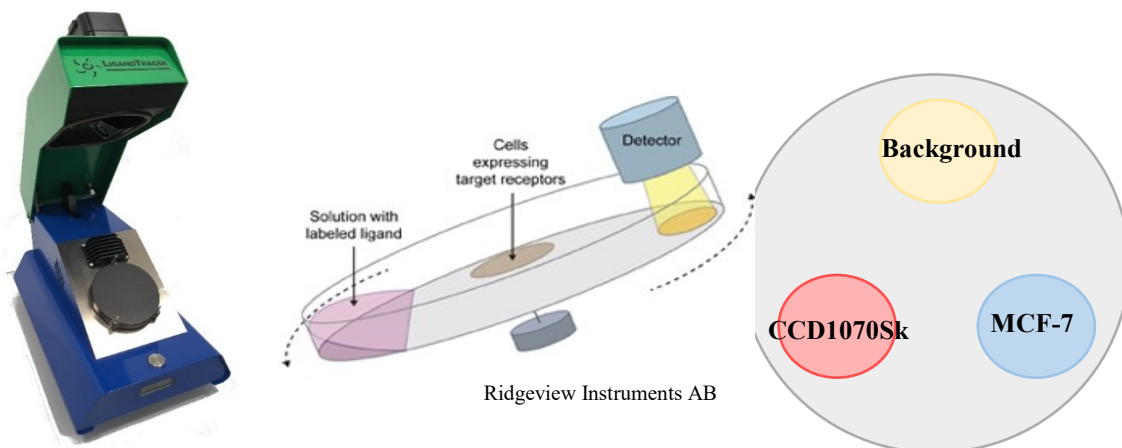
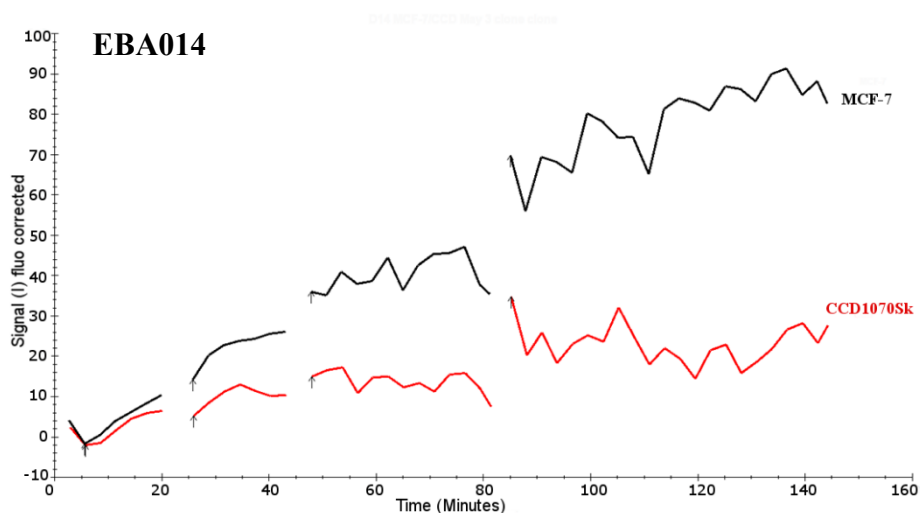


Figure 23. Ligand Tracer Green line. The instrument is suitable for monitoring the interaction of the ligand with cell-surface receptors on living cells in the real-time mode. It allows determination of on- and off-rate kinetics as well as binding affinity. The technology is based on repeated differential measurements of surface-associated proteins. Cells are seeded in a local part of the cell dish and one side is used as a reference. The dish is placed on an inclined, slowly rotating support and a liquid containing the labeled protein is added. The detector, which is mounted over the upper part, registers the additional activity of the proteins bound to the cells.

The values were obtained by LigandTracer Green Line with an APC-compatible detector and analyzed using Trace Drawer 1.8 software (Fig. 24). The binding curves show that EBA014 and EBA062 bind to EpCAM-positive cells but not to EpCAM-negative cells, thus demonstrating the required cell selectivity. In case of the CAB101 binder, attachment to N-cadherin-positive cells was specific only in higher concentrations (90 nM) of the protein. The estimated KD values are 56 nM for EBA014, 215 nM for EBA062, and ~ 500 nM for CAB101. The binding kinetics for the CAB043 binder variant was not measured due to the precipitation of the tested protein in the medium during the measurement.



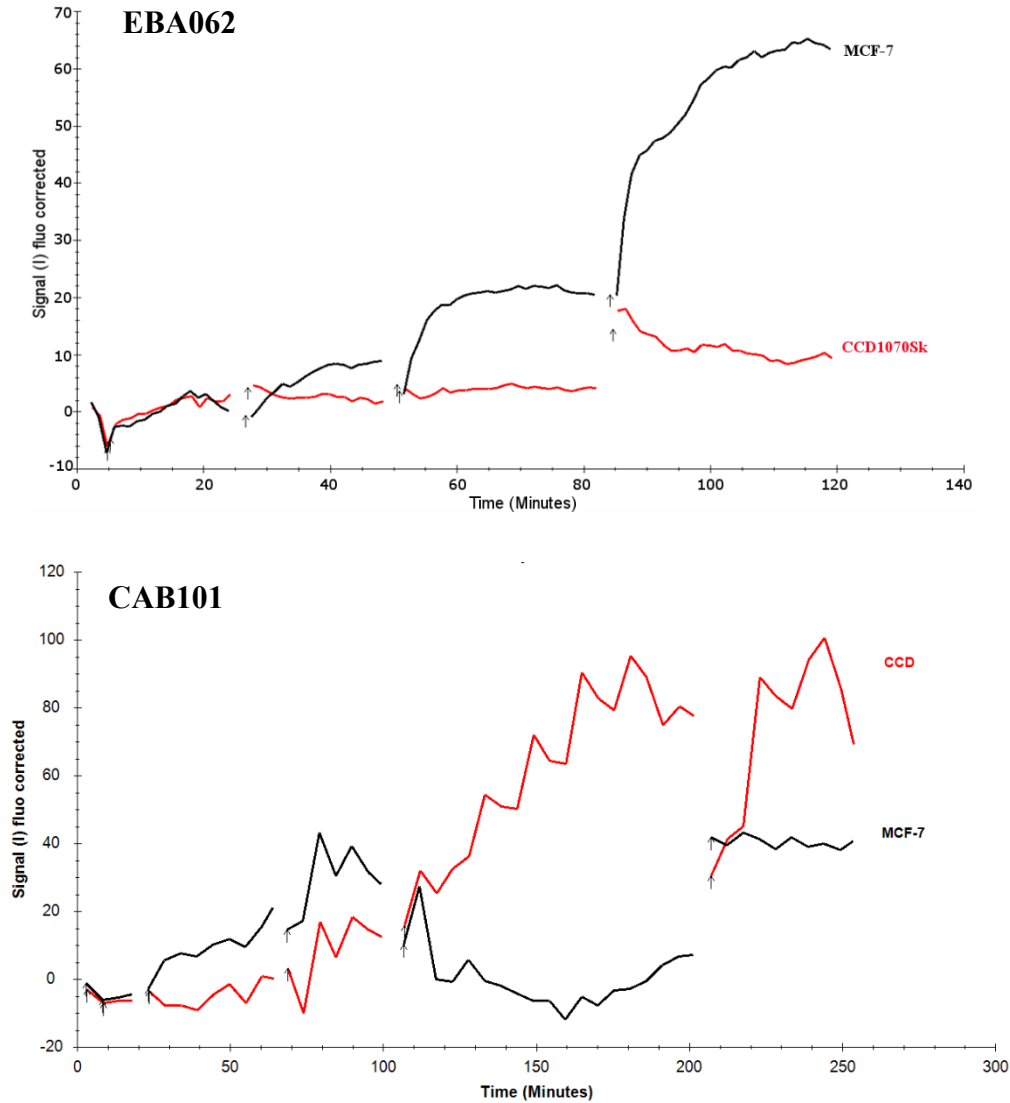


Figure 24. Binding of EBA014, EBA062, and CAB101 to MCF-7 and CCD1070Sk cells as tested by LigandTracer Green Line in the real-time mode. MCF-7 as a model of EpCAM-expressing cell line and CCD1070Sk as a model of N-cadherin-expressing cell line were selected for the binding experiment. *In vivo* biotinylated variants EBA014, EBA062, CAB043, and CAB101 were labeled using a streptavidin-APC conjugate and diluted to the final concentration of 10 nM, 30 nM, and 90 nM in the culture medium. Two separate cell populations of MCF-7 and CCD1070Sk cells were seeded into the same circular plastic dish. Each fluorescently labeled ligand was incubated with the two cell populations simultaneously. The values were obtained by LigandTracer Green Line with an APC-compatible detector and analyzed using Trace Drawer 1.8 (Ridgeview Instruments AB).

Affinity maturation of the EBA014 binder

To increase the binding affinity of the most promising variant EBA014, error-prone PCR was performed as an affinity-maturation approach for the selection of 2nd-generation binders. Primers for mutagenesis were designed to incorporate mutations only within the originally randomized region of the ABD scaffold (amino acids 20-44), corresponding to the 75bp long DNA fragment. The conditions for error-prone PCR were optimized according to the GeneMorph II Random Mutagenesis Kit protocol. The DNA library was cloned into the pET28b vector and the efficiency of the mutagenesis was tested by sequencing, followed by subsequent analysis of the mutations of in the particular variants (Table 6).

Table 6. Analysis of mutations of new EBA014 variants after error-prone PCR. Amino acids 1-46 of ABD are displayed. EBA014-WT is the sequence of the original EBA014 variant. ABD-WT is the sequence of the parental non-mutated variant.

Name	Amino acid sequence
ABD-WT	LAEAKVLANRELDKYGVSDYYKNLINNAKTVEGVKALIDEILAAALP
EBA014-WT	LAEAKVLANRELDKYGVSDDYKNQINAAATVTGVNIEIDRILARLP
EBA014-1	LAEAKVLANRELDKYGVSDDCKNQINAAATVTGVNIEIDRILARLP
EBA014-4	LAEAKVLANRELDKYGVSDDNKNQINAAATVTGVNIEIDRILARLP
EBA014-5	LAEAKVLANRELDKYGVSDDYKNQINAAATVTGNGNIEIDRILARLP
EBA014- 8	LAEAKVLANRELDKYGVSDDYKNWINAAATVTGVNIEIDRILARLP
EBA014-9	LAEAKVLANRELDKYGVSDDYKNQINATATVTDVNIIDRILARLP
EBA014-10	LAEAKVLANRELDKYGVSDDYKNQINAAATVTGVNIEIDRILAQLP
EBA014-16	LAEAKVLANRELDKYGVSDDYKNQINAAATVTGVNIEIDRILVRLP
EBA014-18	LAEAKVLANRELDKYGVSDDYKNQINAAATVTGVNIEIDRISARLP
EBA014-22	LAEAKVLANRELDKYGVSDDYKNQINAAATVTGVNIEIDRILARLP
EBA014-27	LAEAKVLANRELDKYGVSDDYKNQINAAATVTGVNIEIDRIARLP
EBA014-29	LAEAKVLANRELDKYGVSDDYKNQINAAATVTGVNTEIVRILARLP

.. original randomized region . new mutations

The analyzed sequences of 30 clones revealed 11 unique EBA014 variants containing 1-2 amino acid alterations in the mutated scaffold region, suggesting that optimized conditions for error-prone PCR were found. This 2nd-generation plasmid library is ready for further large-scale screening of novel EBA014 variants with an improved binding affinity and required cell selectivity.

3.2.2. Binders derived from the Myomedin scaffold

Development of the new Myomedin scaffold and generation of a new combinatorial library

The three-helix bundle ABD scaffold has already been successfully used for generation of several types of protein binders raised against a portfolio of protein structures with sub- to nanomolar affinity range, with the required specificity or arranged neutralization activity. However, the flat randomized surface between helices 2 and 3 may, in some cases, limit identification of the best mimicking candidates of the surface (glyco)peptide epitopes recognized by broadly neutralizing antibodies. In addition, some ABD-derived binders still retain a residual affinity to serum albumins, yet weakened by several orders of magnitude by scaffold randomization, which might complicate their diagnostic use for detection of low-level cytokine targets or body fluid oncomarkers. Therefore, another model of a protein domain scaffold based on randomized loops or β -sheets can bring a valuable structural alternative for the development of high-affinity protein binders by directed evolution from combinatorial libraries. To reach this goal, we selected the human myomesin domain as a model for alternative scaffold development. This scaffold, called **Myomedin**, could generate protein binders with improved thermal stability, suppressed serum albumin cross-reactivity, and produce a higher combinatorial complexity over the ABD scaffold-derived library. The structure of the Myomedin scaffold is based on the immunoglobulin type II domain of human myomesin, one of the major components of the M band in the sarcomere. Myomesin is a long molecule sometimes called “a spring with beads” because of its repetitive domain composition (Fig. 25).

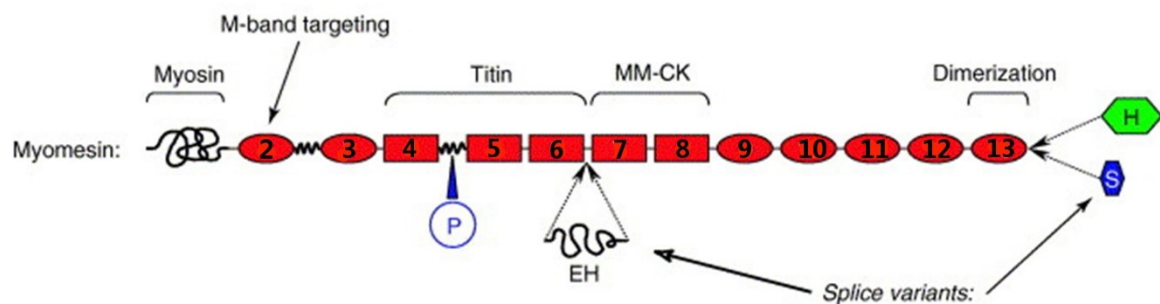


Figure 25. Scheme of human myomesin. Myomesin is composed of a unique head domain, responsible for binding to myosin, followed by 12 repetitive structural modules with homology to fibronectin type III (rectangles) or immunoglobulin type II domains (ellipses). Some domains are responsible for binding to a variety of proteins; C-terminal domain 13 is responsible for antiparallel dimerization of two myomesin molecules (the figure was modified according to [95]).

To generate a new combinatorial library, one myomesin domain was selected and biophysically characterized. The nucleotide sequence of the wild-type domain (Myo-wt) was optimized for expression in the *E. coli* host (GeneArt) and cloned into the pET vector to contain HisTag at its N-terminus. This construct has an MW of 15 kDa, the appropriate size for a small binding protein scaffold. Myo-wt was expressed in the *E. coli* BL21 (DE3) host strain as a soluble form in the cytoplasm. The soluble protein was purified using NiNTA affinity chromatography and the elution were further purified using gel size-exclusion chromatography. Both size exclusion chromatography and SDS-PAGE analysis revealed monodispersity of the protein (Fig. 26).

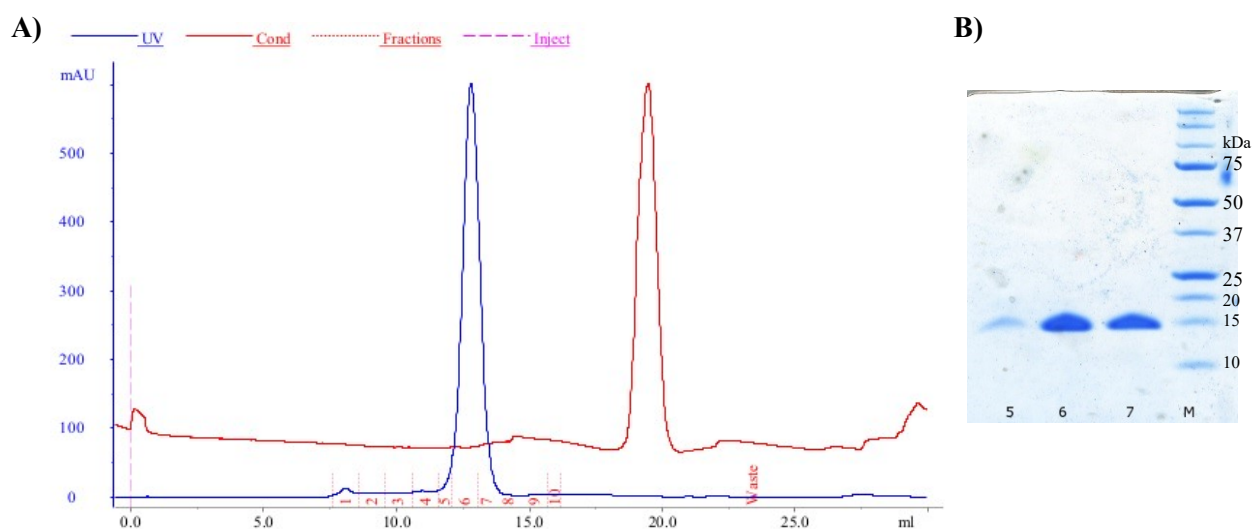


Figure 26. Elution profile of Myo-wt from size-exclusion chromatography (A). SDS-PAGE analysis of purified Myo-wt (B). The elution volume corresponds to a molecular weight of 15 kDa, as expected for the monomeric Myo-wt. M = molecular standard.

The thermal stability of Myo-wt was tested using the thermal shift assay (Fig. 27.). The measured temperature melting point of 72°C indicates high stability of the wild-type molecule. This T_m is much higher than the T_m of 58°C of wild-type ABD. The characterization of Myo-wt was completed by crystallization of the protein and refining its structure (data not shown).

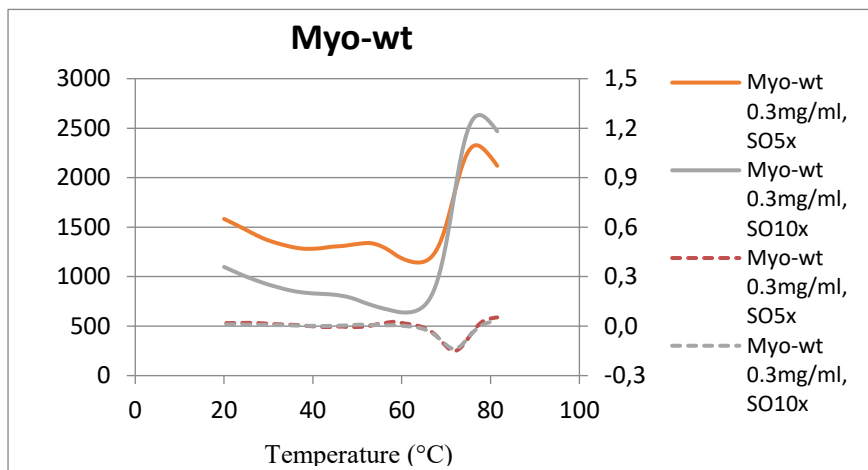


Figure 27. Thermal melting fluorescence curves of Myo-wt. The first derivative of fluorescence versus temperature curves is shown as a dashed line. The melting point is given as the lowest point of the curve. The estimated $T_m = 72^\circ\text{C}$. SO = sypro orange stain solution.

The *in silico* modeling of a new library proposed two different strategical approaches (Fig. 28). In the first one, amino acid residues of three different loops are randomized, while in the second case, residues of anti-parallel beta sheets were selected for the randomization.

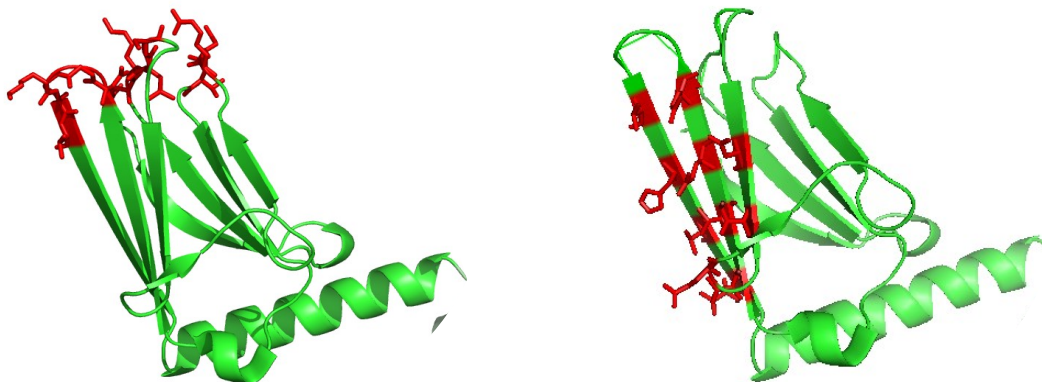


Figure 28. The structure scheme of the two proposed strategical approaches to Myomedin randomization. Drawings of structures are based on PDB structure 3RBS. The randomized amino acids are displayed as sticks in red. In the first model (left), loops are randomized, and in the second model (right), beta sheets were selected for the randomization.

According to the model, sequences with randomized oligonucleotides were designed and synthesized using the TRIM or NNK technology, and corresponding DNA libraries were assembled. To test the efficiency of the assembly and the complexity of the assembled libraries, they were cloned into the pET vector for the selection of random variants. The obtained

sequences were analyzed for the presence of nucleotide variability in the randomized regions and undesired sequence changes caused by frameshifts or mutations. The analysis confirmed that both libraries were suitable for the use in RD selection.

Selection of binders to EpCAM and N-cadherin

In the selection campaign, consisting of three rounds of ribosome display, recombinant commercial EpCAM and N-cadherin were used as target molecules for direct coating. Both libraries, named Myomedin-loop and Myomedin-betasheet, were used in parallel to altogether generate four collections of novel binders. After the third round of the selection, all four DNA collections of the new variants were cloned into the modified pET vector to contain HisTag at their N-terminus and AviTag at their C-terminus. First, a collection derived from the Myomedin-loop library, targeting N-cadherin, was selected for detailed characterization. Altogether 20 sequentially correct variants, named **LN clones**, were compared in the similarity tree to reveal 17 unique variants (Fig. 29).

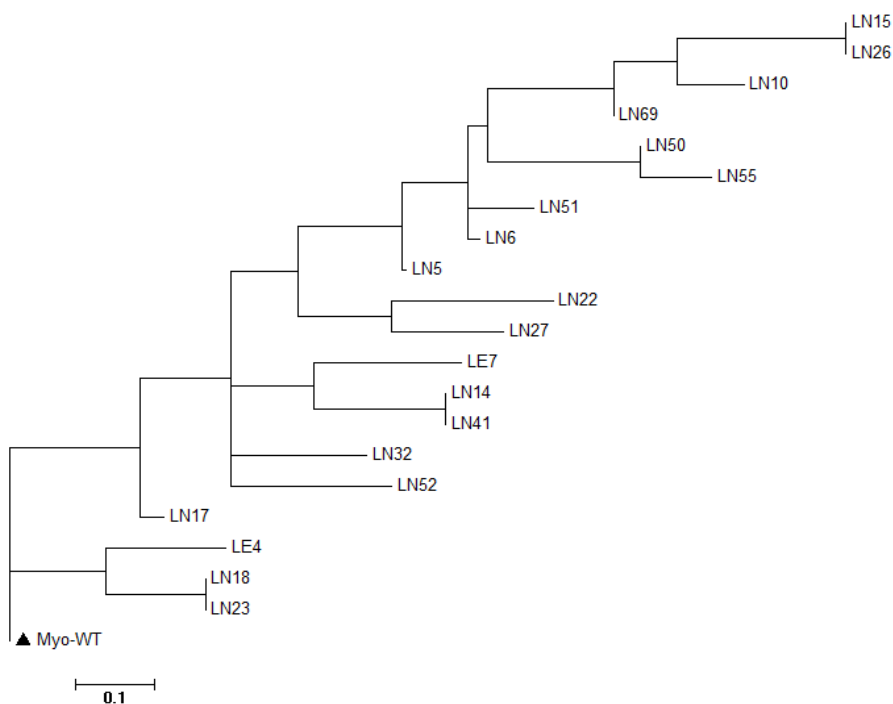


Figure 29. Similarity tree of polypeptide sequences of the obtained LN clones. Sequence analysis of 20 LN clones revealed 17 unique sequence variants. The sequence of the parental myomedin wild-type molecule Myo-WT type (marked as a triangle) was used as a root of the tree.

All LN variants, except for LN10 and LN27 that contained mutations in the initial HisTag sequence and therefore had to be re-cloned, were produced as soluble *in vivo* biotinylated proteins in *E. coli* and purified via HisTag using NiNTA affinity chromatography (Fig. 30). The

LN5 variant showed lower molecular mass in SDS-PAGE analysis as it contains a deletion in the N-terminal part of the sequence including the first randomized loop (sequences not shown).

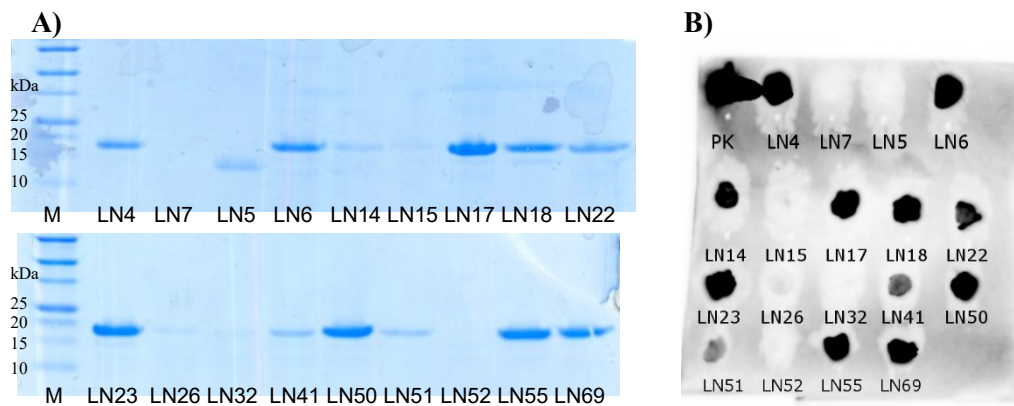


Figure 30. Analysis of the purified LN clones by SDS-PAGE (A) and by dot blot (B). LN clones were produced as soluble *in vivo* biotinylated proteins and purified using NiNTA affinity chromatography. Eluted fractions were transferred onto nitrocellulose membrane and detected using a streptavidin-HRP conjugate. PK = positive biotinylated control; M = molecular standard.

The LN variants that were successfully produced in soluble form in *E. coli* (LN7, LN32, LN52 variants, negative on SDS-PAGE and dot blot, were omitted from the analysis) were used for a pilot ELISA binding experiment (Fig. 31). Two variants of recombinant N-cadherin (the commercial glycosylated whole extracellular moiety and bacterial non-biotinylated N-cadherin), recombinant EpCAM, and BSA were applied to a Medisorp plate. The bound biotinylated soluble LN variants were detected using a streptavidin-HRP conjugate. Strong binding to both N-cadherin targets in comparison to negative controls was observed for LN4 and LN22 variants. LN5 and LN23 variants also showed a weak positivity in binding to both N-cadherin targets. LN14, LN17, and LN18 bound only to the bacterial N-cadherin product. Some LN variants appear to be non-specific, as they bound to EpCAM and BSA negative controls.

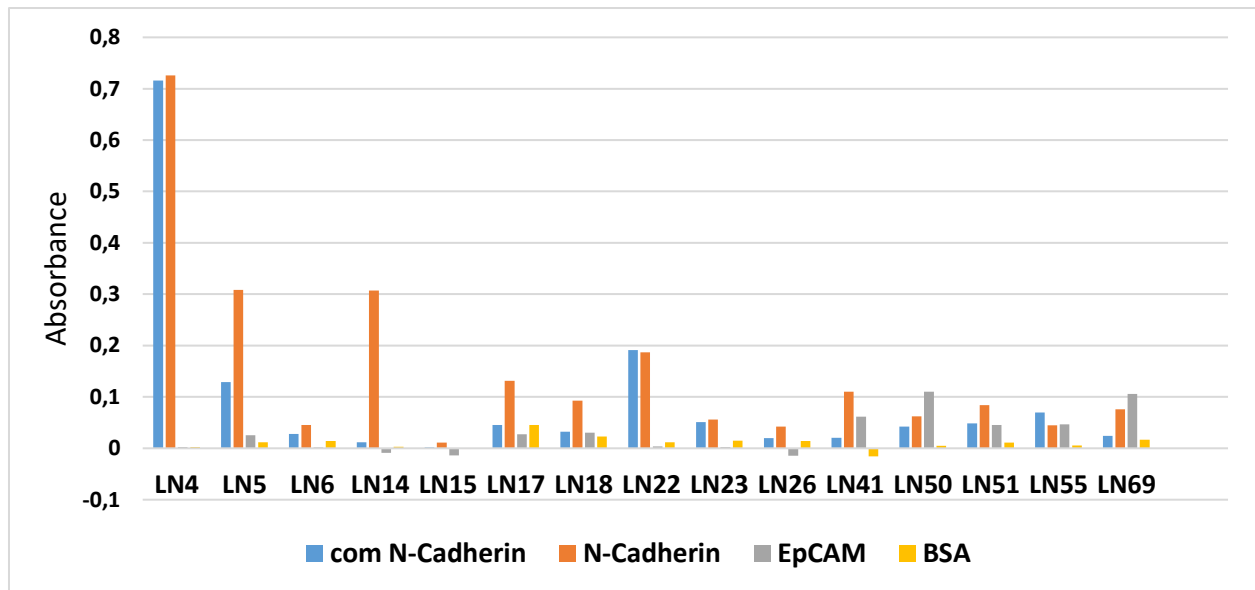


Figure 31. Test of binding of the purified LN variants to recombinant N-cadherin using ELISA. Soluble LN clones produced as *in vivo* biotinylated proteins were applied to a Medisorp microtiter plate coated with two recombinant variants of N-cadherin, EpCAM, and BSA. Streptavidin-HRP was used to detect the bound clones.

Summary

Using a combinatorial library derived from the ABD scaffold in combination with RD selection, DNA collections of CAB binders, targeting the mesenchymal membrane marker N-cadherin, and EBA binders, targeting the epithelial membrane marker EpCAM, were generated and cloned into a plasmid vector, thus providing a DNA library for the production and screening of the best binding variants. The binding profiles of the most promising variants were analyzed using ELISA with immobilized recombinant EpCAM, N-cadherin, and BSA. Alternatively, ELISA with an inverted arrangement was performed. EBA014, EBA062, CAB043, and CAB101 were shown to bind their recombinant protein targets but not the BSA control. EBA014, EBA062, and CAB101 variants exhibited selective binding properties as demonstrated on MCF-7 and CCD1070Sk cell lines expressing either EpCAM or N-cadherin using the LigandTracer Green Line system. All variants showed the binding affinity to living cells in a nanomolar range. Currently, we work on increasing the binding affinity of the EBA014 variant by affinity maturation.

Four collections of Myomedin-derived binders, targeting N-cadherin and EpCAM, were generated and cloned into a plasmid vector for the production and screening of the best binding variants. The N-cadherin binders selected from the Myomedin-loop library (LN binders) were expressed, and cell lysates were used for a pilot ELISA experiment. More detailed

characterization of the LN clones along with characterization of the particular variants from other Myomedin collections will yet be performed. The developed binders might serve as robust capture agents required for the development of a microfluidic chip unit for the detection and separation of CTCs. Selection of cell populations of different cell phenotypes via two surface biomarkers might significantly enhance the sensitivity and accuracy of the diagnostic method and serve as an alternative tool for the clinical practice.

3.3. Binding proteins specific for Shiga toxin 1 B Subunit

Scientific outcomes:

Publication:

Zdravec P., **Marečková L.**, Petroková H., Hodnik V., Nanut M., Anderluh G., Strukelj B., Malý P., Berlec A. Development of Recombinant *Lactococcus lactis* Displaying Albumin-Binding Domain Variants against Shiga Toxin 1 B Subunit. *PLoS ONE*, 2016, vol. 11. ISSN 1932-6203.

Production and characterization of recombinant Stx1B

To generate binders derived from the ABD scaffold using ribosome display, a recombinant shiga toxin 1B subunit (Stx1B) was produced in the form of a fusion protein with HisTag. The gene for Stx1B was synthesized and cloned into the pET28b vector. Different expression conditions (growth at 37°C, 30°C, and 25°C; induction at $A_{600} = 0.5, 1, 2,$ and 3.5-4.0) were tested (data not shown). The highest total level of Stx1B expression was achieved by growing the bacteria at 37 °C to $A_{600} = 3.5-4.0$, followed by induction with 1 mM IPTG for 3 h at 28 °C. Most of the fusion protein was produced in the form of inclusion bodies, which were dissolved in 6 M guanidinium HCl and efficiently purified with immobilized metal affinity chromatography (IMAC) (data not shown). We screened different refolding conditions, and Stx1B was effectively solubilized with a rapid dilution method by using 0.5 M arginine and 0.01 % Brij-35-containing 50 mM Tris buffer. The solubilized product was stored in Tris or PBS buffer for characterization. The molecular weight of recombinant Stx1B was determined by analytical gel filtration chromatography (data not shown). The recombinant Stx1B was eluted from the calibrated column as one sharp symmetrical peak, with molecular weight that corresponded to the pentameric form of recombinant Stx1B. The functionality of recombinant Stx1B was tested by its ability to bind to immobilized globotriosyl ceramide (Gb₃) receptor *in vitro*, and by its internalization into HeLa cells, which naturally contain Gb₃ on their surface. Strong, specific, and concentration-dependent binding of recombinant Stx1B to the immobilized Gb₃ receptor was demonstrated by ELISA (Fig. 32.A). In HeLa cells, 1 h after co-incubation with Stx1B, the latter was internalized in the cells and co-localized with Golgi marker Golgin 97 (Fig. 32.B).

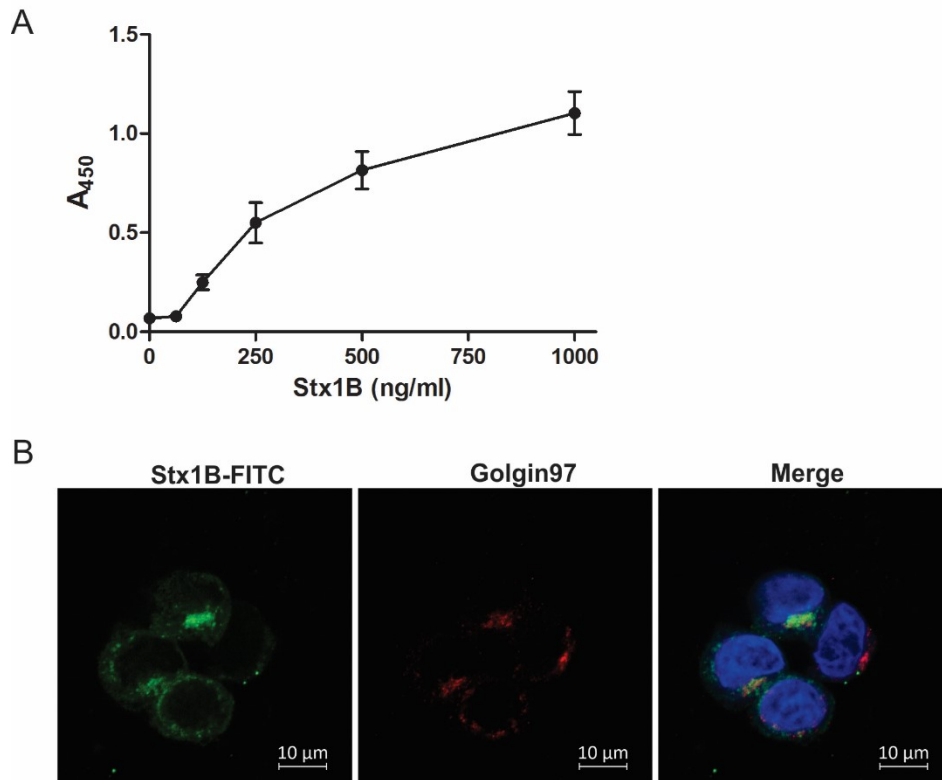


Figure 32. Ability of recombinant Stx1B to bind to Gb₃ receptor *in vitro* (A). Binding of serially diluted Stx1B to Gb₃ as determined by ELISA using THE™ His Tag antibody. A₄₅₀: Absorbance at 450 nm. Error bars denote standard deviations. **Internalization of FITC-labeled Stx1B into HeLa cells (B).** Golgi was detected with mouse anti-human Golgin97 primary antibody and Alexa Fluor 555-conjugated goat anti-rabbit secondary antibody (red). DAPI staining was used to label nuclei (blue).

Ribosome display selection of Stx1B binders

To select unique binders of Stx1B, a high-complex combinatorial ABD library was used. Five cycles of ribosome display selection were performed, yielding a collection of 17 unique Stx1B-binders designated as **S1B binders** (Fig. 33.A). The identified S1B binders were produced in *E. coli* as fusion proteins with TolA spacer containing AviTag at the C-terminus and HisTag at the N-terminus (His-S1B-TolA-Avi). The expression level of the corresponding fusion protein was tested by SDS-PAGE and Western blot analysis (data not shown) and the binding affinity was verified by ELISA (Fig. 33.B). ELISA-positive cell lysates with the appropriate expression level of S1B binders were selected for further analysis.

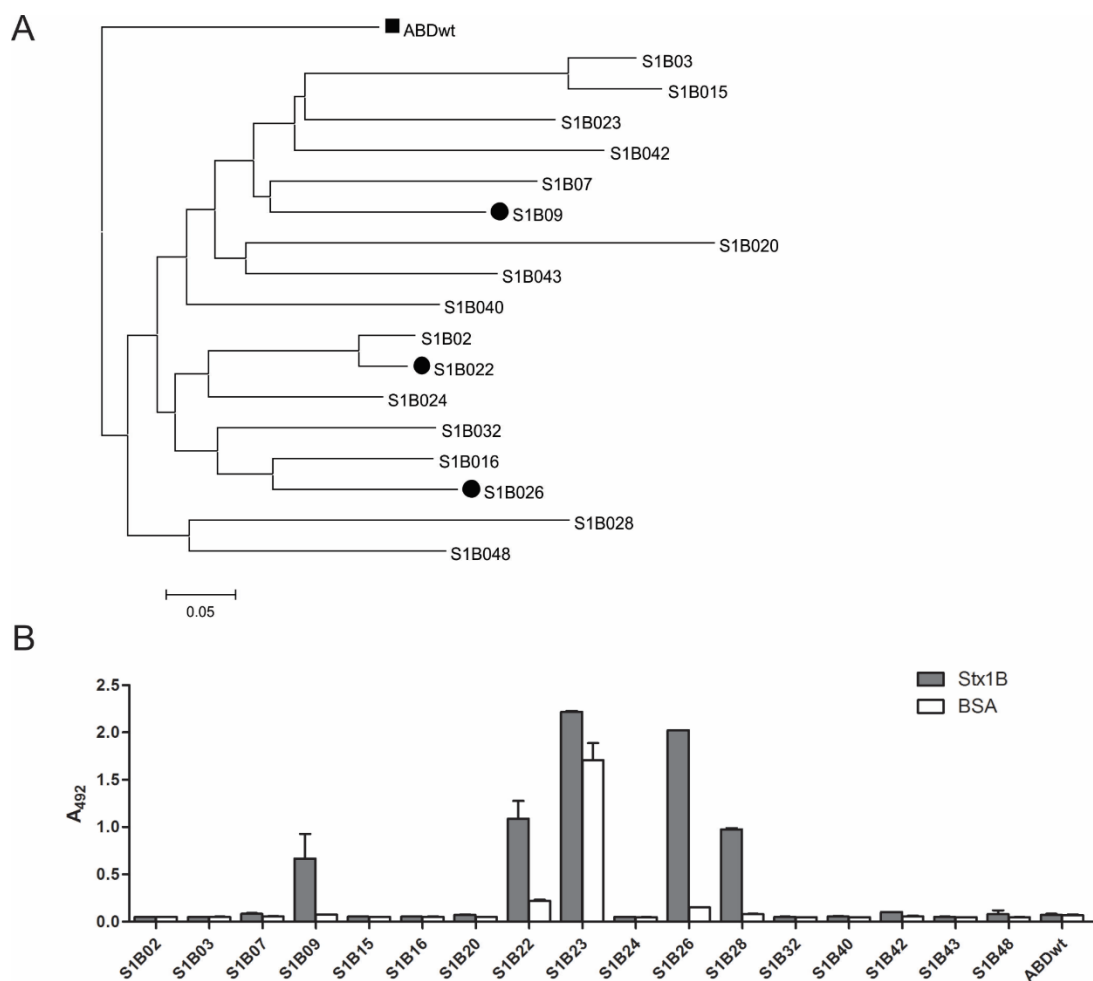


Figure 33. Sequence similarity analysis (A) and binding affinity (B) of 17 S1B binders selected after five rounds of ribosome display. A: The sequence of the parental ABD wild-type domain was used as a root of the tree and is highlighted as a square, while S1B variants selected for more detailed analysis are highlighted as circles. B: S1B binders-containing cell lysates were incubated with immobilized Stx1B (grey bars) or BSA (white bars) and detected with HRP-conjugated streptavidin. Error bars denote standard deviations.

Characterization of the selected S1B binders

The selected binders were produced in *E. coli* on a large scale, purified with IMAC or HisTrap FPLC, and verified by SDS-PAGE electrophoresis, where a low level of expression and some proteolytic degradation of the S1B9 variant were observed (Fig 34.A). Stx1B was immobilized and incubated with serial dilutions of selected S1B binders, detected with HRP-streptavidin. A gradual increase of the ELISA signal confirmed binding of S1B binders to recombinant Stx1B (Fig 34.B). Variant S1B26 showed the strongest binding, while binding of the S1B9 variant was the weakest, which may be the consequence of the degradation noted above. Sequence similarity comparison of selected binders S1B9, S1B22, and S1B26 with parental non-mutated ABDwt is presented in Figure 34.C.

Based on ELISA tests and SDS-PAGE analysis, clones S1B22 and S1B26 were selected for further characterization of binding using surface plasmon resonance (SPR) and microscale thermophoresis (MST), and of stability with the thermal shift assay (TSA).

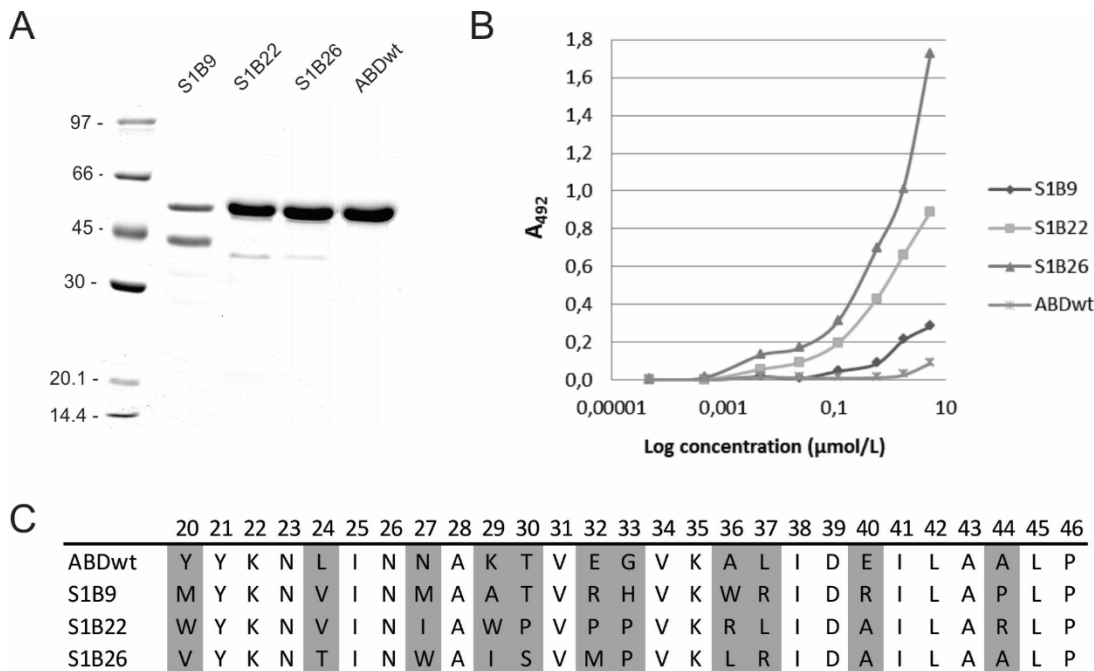


Figure 34. SDS PAGE analysis of selected binders S1B9, S1B22, and S1B26 after purification from *E. coli* cell lysates, stained with Coomassie brilliant blue (A). ELISA-determined binding of serially diluted biotinylated selected binders to immobilized recombinant Stx1B (B). The binding was detected with HRP-conjugated streptavidin. Sequence similarity comparison of selected binders with parental non-mutated ABDwt (C). Randomized sequences between residues 20 and 46 were compared. Randomized positions are indicated in grey.

The first setup of SPR affinity measurements included immobilization of Stx1B on the sensor chip surface and injecting S1B proteins over the surface. Binding was confirmed with different dilutions of both binders, S1B22 and S1B26. Nevertheless, we could not determine the binding constant (K_D) for the tested interactions with any of the available kinetic modules in the BiacoreT100 software. This was probably due to a complex interaction between S1B variants and Stx1B, which is in pentameric form, and probably binds more than one S1B molecule. The binding mode between Stx1B and S1B binders could be investigated by structural analysis, such as molecular docking, or by solving the structure of the complex. Protein variants S1B22, S1B26, and the ABDwt control were injected at 1 μM concentration over the immobilized Stx1B, and the specific binding is shown in Figure 35. A significantly higher sensor response

was observed in the case of S1B22 and S1B26 proteins in comparison to the parental ABDwt control.

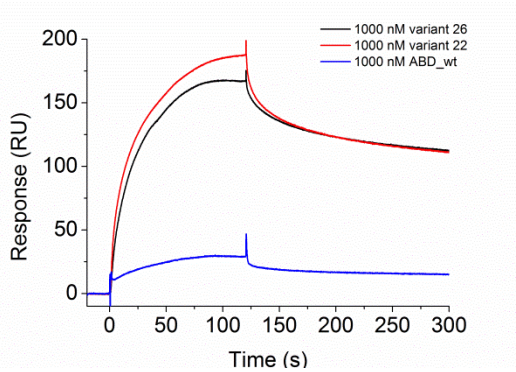


Figure 35. Binding of S1B22 and S1B26 in fusion with Tola-Avi to the immobilized recombinant Stx1B.

In a reversed setup, clones S1B22 (Fig. 36.A) and S1B26 (Fig. 36.B) were attached to the sensor chip surface, and twofold dilutions of recombinant Stx1B, starting with 4 μM concentrations, were injected over the chip surface. To calculate the affinity constant, we applied the Steady State Affinity model, and an average of three experiments was considered. The binding affinity of recombinant Stx1B to S1B22 and S1B26 was $0.70 \pm 0.03 \mu\text{M}$ and $1.00 \pm 0.09 \mu\text{M}$, respectively.

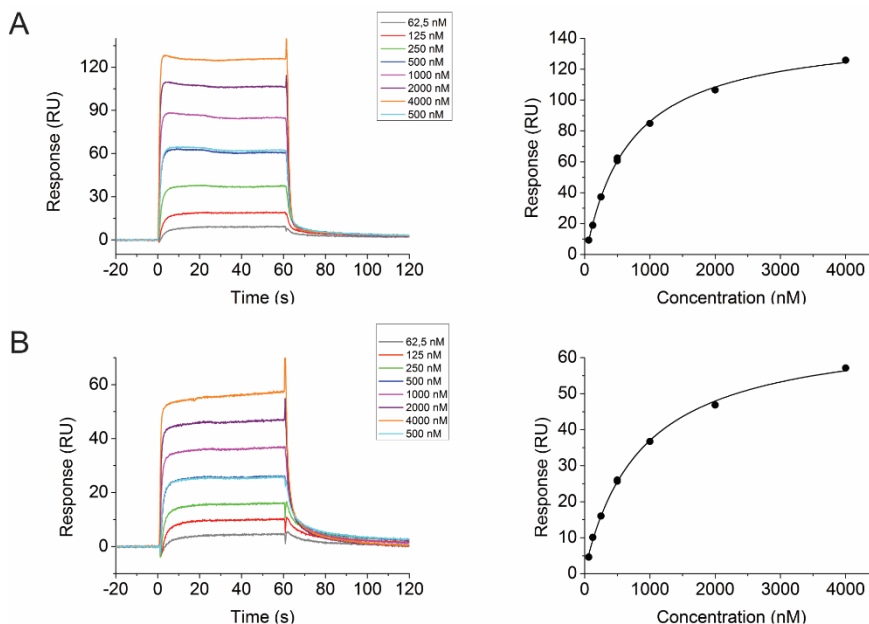


Figure 36. SPR analysis of the binding of recombinant Stx1B to CM5-chip-immobilized S1B22-Tola-Avi (A) and S1B26-Tola-Avi (B). Recombinant Stx1B in seven different concentrations was injected over the chip surface (left figures). To calculate the affinity constant, we applied the Steady State Affinity model (right).

The binding affinity of S1B22 and S1B26 to fluorescently-labeled recombinant Stx1B in solution was confirmed by microscale thermophoresis (MST). The binding curves obtained from three repeated measurements for S1B22 and S1B26 are shown in Figure 37. The commercial analysis software was used to plot and fit the change in initial fluorescence to yield binding affinities in the micromolar range of $0.4 \pm 0.05 \mu\text{M}$ for S1B22 and $0.6 \pm 0.05 \mu\text{M}$ for S1B26.

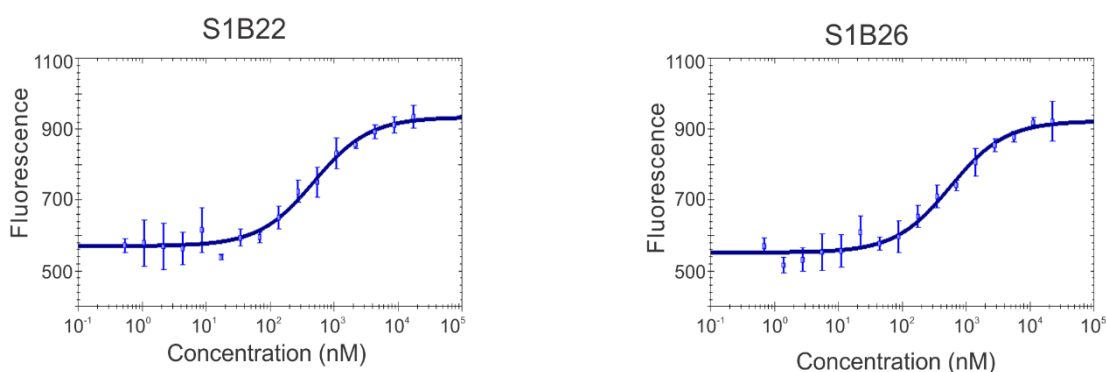


Figure 37. The binding affinity of S1B22 and S1B26 to fluorescently-labeled recombinant Stx1B measured by MST. Sixteen serial dilution concentrations of S1B22 or S1B26 were mixed with fluorescently labeled Stx1B at 5 nM final concentration. Fluorescence change K_d fit in NanoTemper software was used to calculate K_d . Error bars denote standard deviations.

The thermal stabilities of binders S1B22 and S1B26 in fusion with TolA-Avi were investigated by the fluorescence-based thermal shift assay (data not shown). The denaturation temperature (T_m) determined for the binder S1B26 was 53 °C in PBS buffer and 54 °C in Tris-NaCl buffer. T_m for the binder S1B22 could not be determined in any of the tested buffers, probably due to the presence of two tryptophanes and three prolines in the randomized part of S1B22, which might destabilize the helical structure of the protein.

Expression and surface display of the selected S1B binders on *L. lactis* NZ9000

Genes for S1B9, S1B22, S1B26, ABDwt, and ABDwtHis without tolA spacer or tags were amplified by PCR and cloned into plasmid pSDLBA3b [96], which was previously designed for surface display of target proteins in fusion with the Usp45 secretion signal and surface anchoring C-terminal domain of AcmA (cA). Fusion proteins were expressed in *L. lactis* by induction with nisin and visualized in the cell lysates by SDS PAGE and Coomassie brilliant blue staining (Fig. 38.A). The surface display of ABDs was confirmed for ABDwt and ABDwtHis using flow cytometry. *L. lactis* cells expressing ABDwt on their surface efficiently

bound FITC-conjugated HSA (Fig. 38.B), which also indicates functionality of the displayed binder. Display of ABDwtHis on the surface of *L. lactis* cells was also confirmed with FITC-conjugated antiHis antibody (data not shown).

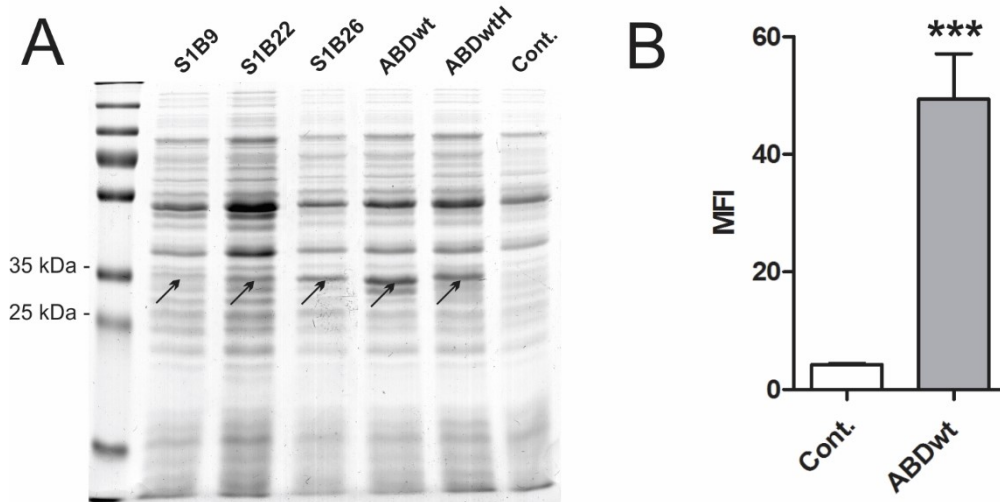


Figure 38. SDS PAGE analysis of lysates of *L. lactis* cells expressing S1B9, S1B22, S1B26, ABDwt, and ABDwtHis (ABDwtH) (A). All products in fusion with the Usp45 secretion signal and LysM-containing cA domain, stained with Coomassie brilliant blue. ABD fusion proteins are highlighted with arrows. **Flow cytometric analysis of ABD surface display (B).** Detection with FITC-conjugated human serum albumin. The MFI value of ABDwt was compared to the control using Student's t test. *** $p < 0.001$. Cont. = control containing empty plasmid pNZ8148.

Evaluation of Stx1B binding by recombinant *L. lactis* with surface-displayed S1B binders

Binding of Stx1B by recombinant *L. lactis* with surface-displayed S1B binders was evaluated by flow cytometry (Fig. 39.A) and whole-cell ELISA (Fig. 39.B). Using flow cytometry we observed statistically significant binding of fluorescently-labeled Stx1B by *L. lactis* cells displaying S1B9 or S1B26 on their surface in comparison with control *L. lactis* cells expressing ABDwt. Using the whole-cell ELISA, the binding of Stx1B by *L. lactis* cells displaying S1B9, S1B22, or S1B26 was confirmed. Based on these results, S1B26 was selected as the most promising Stx1B binder for the display on the surface of *L. lactis*, even though S1B22 exhibited lower binding constants in SPR and MST, possibly due to the fusion with TolA-Avi in isolated S1Bs.

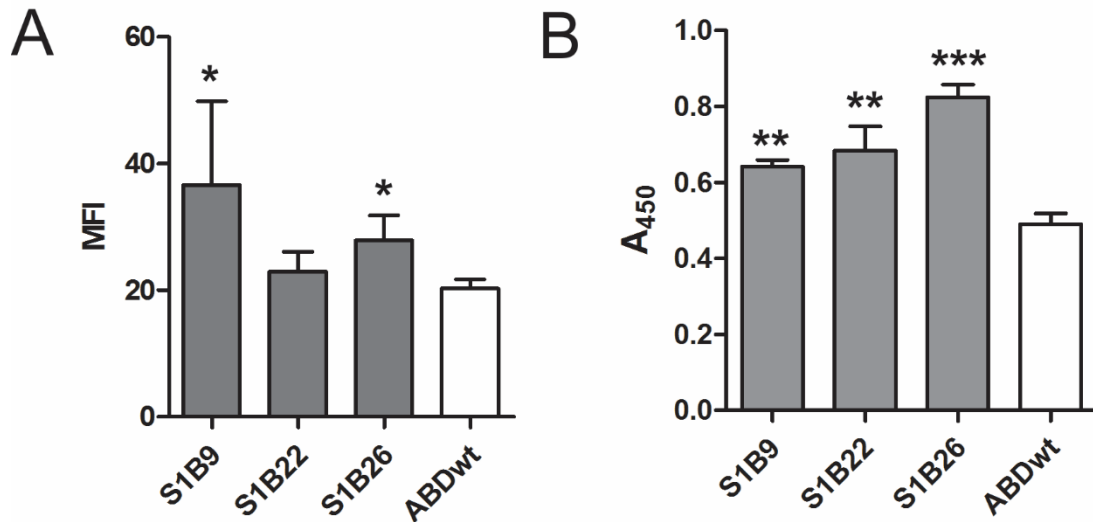


Figure 39. Flow cytometric (A) and whole-cell ELISA (B) analyses of binding of recombinant Stx1B by *L. lactis* cells displaying S1B variants or ABDwt on their surface. (A) Alexa488-conjugated Stx1B was used for the detection. MFI: Mean fluorescence intensity. (B) Mouse antiStx1B antibody and HRP-conjugated anti-mouse antibody were used for Stx1B detection. A₄₅₀: Absorbance at 450 nm. Vertical bars denote standard deviation. MFI or A₄₅₀ values of S1B binders were compared to ABDwt control using Student's t test. *: p<0.05, ** p<0.01, *** p<0.001.

Redirection of Stx1B transport in HeLa cells by selected S1B binders

S1B22 and S1B26 in fusion with TolA-Avi were tested for their ability to prevent binding of Stx1B to HeLa cells, or to interfere with retrograde transport of Stx1B to the Golgi apparatus (GA) in HeLa cells. When fluorescently labeled, Stx1B (Stx1B-Alexa Fluor 488) was mixed with S1B binders prior to incubation with HeLa cells, and no decrease in the mean fluorescence intensity (MFI) compared to the control (incubated with Stx1B-Alexa Fluor 488 alone) was observed using flow cytometry. This result is in correlation with the inhibition of binding to the HeLa cells. Contrary to that, a higher MFI was observed in cells incubated with the mixtures of S1Bs and Stx1B-Alexa Fluor 488 (Fig. 40.A and 40.B), indicating a higher amount of the bound Stx1B-Alexa Fluor 488 or different cell distribution of the internalized toxin. ABDwt-TolA-Avi had no effect on the internalization of the Stx1B-Alexa Fluor 488 conjugate into HeLa cells (Fig. 40.A and 40.B). To investigate the effect of S1Bs in more detail, we performed fluorescence microscopy using membrane-labeling marker PKH26 (Fig. 40.C) and marker for GA (Fig. 40.D). In cells incubated with Stx1B-Alexa Fluor 488 alone, or mixture of Stx1B-Alexa Fluor 488 and ABDwt, the majority of Stx1B-Alexa Fluor 488 was co-localized with the marker of GA 1 h after addition to HeLa cells (Fig. 40.D), as shown before with FITC-conjugated Stx1B. When Stx1B-Alexa Fluor 488 was pre-incubated with S1B22 or S1B26, the

distribution of Stx1B in HeLa cells was completely altered. Stx1B-Alexa Fluor 488 was partially co-localized with the membrane dye, indicating localization at the cell membrane or in membrane-bound vesicles, while the co-localization with the GA marker was completely lacking, indicating its absence from GA. S1B22 and S1B26 interfered with the conventional internalization route of Stx1B into the HeLa cells, suggesting a possible inhibitory function of S1B variants on Stx1B retrograde transport. However, more analyses need to be performed to prove the exact mechanism of effect of S1Bs on Stx1B trafficking.

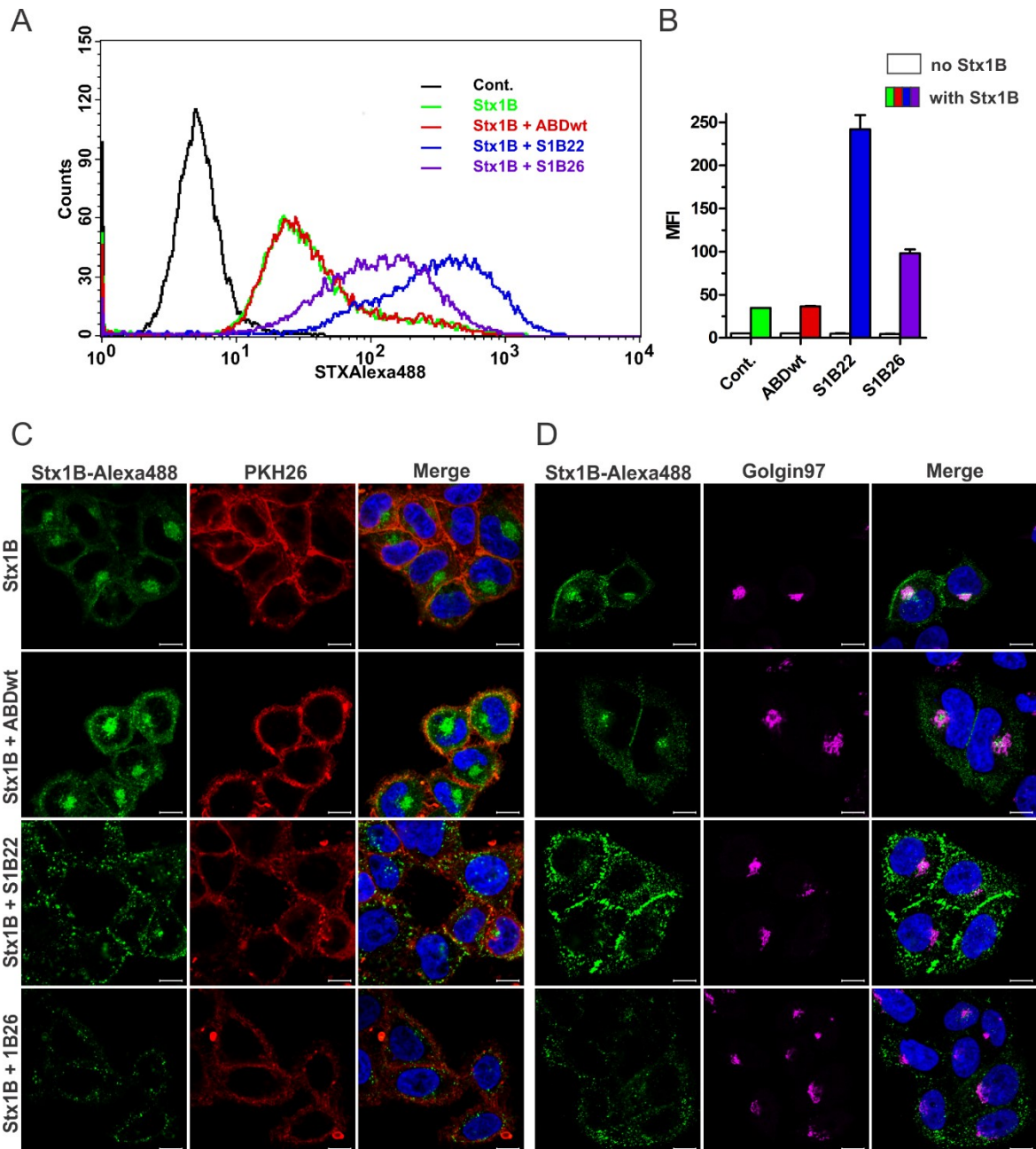


Figure 40. Effects of S1B binders on Stx1B transport into HeLa cells. Flow cytometric analysis of HeLa cells demonstrating a shift in fluorescence intensity (A) and mean fluorescence intensity (MFI; B). MFI upon 1h incubation of HeLa cells with mixtures of S1B22, S1B26, or ABDwt and Alexa Fluor 488-labeled Stx1B. Cont. = unstained HeLa cells. Stx1B = HeLa cells incubated with Stx1B-Alexa Fluor 488 alone. Fluorescence microscopy images of HeLa cells incubated with Alexa Fluor 488-labeled Stx1B (green) with or without pre-incubation with S1B22 and S1B26 (C, D). DAPI staining (blue) was used to label nuclei. Cells were stained with the PKH26 membrane labeling dye (red; C) and the Golgi apparatus was detected with mouse monoclonal Golgin-97 antibody and secondary polyclonal goat anti-mouse antibody conjugated with Alexa Fluor 633 (purple; D). Bars = 10 μ m.

Summary

An efficient and functional display of ABD-derived Stx1B binding proteins (named S1B binders) on the surface of *L. lactis* was demonstrated. For the selection of S1B binders using ribosome display, recombinant Stx1B was expressed in the form of inclusion bodies and efficiently refolded. Recombinant Stx1B was demonstrated to form a pentamer that should bind to the Gb₃ receptor *in vitro*. Furthermore, fluorescently-labeled Stx1B bound to the receptor on HeLa cells was internalized into the cells and then transferred into the Golgi apparatus 1 h after addition to HeLa cells, indicating that recombinant Stx1B was fully functional and can be used as a suitable target for the selection of binders by RD. Of all selected S1B variants, four cell lysates that contained S1B binders S1B9, S1B22, S1B26, or S1B28 showed specific binding to immobilized recombinant Stx1B using ELISA. The S1B28 variant showed a lower level of expression, possibly due to unintended mutation in the non-randomized part of the sequence, and this protein was, therefore, excluded from further characterization. Binding of serially diluted S1B9, S1B22, S1B26 binders to immobilized Stx1B was observed. The most promising variants S1B22 and S1B26 were chosen for further biophysical characterization using SPR. The binding affinities could not be determined with any of the predetermined kinetic modes when Stx1B was immobilized on the sensor surface. This was probably due to a complex interaction mode between S1B variants and Stx1B, which is in pentameric form, and probably binds more than one S1B molecule. On the contrary, by reverting the SPR setup with immobilization of S1B variants and flowing Stx1B over the sensor, the affinity constants of S1B22 and S1B26 were determined to be in the micromolar range (0.70 μM for S1B22 and 1.00 μM for S1B26). This low affinity of S1B binders could be further improved by an affinity maturation approach.

L. lactis capable of binding Stx1B by displaying S1B binders on its surface were engineered. To display the S1B binders on the surface of *L. lactis*, the genes for S1B9, S1B22, S1B26, and ABDwt control without TolA spacer or AviTag were fused to the gene for peptidoglycan-binding C terminus of AcmA protein and to the Usp45 secretion signal. The fusion proteins were expressed in *L. lactis* by using a nisin-controlled expression system (NICE), as confirmed by SDS PAGE analysis. Although the S1B9 variant was eliminated from further biophysical characterization, it was expressed in *L. lactis* cells and no truncation was observed. Surface display of all four variants was confirmed using flow cytometry or whole-cell ELISA. Using flow cytometry, binding of fluorescently-labelled Stx1B was observed with surface-displayed S1B9 and S1B26, whereby the S1B9 variant showed stronger binding. On the contrary, whole-cell ELISA revealed significant binding of all three S1B variants, the strongest with S1B26 and

the weakest with S1B9. Thus, S1B26 was indicated as the most promising Stx1B binder for the *L. lactis* surface display.

3.4. Development of procedures and tools for validation of the polyvalent vaccines against bacterial enteral diseases

Scientific outcomes:

Utility models:

0477716 - BTO-N 2018 RIV CZ cze L - Recombinant protein – Toxin A (*C. difficile*)
 0477715 - BTO-N 2018 RIV CZ cze L - Recombinant protein – Toxin Epsilon type B (*C. perfringens*)
 0477714 - BTO-N 2018 RIV CZ cze L - Recombinant protein – Toxin Beta2 (*C. perfringens*)
 0477713 - BTO-N 2018 RIV CZ cze L - Recombinant protein – Toxin Beta (*C. perfringens*)
 0477712 - BTO-N 2018 RIV CZ cze L - Recombinant protein – Toxin Alpha (*C. perfringens*)

Expression and characterization of recombinant antigens

To develop ELISA protocols for the determination of antibodies against *Clostridium perfringens* toxin Alpha (CPA), Beta (CPB1), Beta2 (CPB2), Epsilon (ETX) and *Clostridium difficile* Toxin A (TcdA), five recombinant antigens were produced and characterized (Table 7.). Genomic DNA of *C. perfringens* (types A, B) and *C. difficile* were isolated from bacteria of veterinary isolates (provided by Dyntec s.r.o.) and the purified DNA was used as a template for amplification of CPA, CPB1, CPB2, ETX, and TcdA sequences using PCR. For PCR amplification, specific primers for each of the antigens were designed.

Table 7. Schematic overview of five produced antigens

Name	Abbreviation	Bacterial strain	Produced part of the protein	Length MW	UniProt ID
Toxin Alpha (α)	CPA	<i>C. perfringens</i> toxinotype A	C-terminal domain	134 aa 16 kDa	Q0TV31
Toxin Beta (β)	CPB1	<i>C. perfringens</i> toxinotype B	Full-length	324 aa 36 kDa	Q46308
Toxin Beta2 (β2)	CPB2	<i>C. Perfringens</i> toxinotype A, B	Full-length	250 aa 29 kDa	Q5MQ79
Toxin Epsilon (ϵ)	ETX	<i>C. perfringens</i> toxinotype B	Full-length without pro-peptide	298 aa 33 kDa	Q02307
Toxin A	TcdA	<i>C. difficile</i>	C-terminal repetitive domain	359 aa 36 kDa	Q189K5

Production of recombinant toxin Alpha of *C. perfringens* (CPA)

CPA has been shown to be the key virulence factor in infection with type A strains of *C. perfringens*. According to the literature [97], specific primers for amplification of the immunogenic but non-toxic C-terminal domain of CPA were designed (Fig. 41). The amplified product was cloned into the pET vector and sequentially verified. The final construct of 134 aa containing HisTag at its N-terminus was produced in soluble form in *E. coli* BL21 (DE3). Recombinant CPA was purified from the cytosolic extract by affinity chromatography in NiNTA-agarose and analyzed using SDS-PAGE and Western blot (Fig. 42).

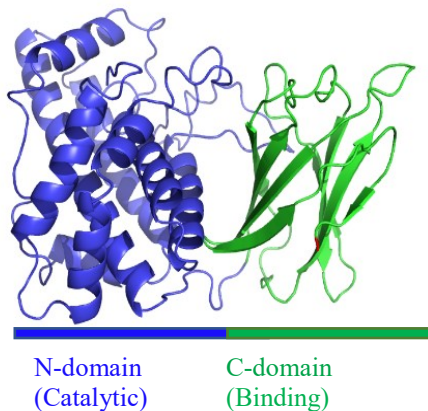


Figure 41. The structure of CPA. (PDB:1CA1). Toxin A from *C. perfringens* is composed of two domains: the N-terminal catalytic domain (blue) responsible for phospholipase activity of the toxin, corresponding to the phospholipase C activity, and immunogenic C-terminal domain (green) responsible for binding to the cell membrane.

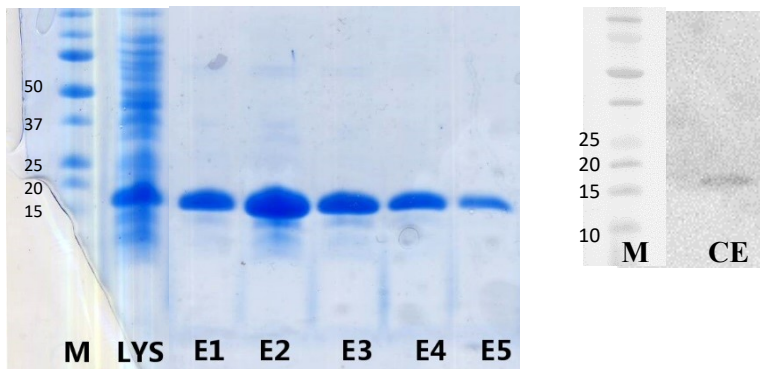


Figure 42. Analysis of purified CPA by SDS-PAGE (left) and by Western blot (right). CPA was produced in soluble form in BL21 (DE3) and purified using NiNTA affinity chromatography. The expression of CPA was detected using anti-HisTag HRP conjugate. LYS = cell lysate; E = eluted fractions; CE = cytosolic extract; M = molecular standard.

Production of recombinant toxin Beta of *C. perfringens* (CPB1)

Beta toxin is the main disease-causing agent in type B strains of *C. perfringens* [98]. Specific primers for amplification of the full-length CPB1 toxin DNA were designed. The amplified product was introduced into the pET vector and sequentially verified. The final product of 324 aa containing the N-terminal HisTag sequence was predominantly found in inclusion bodies of *E. coli* BL21 (DE3). Higher production of the soluble protein in the cytosolic extract was achieved by expression in the ArticExpress RIL (DE3) host cells at 13°C, a special *E. coli* strain designed for the production of proteins with rare codons. Recombinant soluble CPB1 was purified from the cytosolic extract by affinity chromatography in NiNTA-agarose and analyzed using SDS-PAGE and Western blot (Fig. 43).

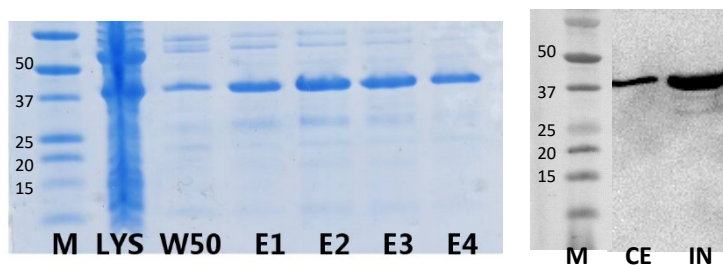


Figure 43. Analysis of purified CPB1 by SDS-PAGE (left) and Western blot (right). CPB1 was produced in soluble form in ArcticExpress (DE3) RIL and purified using affinity chromatography in NiNTA-agarose. The expression of CPB1 was detected using anti-HisTag HRP conjugate. E = Eluted fractions; LYS = cell lysate; W50 = wash with 50 mM imidazole, 300 mM NaCl, 50 mM Tris buffer pH 8; CE = cytosolic extract; IN = inclusion bodies; M = molecular standard.

Production of recombinant toxin Beta2 of *C. perfringens* (CPB2)

Beta2 toxin can be found in type A and B strains of *C. perfringens*. Its amino acid sequence has no significant homology with *C. perfringens* CPB1 or any other known toxins [99]. Specific primers for amplification of the full-length CPB2 toxin DNA were designed. The amplified product was cloned into the pET vector and sequentially verified. The final construct of 250 aa containing N-terminal HisTag was produced in the soluble form in BL21 (DE3) *E. coli* host cells. Recombinant soluble CPB2 was purified from the cytosolic extract by IMAC chromatography using NiNTA-agarose and further analyzed using SDS-PAGE and Western blot (Fig. 44).

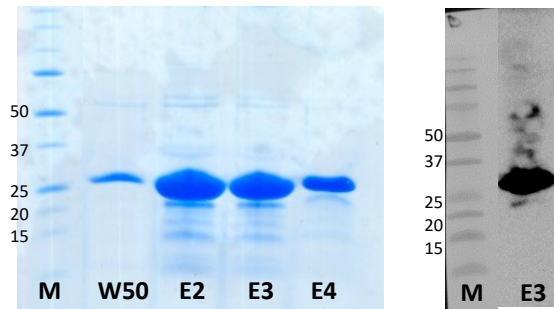


Figure 44. Analysis of purified CPB2 by SDS-PAGE (left) and by Western blot (right). CPB2 was produced in soluble form in BL21 (DE3) host cells and purified using affinity chromatography in NiNTA-agarose. The expression of CPB2 was detected using anti-HisTag HRP conjugate. E = Eluted fractions; W50 = wash with 50 mM imidazole, 300 mM NaCl, 50 mM Tris buffer pH 8; CE = cytosolic extract; IN = inclusion bodies; M = molecular standard.

Production of recombinant toxin Epsilon of *C. perfringens* (ETX)

Epsilon toxin is produced by type B and type D strains of *C. perfringens* [98]. Specific primers for the amplification of the complete ETX toxin without the pro-sequence were designed. The amplified product was cloned into the pET vector and sequentially verified. The final construct of 298 aa containing HisTag at its N-terminus was produced in the soluble form in BL21 (DE3) *E. coli* host cells. Recombinant soluble ETX was purified from the cytosolic extract by IMAC chromatography in NiNTA-agarose and analyzed using SDS-PAGE and Western blot (Fig. 45).

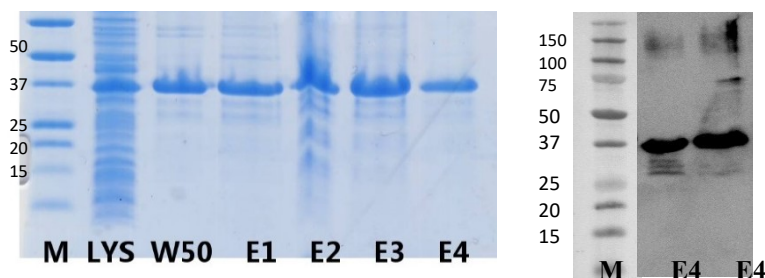


Figure 45. Analysis of purified ETX by SDS-PAGE (left) and by Western blot (right). ETX was produced in soluble form in BL21 (DE3) and purified using affinity chromatography in NiNTA-agarose. The expression of ETX was detected using anti-HisTag HRP conjugate.; LYS = cell lysate; E = eluted fractions; W50 = wash with 50 mM imidazole, 300 mM NaCl, 50 mM Tris buffer pH 8; M = molecular standard.

Production of recombinant A of *C. difficile* (TcdA)

TcdA is a large 308 kDa protein that belongs to a larger family of clostridial toxins. The C-terminus of TcdA consists of highly repetitive structures termed “combined repetitive oligopeptides”, which are found between amino acids 1832–2710 (Fig. 46). This region is responsible for binding to the receptor, and it is, therefore, called “the receptor-binding domain

(RBD).” RBD has been shown to be an excellent immunogen [100-102]. For the recombinant TcdA expression, specific primers for amplification of the part of the C-terminal repetitive domain were designed (Fig. 46). The amplified product was cloned into the pET vector and sequentially verified. The final construct of 359 aa containing HisTag at its N-terminus was produced in the soluble form in the ArcticExpress RIL (DE3) host cells at 13°C. Recombinant soluble TcdA was purified from the cytosolic extract by affinity chromatography in NiNTA-agarose and analyzed using SDS-PAGE and Western blot. Purified TcdA, beside the monomeric form having an apparent molecular mass of 36 kDa, was shown to form multimers (Fig. 47).

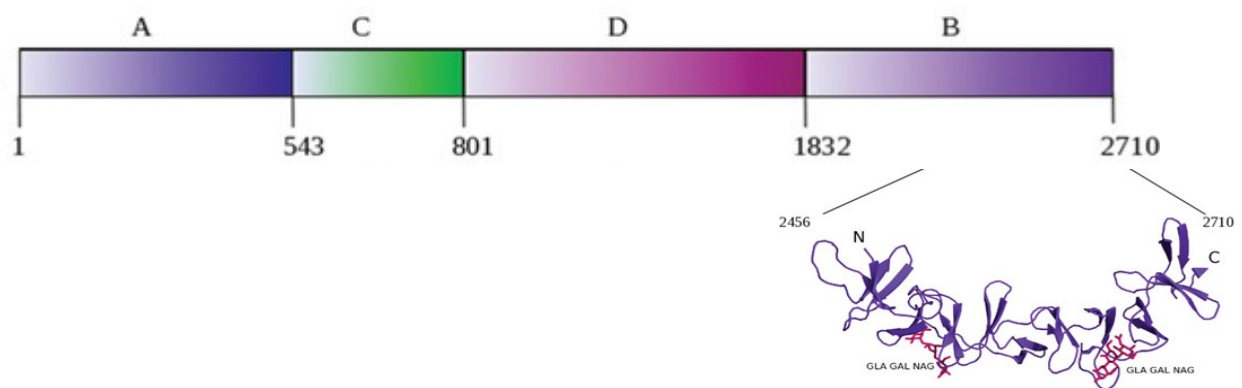


Figure 46. Schematic representation of the toxin A of *C. difficile*. The structure of the part of C-terminal domain (B) corresponding to the expressed region of recombinant TcdA is indicated. The figure was modified according to the original described in [100].

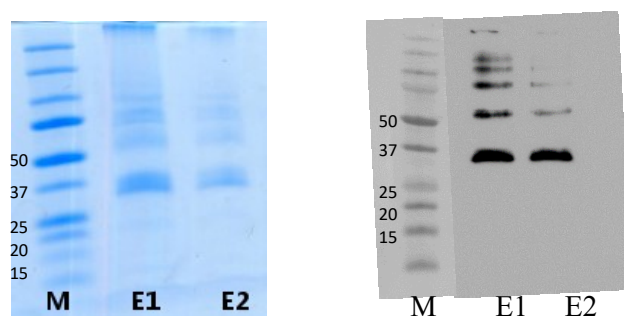


Figure 47. Analysis of purified TcdA by SDS-PAGE (left) and by Western blot (right). TcdA was produced in soluble form in ArcticExpress (DE3) RIL and purified using affinity chromatography in NiNTA-agarose. The expression of TcdA was detected using anti-HisTag HRP conjugate; E = eluted fractions; M = molecular standard.

Development and validation of the ELISA method for the detection of antibodies against CPA, CPB1, CPB2, ETX, and TcdA

The vaccine efficacy is declared by determination of antibodies against recombinant antigens CPA, CPB1, CPB2, ETX, and TcdA. Purified recombinant toxins and specific antibodies were used to optimize the antigen-coating conditions in ELISA. The surface of different types of microtiter plates (Polysorp, Maxisorp) was tested for the optimization in combination with different coating buffers (bicarbonate/carbonate buffer pH 9.6, acetate buffer pH 3, and PBS buffer pH 7.4). Serial dilutions of recombinant proteins were prepared to find the optimal coating concentration for each antigen (Table 8).

Table 8. Optimal coating conditions for each recombinant antigen used in ELISA

Antigen	Microtiter plate	Coating buffer	Concentration
CPA	Maxisorp	bicarbonate/carbonate buffer pH 9.6	4 µg/ml
CPB1	Maxisorp	bicarbonate/carbonate buffer pH 9.6	5 µg/ml
CPB2	Maxisorp	bicarbonate/carbonate buffer pH 9.6	2 µg/ml
ETX	Maxisorp	bicarbonate/carbonate buffer pH 9.6	3 µg/ml
TcdA	Polysorp	bicarbonate/carbonate buffer pH 9.6	5 µg/ml

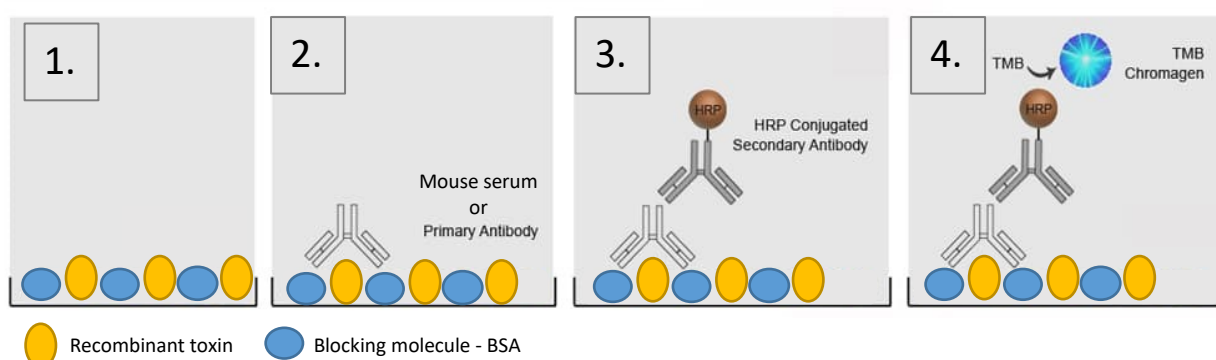


Figure 48. Schematic representation of the ELISA arrangement

The scheme of the ELISA arrangement is displayed in Figure 48. Each antigen, i.e. recombinant toxin, was diluted in the coating buffer to the particular concentration (Table 8.). The microtiter plate with the antigen was incubated overnight at a temperature of 5 ± 3 °C. After the incubation period, the unbound antigen was removed from the wells. All wells were washed three times with washing solution. After that, blocking was performed using blocking solution containing

BSA. The incubation time for blocking was 2 hours at RT. The blocking solution was removed from the wells with washing solution. To test the particular mouse sera on the microtiter plate, both positive and negative serum were added as controls. All sera were diluted 1000x to 128000x in dilution solution. Diluted sera were applied to each well of the microtiter plate. To optimize the protocol, sera of mice vaccinated with the studied vaccine were used. The plate with the diluted sera was covered and incubated for 1 hour at RT. After the incubation period, the unbound serum was removed from the wells. All wells were washed three times with washing solution. After that, the HRP conjugate diluted in the dilution solution was applied to each well and incubated for 1 hour at RT. After the incubation period, the unbound conjugate was removed from the wells and the wells were repeatedly washed. Then the substrate 3,3',5,5'-tetramethylbenzidine (TMB) was applied to each tested well. The plate was incubated for 5 minutes at RT and the reaction was terminated by the addition of stop solution 2M H₂SO₄. The color intensity was measured using a spectrophotometer at a wavelength of 450 nm.

For validation of the ELISA protocol, the parameters and criteria of acceptability were tested. The following parameters were evaluated: specificity, precision, reproducibility, intermediate precision, range, and linearity.

Control wells

Control well A = without antigen, without serum, the result is negative

Control well B (BLANK) = with antigen, without serum, the result is negative

Control well C = without conjugate, the result is negative

Specificity

The negative sample should be mouse serum, where the color reaction is not expected by any dilution (absorbance under 0.12 – quantification limit). Two negative samples in three days at all dilutions were tested. Absorbance of samples without conjugate, samples without antigen and serum, and samples without serum were not higher than 0.12.

Precision

Precision describes the agreement among samples and is expressed as variation coefficient (CV).

$$CV = (SD/mean) \times 100$$

Reproducibility

Six positive samples in one day were tested. CV for reproducibility was ≤ 15 % for samples with absorbance higher than 0.12.

Intermediate precision

Six (first day) or two positive samples in three days were tested. CV for reproducibility was ≤ 15 % for samples with absorbance higher than 0.12.

Range

The range for the method was set from the first dilution to the last dilution where the absorbance was higher than 0.1. The range for this validation was dilution 1000x - 128000x of the tested sera.

Linearity

Linearity was approved by using linear regression for the dependence of the logarithm of absorbance on the logarithm of the dilution that is usually used for the ELISA method. Calculation was performed in software Combistat. The correlation coefficient was higher than 0.95. Analysis of variance (ANOVA) was used for evaluation of regression significance and non-significance of parameter “non-linearity”. Linearity from three separate days confirmed parallelism.

The validation of the method confirmed that the method is suitable for verifying the efficacy of the product containing toxins of *Clostridium perfringens* and *Clostridium difficile*. The ELISA protocol and the validation report is attached in **Supplementary data**.

Detection of antibodies against CPA, CPB1, CPB2, ETX, and TcdA in the serum of mice immunized with commercial vaccines using the optimized ELISA method

The optimized ELISA protocols were used to test 45 murine sera for the presence of antibodies against CPA, CPB1, CPB2, ETX, and TcdA. Mice (groups of 5) were immunized with two vaccines already developed by Dyntec s.r.o. (named Dyn 1 and Dyn 2), four vaccines under development by Dyntec s.r.o. (named DV 1-4), and three commercial competitive vaccines (named CV 1-3) (Table 9.). Individual vaccines were then compared based on the level of detected antibodies.

Table 9. Summary of the nine tested vaccines

Name	Listed antigens	Tested antigens
Dyn 1	C. perfringens A, C; C. Difficile	CPA, CPB1, CPB2, ETX, TcdA
Dyn 2	C. perfringens A, C; C. Difficile	CPA, CPB1, CPB2, ETX, TcdA
CV 1	C. Perfringens C	CPA, CPB1, CPB2
CV 2	C. Perfringens B, C, D	CPA, CPB1, CPB2, ETX
CV 3	C. Perfringens A, C, D	CPA, CPB1, CPB2, ETX
DV 1	C. perfringens A, C	CPA, CPB1, CPB2, ETX
DV 2	C. perfringens A, C	CPA, CPB1, CPB2, ETX
DV 3	C. perfringens A, C	CPA, CPB1, CPB2, ETX
DV 4	C. perfringens A, C	CPA, CPB1, CPB2, ETX

The overall comparison of all vaccine samples (Fig. 49) suggests that the vaccines under development by Dyntec s.r.o. have parameters at least comparable to those found in the best commercial competitive vaccines. The test also confirmed the presence of antibodies against toxin A from *C. difficile* in Dyn 1 and Dyn 2 vaccines, unique vaccines containing this significant antigen.

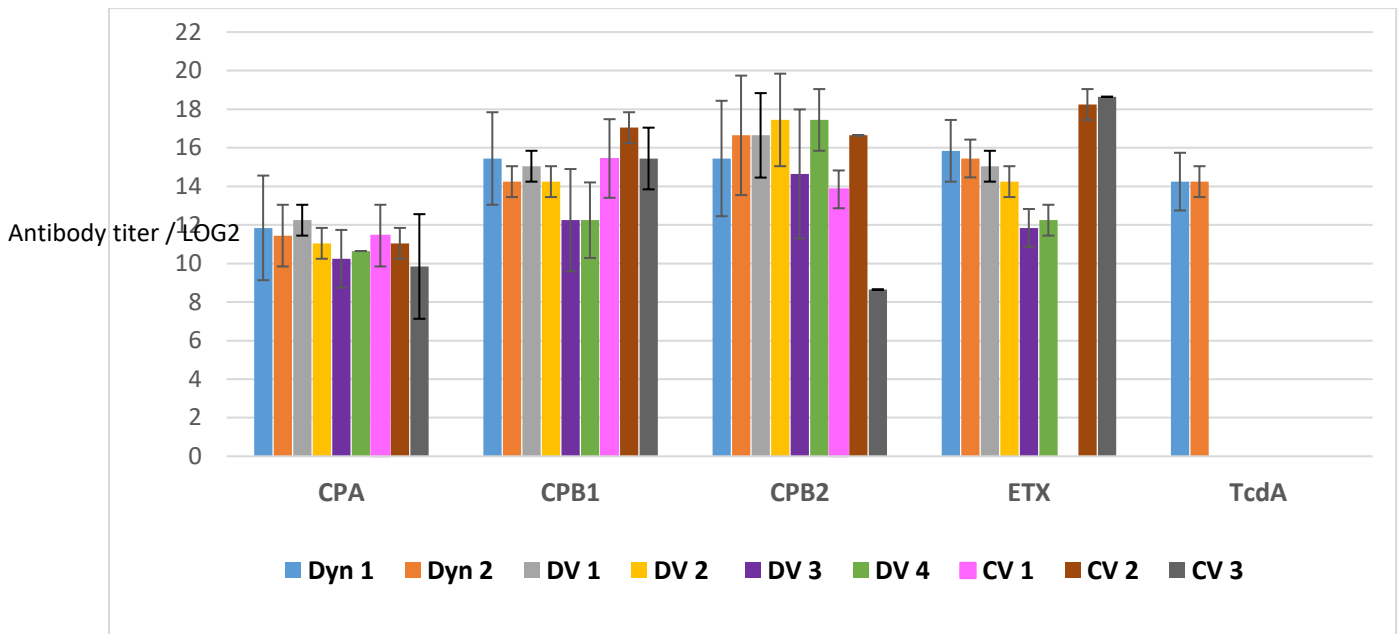


Figure 49. Overall comparison of the efficiency of nine vaccines tested by the validated ELISA protocols. Mice (groups of 5) were immunized with nine different vaccines. Two vaccines already developed by Dyntec, s.r.o. (Dyn 1 and Dyn 2), four vaccines under development by Dyntec, s.r.o. (DV 1-4), and three commercial competitive vaccines (CV 1-3). In total, 45 murine sera were compared based on the antibody titer against five different antigens (CPA, CPB1, CPB2, ETX, and TcdA).

Summary

Clostridium perfringens and *Clostridium difficile* are widespread gram-positive anaerobic bacteria whose most significant virulence factors include secreted toxins. *C. perfringens* is classified into five toxinotypes (A–E) based on the production of one or more of the four major toxins alpha, beta, epsilon, and iota. In addition to the so-called “major” toxins, there are other toxins, such as beta 2 toxin, produced by some strains of *C. perfringens*. Recombinant toxins CPA, CPB1, CPB2, ETX from *C. perfringens* and TcdA toxin from *C. difficile* were successfully expressed in *E. coli* in the soluble form and characterized using SDS-PAGE and WB. These recombinant antigens were then used as standards for the development of sensitive and specific ELISA protocols for the quantitation of antibodies in murine sera. Parameters and criteria of the acceptability for the ELISA validation were tested, demonstrating that the ELISA test developed in this study provides the required specificity and sensitivity for detection of

clostridial toxins CPA, CPB1, CPB2, ETX, and TcdA. In addition, the optimized ELISA protocols were used for comparison of the efficacy of the vaccines, currently under development by Dyntec s.r.o., with the corresponding commercial best-of-class vaccines. The results demonstrate that samples of the Dyntec vaccines have at least comparable parameters in the four tested valences as the competitor products, but novel vaccines will be produced as 10-valent protective vaccines currently not available on the market. These developed ELISA protocols, therefore, form an integral part of the official validation documentation required for certification of the vaccines by both Czech and European veterinary authorities and will be used by Dyntec s.r.o. for the quality testing of their future commercial products.

4. Discussion

The natural mammalian Ig repertoire, a highly efficient mechanism of humoral defense, has been successfully exploited for scientific and commercial purposes for generation of antibodies with the desired binding properties. Monoclonal antibodies have become the "gold" standard of biomedicine. Although they continue to lead in the field of medical therapy, they still possess some limitations in many other applications such as *in vitro* and *in vivo* diagnostics. The rapid development of *in vitro* selection techniques such as ribosome display technology has proven to be a powerful tool for generating binding molecules to almost any antigen of interest. Diversity can be artificially introduced into non-immunoglobulin (non-Ig) scaffolds, making it possible to derive binders with specificities and affinities comparable to those derived from antibody-based genetic libraries. These novel binders exhibit features that had previously been solely attributed to antibodies. Furthermore, they possess several beneficial properties, such as small size, efficient refolding ability, high protein stability and solubility, and simple production that can lead to a reduction in cost in downstream processing. In addition, construction of novel binders using different non-Ig scaffolds has the advantage of creating new binding surfaces of different geometries, making it possible to target a broader spectrum of molecules. Some epitopes have been shown not to be sufficiently immunogenic to be effectively detected by antibodies such as polysaccharides, nucleic acids and lipids, or they are just inaccessible to such large molecules as antibodies. In these cases, a niche for small binding proteins has been created to overcome such limitations. As a consequence, the number and complexity of these types of binders continues to grow every year.

The ABD scaffold, derived from the three-helix bundle of the albumin-binding domain of streptococcal protein G, represents one of small non-Ig scaffolds. In our laboratory, we have established a highly complex combinatorial library developed on the ABD scaffold. It has been already demonstrated that this library can be used for generation of high-affinity binders of human interferon gamma [23] or for novel IL-23 receptor antagonists with a promising anti-inflammatory potential [26]. Therefore, we used this ABD scaffold-derived library to generate unique binders of human PSP94, KLK2, KLK11 for the diagnosis of prostate cancer, binders of human EpCAM and N-cadherin for the detection of circulating tumor cells in the diagnosis of lung adenocarcinoma, and binders of B subunit of Shiga Stx1 toxin for their directed exposure on the surface of engineered *Lactococcus lactis* cells.

The first part of the thesis was aimed to the development of unique binders to prostate cancer (PCa) biomarkers for more accurate diagnosis of PCa. In 1986, PSA (prostate-specific antigen) screening was approved by the US Food and Drug Administration (FDA) as a supplementary test to the digital rectal examination (DRE) for PCa diagnosis. Since that, PSA screening has been broadly implemented among physicians and massively exploited for PCa diagnosis. Currently, the PCa diagnosis that relies on the detection of the serum level of PSA has become controversial due to the lack of specificity and increasing rates of overdiagnosis. Many men were diagnosed with clinically indolent cancer while they were asymptomatic, leading to unnecessary therapeutic intervention. Although the elevated level of PSA is a very important indicator, no single biomarker is likely to have the appropriate degree of certainty to efficiently diagnose all patients due to the heterogeneity of PCa. Consequently, the future of PCa diagnosis might rely on the combination of multiple biomarkers that can give accurate information about the cancer presence, disease stage, metastasis, and the need for targeted systemic therapy. Therefore, a simple and accurate device must be developed for this purpose. In an effort to improve PCa screening methods, a new wave of PCa biomarkers has emerged that have higher PCa specificity than PSA and its isoforms [103]. The newly found biomarkers have become the basis for the development and approval of new tools for the PCa diagnosis. Except for the already mentioned PSA (KLK3), other members of kallikrein family such as KLK2 and KLK11 have been considered as valuable prognostic markers in combination with other screening tools. For example, the 4Kscore® Test (OPKO Health, Miami, FL) measures the plasma levels of four prostate-derived kallikrein proteins. The levels of these biomarkers are combined with age and digital rectal examination to predict the risk of finding the Gleason score ≥ 7 upon biopsy. The 4Kscore decreases the number of unnecessary biopsies by 49 % to 57 % among men being screened for the first time, but is not appropriate for men who have undergone DRE in the previous 96 hours or men who have undergone any therapy or procedure for symptomatic benign prostate hyperplasia. Another example of a newly developed blood test is Apifyny (Armune Bioscience, Kalamazoo, MI), which measures the expression of eight PCa-specific autoantibodies. Beside direct detection of protein biomarkers in the blood or urine, other approaches have emerged to diagnose PCa. Currently, the assays based on the detection of mRNA specific for PCa have been considered as promising (e.g. mRNA corresponding to the fusion gene *TMPRSS2:ERG*, long noncoding RNA, elevated mRNA levels of distal-less homeobox 1 (*DLX1*) and homeobox C6 (*HOXC6*)). With the progress in high-throughput methods and automatization, quantitative multiplex proteomic-based tests are also on the rise [103].

We favored a proposal of a simple biosensor that can simultaneously detect multiple biomarkers in human serum as a possible solution that could reduce overtreatment of the prostate cancer patients. Therefore, we focused on serum protein biomarkers. According to the literature, we selected PSP94, KLK2, and KLK11 PCa biomarkers for the generation of novel binders. The serum levels of kallikreins, including PSA, have been shown to increase during the development of PCa, while the expression of PSP94 declines from normal physiological values. Monitoring of the serum ratio of kallikreins/PSP94 can be more confirmative, and therefore improving the accuracy of the diagnosis. It is obvious that the assay will never be a self-explaining outcome and consequently must be combined with other clinical characteristics such as the patient's age, weight, and prostate size. However, the detection and evaluation of these biomarkers can offer additional valuable information that can help physicians and patients in the assessment of the PCa severity and for decision making on further therapy.

Novel binders targeting PSP94 PCa biomarker (PAB binders), KLK2 and KLK11 PCa biomarkers (KLA and HIP binders) were generated and registered in the RIV database (the database of research results, experimental development and innovations administered by the *Ministry of Education, Youth and Sports of the Czech Republic*). The most promising binders were biophysically and functionally characterized. To characterize the PAB binders using flow cytometry, LNCaP prostate cells were successfully used as a model cell line expressing native PSP94. Despite that PSP94 is a secreted protein lacking a transmembrane anchor, its presence has been localized on the cell surface by its autoreceptor, 37kDa laminin receptor precursor [63]. Very little is known about its binding proteins on the cell surface, and there are likely more binding proteins to be elucidated in this process. Based on the flow cytometry experiments, PAB046 and PAB050 variants were shown to recognize the PSP94 target protein in its native conformation and were selected as the most promising binders of PSP94. The presented PAB, KLA, and HIP binders, after subsequent modifications, are available for the development of novel multi-factorial biosensors for more precise PCa diagnosis.

The ABD scaffold appears to have appropriate properties for the development of biosensors, where high shearing forces, pH changes, and reducing or denaturing conditions usually lead to the loss of antibody function, complicating its utilization. Consequently, this proven library was used for generation of the binders intended to selectively recognize different phenotypes of circulating tumor cells (CTCs) as a part of the cell capture zone of the microfluidic chip for the diagnosis of lung adenocarcinoma. CTCs have been shown to be a valuable clinical marker for diagnosis of different kinds of cancer. Unfortunately, the cellular heterogeneity and low

abundance of CTCs in the blood represent a big analytical challenge. In patients with advanced solid cancer, CTCs often occur at a concentration of one CTC per 10 million of white blood cells (WBCs) surrounded by millions of small red blood cells in one ml of the blood sample. Since very sophisticated separation approaches for red blood cell depletion have been developed, the leukocyte contamination remains the most common contamination of samples that may lead to false-positive results and false interpretation. Most detection strategies of CTCs are based on the detection of epithelial marker EpCAM, which is missing on WBCs. Although antibodies are the most common detection molecules, non-Ig binders of EpCAM have been already demonstrated [104, 105]. The disadvantage of all detection methods solely based on EpCAM is that due to the epithelial-mesenchymal transition process, many CTCs lose their epithelial phenotype and become cells with mesenchymal properties. Such assays result in reduction of the already low number of captured cells during the selection. Therefore, we focused on the development of two collections of binders: EBA binders, targeting epithelial membrane marker EpCAM, and CAB binders, targeting mesenchymal membrane marker N-cadherin. The study of mesenchymal cancer cells is complicated by their demanding cultivation. The majority of the described markers of mesenchymal cells are intracellular molecules (e.g. vimentin) unsuitable for separation and detection purposes. N-cadherin belongs to the small group of identified surface mesenchymal markers. It is composed of five extracellular domains protruding from the surface of the cell membrane and convenient for targeting by capture molecules.

Out of the collections of EBA and CAB binders, three selected variants EBA014, EBA062, and CAB101 appear to be the most promising binders based on their cell selectivity demonstrated by binding to real cells of particular phenotype using the LigandTracer device. EBA014, which showed the highest affinity in LigandTracer experiment, was chosen for *in vitro* affinity maturation using error-prone PCR. This 2nd-generation plasmid library is currently being analyzed for novel EBA014 variants with an improved binding affinity and required cell selectivity.

In addition to the collection of binders derived from the ABD scaffold, there was a motivation to use N-cadherin and EpCAM as model targets for testing the potential of newly developed libraries derived from the Myomedin scaffold to yield a novel kind of binders that will be able to recognize other epitopes on the target molecules. The development of a combinatorial library based on a new scaffold was triggered by the fact that the flat randomized ABD surface between helices 2 and 3 may limit identification of the binding candidates of some surface (glyco)peptide

epitopes. In addition, some ABD-derived binders still retain a residual affinity to serum albumins, yet weakened by several orders of magnitude by scaffold randomization. However, it could still cause complications in diagnostic use of the binders expected to detect markers of very low concentration in the serum. Moreover, the human origin of Myomedin allows its easier utilization for therapeutic purposes by minimizing the response of the immune system. Starting from a stable Myomedin scaffold optimized for expression in an *E. coli* host, computational analysis of its structure and binding properties was performed in order to identify residues suitable for randomization with the purpose of generating a combinatorial library. Two different strategical approaches were proposed. In the first one, amino acid residues of three different loops were randomized, while in the second case, residues of anti-parallel beta sheets were selected for the randomization. Both libraries were used for the generation of binders targeting EpCAM and N-cadherin, now being analyzed for the best binding individuals. The developed protein binders with engineered selectivity and sufficient binding affinity will be used for construction of a cell-sorting unit of the microfluidic chip in the collaborating laboratory at the University of J.E. Purkinje. The proposed microfluidic device is intended to capture and in the next step release the cell of the particular phenotype for subsequent cultivation and further characterization. It is a unique system that requires special properties of the capture agents. Our generated binders are going to be modified to fulfil these tough requirements.

The third part of the thesis was devoted to the generation of ABD-derived binders to the Shiga toxin (Stx) B subunit (S1B binders). It has been shown that Shiga toxin receptor analogs, which bind to the toxin in the gastrointestinal tract (GI), are able to prevent its activity, and thereby have been considered as a potential therapeutic tool for treating infections with Shiga toxin-producing bacteria. The current treatment only relies on nonspecific supportive therapy such as conventional antibiotic treatment, which increases risk of the development of hemolytic-uremic syndrome by induction of Stx expression and the toxin release into the gut. It is obvious that new alternative therapies are highly demanded. Various potential therapeutic strategies are currently under development, including monoclonal antibodies against Stx, compounds directed against Stx-producing bacteria, Stx receptor analogs, receptor synthesis and processing inhibitors, and also novel antimicrobial therapies [106]. We have proposed an interesting alternative – a model of engineered *Lactococcus lactis* cells displaying S1B binders capable of binding the Shiga toxin on their surface, and thus scavenging it from the GI tract. Furthermore, *L. lactis* was shown to be able to inhibit Shiga toxin-producing bacteria by the production of lactic acid, thus increasing its therapeutic effect [107]. The display of non-Ig scaffolds such as

Affibodies and DARPins on the surface of *L. lactis* has been already demonstrated, providing the functionality of this model [89]. The ABD scaffold as a small molecule without disulfide bonds capable of fast refolding was selected as an appropriate compound for the *L. lactis* surface display. To generate the S1B binders, only the B subunit of Shiga toxin (Stx1B) was used as a target molecule, because it is capable of binding to the receptor and is not toxic by itself. The most promising S1B binders were biochemically, biophysically and functionally characterized, displayed on the surface of *L. lactis*, and their ability to bind Stx1B was confirmed. Moreover, S1B binders represent an additional class of alternative binding proteins that could be used for neutralization of the Shiga toxin in the human intestine during infections with Shiga toxin-producing bacteria or alternatively for other diagnostic purposes.

This thesis is mainly focused on the diagnosis of different kinds of diseases. The goal of the last part also follows the diagnostic direction and is devoted to the development of an enzyme-linked immunosorbent assay (ELISA) kit for the detection of toxins produced by *Clostridium perfringens* and *Clostridium difficile* to validate the developing polyvalent vaccines against bacterial enteral diseases. The anaerobic bacteria *Clostridium perfringens* and *Clostridium difficile*, etiological agents of diarrheal diseases of pigs and cattle, are becoming drug-resistant and request prevention and control strategies. It has been demonstrated that protection against the various manifestations of diseases caused by *C. perfringens* and *C. difficile* is mediated by antibodies induced to the type-specific clostridial toxins. Therefore, polyvalent vaccines with or without adjuvants prepared by Dyntec s. r. o. were evaluated against five clostridial toxins (CPA, CPB1, CPB2, ETX, and TcdA). Beside mentioned clostridial agents, the developing vaccine consists of five virulent mediators of *E. coli* (data not shown), making it unique by the number of the used valences. The production of such vaccine would have a valuable impact on the survival of piglet and calves without the need for repeated vaccination.

The development, optimization, and analytical validation of an ELISA procedure for the assessment of specific antibodies against five clostridial toxins included in the developing vaccine were described. For this purpose, sera obtained from the mice that received the vaccine were used. We supplied the assay performance validation in terms of sensitivity, reproducibility, precision, and accuracy. The developed ELISA showed reproducibility and reliability, making it valid for evaluation of all tested antigens. In addition, the optimal antigen-coating concentrations and ELISA conditions were described in detail, making it available for laboratories performing these assays in order to standardize the method.

The validated ELISA assay was then used for comparison of the efficacy of the novel vaccines currently under development by Dyntec s.r.o. with commercially available best-of-class vaccines. The comparison included all the appropriate controls, which allowed us to conclude that the developing Dyntec vaccines have at least comparable parameters as the best competitor products. In conclusion, we confirm that the ELISA test can be recommended as a reference method for the determination of antibodies against all tested antigens.

5. Materials and Methods

Cell lines and growth conditions

Androgen-sensitive human prostate adenocarcinoma cell line **LNCaP** (ATCC CRL 1740) was grown in RPMI-1640 medium (Sigma-Aldrich, St. Louis, MO) supplemented with 10% fetal calf serum (FCS) (GIBCO, Grand Island, N.Y.) and antibiotic antimycotic solution (ATB) (Sigma-Aldrich, St. Louis, MO) in 5% CO₂ at 37 °C. Cells of human breast cancer cell line **MCF-7**, prostate cancer cell lines **DU-145** and **PC-3**, normal skin fibroblasts **CCD1070Sk** (ATCC CRL 2091), and human embryonic kidney cells **HEK293** were grown in DMEM medium (Biosera, Nuaille, France) supplemented with 10% FCS and ATB in 5% CO₂ at 37 °C. *L. lactis* **NZ9000** was grown in M-17 medium (Merck) supplemented with 0.5% glucose (GM-17) and 10 µg/ml chloramphenicol at 30 °C without aeration. Bacterial *E. coli* strains **XL1Blue**, **DH5α**, **BL21 (DE3)** and **BL21 (DE3) BirA** were grown at 37 °C, the **SHuffle** strain at 30 °C, unless otherwise stated, with aeration in lysogeny broth (LB) medium supplemented with 60 µg/ml kanamycin. Bacterial *E. coli* strains **ArcticExpress (DE3)** and **ArcticExpress RIL (DE3)** were grown at 30 °C and 13 °C after induction of IPTG with aeration in LB medium supplemented with 60 µg/ml kanamycin and gentamycin.

Antibodies, detection agents and recombinant proteins

The crucial antibodies, detection agents, and commercial recombinant proteins used in this work are summarized in Table 10.

Table 10. Summary of antibodies, detection agents, and recombinant proteins

Targets	Primary antibodies	Secondary antibodies and detection agents	Recombinant proteins
PSP94	Mouse monoclonal antibody to Prostate Secretory Protein/PSP [YSPSP-1] (ab19070) (Abcam, Cambridge, UK) Rabbit monoclonal antibody to Prostate Secretory Protein/PSP [EPR7345] (ab128897) (Abcam, Cambridge, UK) Rabbit polyclonal antibody PSP94 (H-114): sc-68920 (Santa Cruz Biotechnology, Inc., Dallas, USA)	Polyclonal Goat anti-rabbit HRP-conjugated IgG (R&D Systems, Minneapolis, MN) Polyclonal Goat anti-mouse HRP-conjugated IgG (Biolegend, San Diego, CA) Cy5-conjugated goat anti-mouse IgG (F(ab') ₂ fragment) Cy5-conjugated goat anti-rabbit IgG (Jackson ImmunoResearch Laboratories, West Grove, PA)	
KLK2	Goat polyclonal anti-KLK2 antibody (AP16632PU-N) Rabbit polyclonal anti-KLK3 antibody	FITC-conjugated donkey anti-goat IgG (Jackson ImmunoResearch Laboratories, West Grove, PA)	
EpCAM	Rabbit polyclonal Anti-EpCAM antibody ab195577 (Abcam, Cambridge, UK)	Alexa Fluor 647 Donkey anti-rabbit IgG (minimal x-reactivity) antibody (BioLegend, San Diego, CA) Goat Anti-Rabbit IgG H&L (HRP) ab97051 (Abcam, Cambridge, UK)	Recombinant human EpCAM protein ab155712 (Abcam, Cambridge, UK)

N-cadherin	Monoclonal Anti-N Cadherin antibody [8C11] ab19348 (Abcam, Cambridge, UK)	Alexa Fluor 647 Goat anti-mouse IgG (minimal x-reactivity) antibody (BioLegend, San Diego, CA) HRP Goat anti-mouse IgG (minimal x-reactivity) Antibody (BioLegend, San Diego, CA)	Human N-cadherin /CD325/CDH2D Protein (HisTag) (Sino Biological Inc., Beijing, China)
Biotinylated protein		Thermo Scientific Pierce Streptavidin HRP Conjugate High Sensitivity (Thermo Fisher Scientific Inc.) APC streptavidin (BioLegend, San Diego, CA)	Recombinant streptavidin (Sigma-Aldrich, St. Louis, MO)
His-Tag		Anti-His ₆ -Peroxidase (Roche, Basel, Switzerland)	

Production of recombinant proteins

Production of recombinant variants of PSP94

Vector pDNR-LIB containing cDNA of the mature 114 residue-long PSP94 was purchased from Geneservice Ltd. (Cambridge, UK) (GenBank: BC005257.1; UniProt: P08118-1.). Four different recombinant variants of PSP94 were designed and produced in soluble form in different *E. coli* strains.

His-PSP94

The sequence of PSP94 without signal sequence was amplified by PCR using a forward primer containing the start codon and *NdeI* restriction site (ACTTCATATGTCATGCTATTTTCATACCTAATG), and a reverse primer containing the stop codon and *BamHI* restriction site (GCGGATCCTTAGATTATCCATTCACTGACA). The resulting PCR product was inserted into the pET-28b vector (Novagene, Germany) using *NdeI* and *BamHI* cloning sites and introduced into *E. coli* DH5 α cells (New England Biolabs, Ipswich, MA). The obtained plasmid was used for protein production in ArcticExpress (DE3) *E. coli* cells (Agilent Technologies, US). Competent cells were transformed with the protein expression plasmid, using a 37°C cultivation temperature. Several transformants were picked to grow overnight cultures in LB medium containing gentamycin (60 μ g/l) and kanamycin (60 μ g/l) at 37°C. Bacterial cells were grown in 400 ml LB medium without antibiotic selection for 3 hours at 30°C and then induced with 1 mM isopropyl- β -d-thiogalactopyranoside (IPTG) at 10°C, and continued to grow for an additional 24 hours. Cells were harvested by centrifugation at 6,000 g for 15 min. The pellet was resuspended in 20 ml of T50N300 buffer (50 mM Tris, 300 mM NaCl, pH 8.0) and disrupted by ultrasound pulses (Misonix S3000). The lysate was centrifuged for 20 min at 40,000 g and the cytosolic extract (CE) was purified by NiNTA affinity chromatography (QiaGen, Germany). CE was applied to the Ni-NTA columns with 1 ml NiNTA agarose equilibrated with T50N300 buffer and the columns were washed with 20 ml of wash buffer (T50N300 buffer containing 50 mM imidazole). Proteins were eluted with 5 ml of T50N300 buffer containing 250 mM imidazole. The protein expression was analyzed by SDS-PAGE and Western blot (WB). The obtained elution fractions were further purified by gel permeation chromatography (ÄktaTM Purifier; column Superdex 75, 16/60, 50 mM Tris, 100 mM NaCl, pH 8.0).

Strep-PSP94

The sequence of PSP94 without signal sequence was amplified by PCR using a forward primer containing the start codon, *NcoI* restriction site, and Strep Tag II sequence (WSHPQFEK) (CGCGCCATGGCAAGCTGGAGCCACCCGCAGTTCGAAAAGCATATGTCATGCTATTCATACCTAATGAGG) and a reverse primer containing the stop codon and *BamHI* restriction site (GCGGATCCTTAGATTATCCATTCCTGACA). The resulting PCR product was inserted into the pET-28b vector using *NcoI* and *BamHI* cloning sites and introduced into *E. coli* DH5 α cells. The obtained plasmid was used for protein production in BL21 (DE3) *E. coli* cells (New England Biolabs, Ipswich, MA). Competent cells were transformed with the protein expression plasmid, using a 37°C cultivation temperature. Several transformants were picked to grow overnight cultures in LB medium containing kanamycin (60 μ g/l) at 37°C. Bacterial cells were grown in 400 ml LB medium without antibiotic selection for 3 hours at 37°C and then induced with 1 mM IPTG and continued to grow for an additional 4 hours. Cells were harvested by centrifugation at 6,000 g for 15 min. The pellet was resuspended in 20 ml of PBS buffer (137 mM NaCl, 2.7 mM KCl, 10 mM Na₂HPO₄ • 2 H₂O, 2 mM KH₂PO₄, pH 7.4) and disrupted by ultrasound pulses. The lysate was centrifuged for 20 min at 40,000 g and CE was purified by Strep-Tactin Superflow high capacity cartridge H-PR (Iba, Germany) (Äkta™ Purifier). The protein expression was analyzed by SDS-PAGE and WB.

His-PSP94-TolA-Avi

The sequence of PSP94 without signal sequence was amplified by PCR using a forward primer designed to contain the start codon, N-terminal 6xHisTag, and *NcoI* restriction site (ATATCCATGGGCAGCAGCCATCACCATCACCATCATAGCAGCGGCTCATGCTATTTCATACCTAATGAGGG) and a reverse primer missing the stop codon and containing *BamHI* restriction site (CGCGGGATCCGATTATCCATTCCTGACAGAACA). This PCR product was digested with restriction enzymes *BamHI* and *NcoI* and cloned into the pET-28b vector containing the TolA sequence and AviTag consensus sequence (GLNDIFEAQKIEWHE). This plasmid was obtained from the WT-ABD-TolA-AviTag pET28b plasmid (prepared according to Ahmad, J.N. et al., 2012; Kuchař, M. et al., 2013) by restriction digestion using restriction enzymes *BamHI* and *NcoI* (excision of WT-ABD sequence). Ligated plasmid was introduced into *E. coli* DH5 α cells, and the obtained plasmid was used for biotinylated protein production in BL21 (DE3) BirA *E. coli* cells, expressing biotin ligase (BirA). Twenty-five μ l of BL21 *E. coli* BirA competent cells were transformed with 3 μ l of pET28-b plasmid containing the N-6xHisTag-PSP94-TolA-AviTag fusion variant. Two ml of LB medium containing chloramphenicol (60 μ g/l), and kanamycin (60 μ g/l) was inoculated with several transformants to grow overnight cultures at 37°C. Bacterial cells were grown in 5 ml LB medium without antibiotic selection for 3 hours at 37°C and then 50 μ M D-biotin was added (Sigma-Aldrich) in 10 mM bicine buffer, pH 8.34 and induced with 1.5 mM IPTG. The cultivation continued for an additional 4 hours. Cells were harvested by centrifugation at 14,000 g for 5 min. The pellet was resuspended in 700 μ l of lysis buffer (50 mM Tris, 300 mM NaCl, 10 mM imidazole, pH 8.0) containing 70 μ l of lysozyme solution (1 mg/ml), and Benzonase® Nuclease (3 units/ml culture volume) (Merck-Millipore, Darmstadt, Germany). The lysate was purified by NiNTA affinity chromatography according to the NiNTA Spin Columns protocol (QiaGen, Germany). The protein expression was analyzed by SDS-PAGE and WB.

His-Strep-GFP-PSP94

For immobilization of PSP94 to biotinylated surfaces with bound Streptactin and for fluorescent detection, fusion protein His-Strep-GFP-PSP94 was prepared. DNA coding for the entire construct including restriction sites, start codon, GSS and SSG linkers joining particular peptides and protein domains, as well as stop codon and optimized for expression in *E. coli* was synthesized by GeneArt® Gene Synthesis (Life Technologies™). The DNA sequence with restriction sites *NcoI* and *XhoI* was inserted by T4 ligase into vector pET-28b and cloned in *E. coli* XL1blue strain. Protein was produced in *E. coli* SHuffle strain (SHuffle® T7 Express Competent *E. coli*, NEB) to promote disulfide bond formation in PSP-94 in the cytoplasm. Bacterial cells were grown in LB broth with kanamycin (60 µg/l) at 30°C, protein production was induced by adding 0.5 mM IPTG after the culture reached the density of OD₆₀₀ = 0.6, and the cells were collected by centrifugation 4 hours after the induction. The pelleted cells were disrupted by sonication in TN buffer (50 mM Tris, 150 mM NaCl, pH = 8.0) and spun down at 40,000 g for 20 min. Soluble protein was purified using Ni-NTA affinity chromatography and the resulting protein was eluted in elution buffer EB (50 mM Tris, 150 mM NaCl, 250 mM imidazole, pH = 8.0).

Production of recombinant variants of KLK2 and KLK11

Vector pDNR-LIB containing cDNA of the mature KLK2 and KLK11 was purchased from Geneservice Ltd. Two different recombinant variants of KLK2 without the inhibition pro-sequence were produced in *E. coli* BL21 (DE3) and refolded from inclusion bodies. His-KLK11 was produced without the inhibition pro-sequence in soluble form in the *E. coli* SHuffle strain.

His-KLK2 and Strep-KLK2

The sequence of KLK2 without inhibition pro-sequence was amplified by PCR using a forward primer containing the N-terminal HisTag and *NdeI* restriction site (CGCGCATATGATTGTGG GAGGCTGGGAGT) or the N-terminal Strep Tag II and *NdeI* restriction site (CGCGCCATGGCAAGCTGGAGCCACCCGCAGTTCGAAAAGCATATGATTGTGGGAGGCTGGGAGTGT), and a reverse primer containing the stop codon and *BamHI* restriction site (GCGGATCCTCAGGGGTTGGCTGCGA). The resulting PCR products were inserted into the pET-28b vector using *NdeI* and *BamHI* cloning sites and introduced into *E. coli* DH5α cells. After sequencing, the verified plasmids were used for protein production in *E. coli* BL21 (DE3). Competent cells were transformed with the protein expression plasmid, using a 37°C cultivation temperature. Several transformants were picked to grow overnight cultures in LB medium containing kanamycin (60 µg/l) at 37°C. Bacterial cells were grown in 400 ml LB medium without antibiotic selection for 3 hours at 37°C and then induced with 1 mM IPTG and continued to grow for an additional 4 hours. Cells were harvested by centrifugation at 6,000 g for 15 min. The pellet was resuspended in 20 ml of T50N300 buffer and disrupted by ultrasound pulses. The lysate was centrifuged for 20 min at 40,000 g and inclusion bodies (INK) were repeatedly washed in T50N300 buffer pH 8 containing 2M urea and 0.05% tween. INK were dissolved in T50N300 buffer pH 8 containing 8M urea and efficiently refolded to T50N300 buffer pH 8 using gradual dialysis. The soluble His-KLK2 was further purified by gel permeation chromatography (Äkta™ Purifier; column Superdex 75, 16/60, 50 mM Tris, 100 mM NaCl, pH 8.0). The soluble Strep-KLK2 was purified by Strep-Tactin Superflow high

capacity cartridge H-PR (Iba, Germany) (Äkta™ Purifier). The protein expression was analyzed by SDS-PAGE and WB.

His-KLK11

The sequence of KLK11 without inhibition pro-sequence was amplified by PCR using a forward primer containing the *NdeI* restriction site (GCGCCATATGATCATCAAGGGGTTTCGAGTGCA A) and a reverse primer containing the stop codon and *XhoI* restriction site (CGCTCTCGAGCTAATTGTTCTTCATCGTCTCCT). The resulting PCR products were inserted into the pET-28b vector using *NdeI* and *XhoI* cloning sites and introduced into *E. coli* DH5 α cells. The verified plasmid was used for protein production in the *E. coli* SHuffle strain. Bacterial cells were grown in LB broth with kanamycin (60 μ g/l) at 30°C, protein production was induced by adding 1 mM IPTG after the culture reached the density of OD₆₀₀ = 0.6, and the cells were collected by centrifugation 4 hours after the induction. The pelleted cells were disrupted by sonication and spun down at 40,000 g for 20 min. Soluble protein was purified using Ni-NTA affinity chromatography. The protein expression was analyzed by SDS-PAGE and WB.

Production of recombinant variants of EpCAM and N-cadherin

Invitrogen GeneArt® Strings carrying optimized cDNA for expression of the 243 amino acid residue-long extracellular domain of EpCAM (GenBank accession no. M32325) and the two last C-terminal extracellular domains of N-cadherin composed of 224 amino acids (GenBank accession no. X57548), containing N-terminal HisTag and C-terminal AviTag sequences (HEP and HCA) or C-terminal HisTag and AviTag sequences (EPH and CAH), were purchased from Thermo Fisher Scientific Inc. as synthetic double-stranded DNA fragments ready for cloning using *NcoI* and *XhoI* restriction sites into the pET-28b vector. The vector was introduced into *E. coli* DH5 α host cells or, for protein production, into *E. coli* BL21 (DE3) BirA. HEP and EPH were isolated in the form of inclusion bodies and after dissolution purified by affinity chromatography using Ni-NTA agarose in denaturing conditions (Qiagen, Germany). Eluted fractions in 50 mM Tris, 300 mM NaCl, 8 M urea, pH 5.0 were analyzed by SDS-PAGE and Western blot by anti-His₆-peroxidase and streptavidin-HRP conjugate. HCA and CAH were produced in soluble form in CE and purified using Ni-NTA agarose. Eluted proteins were subjected to further purification by gel permeation chromatography (Äkta™ Purifier; column Superdex 75, 16/60, 50 mM Tris, 100 mM NaCl, pH 8.0). Recombinant N-cadherin containing the N-terminal HisTag without C-terminal AviTag (CAD) was generated from DNA of the HCA product using PCR with forward primer (TATACCATGGGCAGCAGC) and reverse primer (TATTCTCGAGTCAAATTCAGGCGGATTATCATTAAC). The PCR product was digested with restriction enzymes *XhoI* and *NcoI* and cloned into the pET-28b vector and sequentially verified. The plasmid was then introduced in BL21 (DE3) *E. coli* cells for protein production. Soluble protein was purified from the cytosolic extract using Ni-NTA affinity chromatography and gel permeation chromatography (Äkta™ Purifier). The protein expression was analyzed by SDS-PAGE and WB.

Production of recombinant Stx1B subunit

The gene for Stx1B was designed, *de novo* synthesized by ATG Biosynthetics (Merzhausen, Germany), and cloned to plasmid pET28b using *NcoI/XhoI* restriction sites, yielding pET28-Stx1B. Overnight culture of *E. coli* BL21 (DE3) harboring plasmid pET28-Stx1B was diluted

(1:100) in 1 l of fresh LB medium and grown to optical density $A_{600} = 3.5-4.0$. Expression of fusion protein Stx1B with a hexa-histidine (his₆) tag was induced by addition of 1 mM isopropyl β -D-1-thiogalactopyranoside (IPTG) for 3 h at 28 °C. The culture was centrifuged at 5,000 g for 15 min and the pellet was resuspended in 30 ml of equilibration/wash (Eq/W) buffer (50 mM NaH₂PO₄, 300 mM NaCl, pH 7.0). The cells were lysed by a cycle of freezing and thawing, and by three times 5 min sonication with a UPS200S sonicator (Hielscher, Teltow, Germany). After cell lysis, the suspension was centrifuged at 15,000 g for 20 min and the supernatant was stored. Inclusion bodies were dissolved in Eq/W buffers with increasing concentrations of guanidinium HCl (1M, 3M and 6M) for 6 h or overnight at 4 °C, followed in each step by centrifugation and supernatant removal. Stx1B-his₆ soluble in Eq/W with 6 M guanidinium HCl was isolated with BD Talon metal affinity resin (BD Biosciences) according to manufacturer's instructions, using batch/gravity-flow column purification and imidazole elution (elution buffer: 45 mM NaH₂PO₄, 270 mM NaCl, 5.4 M guanidinium HCl, 150 mM imidazole, pH 7.0). Fractions containing pure Stx1B were pooled and stored. Recombinant Stx1B was efficiently refolded by 100-fold rapid dilution method in solubilisation buffer (50 mM Tris-HCl with 0.5 M arginine and 0.01% Brij-35, pH 7.5).

Production of recombinant clostridial toxins

Production of recombinant *C. perfringens* toxin Alfa (CPA)

The sequence (134 aa) of the C-terminal domain with flexible linker (275 – 398) of the *C. perfringens* toxin Alpha (CPA) (Uniprot: Q0TV31) and N-terminal HisTag was obtained by PCR amplification of the whole genomic DNA isolated from a veterinary isolate of *C. perfringens* type A using forward (TATACCATGGGCAGCAGCCATCATCATCATCACAATGATCCATCAGTTGGAAAGAATGTAAA) and reverse (GCGCCTCGAGCTATTTGATGTTATAAGTTGAATTCCTGAAATCCACTC) primers. The resulting PCR product was inserted into the pET-28b vector using *Nco*I and *Xho*I cloning sites and introduced into *E. coli* DH5 α cells for sequence verification. The verified plasmid was used for protein production in *E. coli* BL21 (DE3).

Production of *C. perfringens* recombinant toxin Beta (CPB1)

The full-length sequence of the *C. perfringens* toxin Beta (CPB1) (Uniprot: Q46308) without signal sequence (28 – 336) containing the N-terminal HisTag (324 aa) was obtained by PCR amplification of the whole genomic DNA isolated from a veterinary isolate of *C. perfringens* type B using forward (GCGCCCATGGGCAGCAGCCACCACCACCACCACCACAGCAGCGGCAATGATATAGGTAAAATACTACTATACTAGAA) and reverse (TAATCTCGAGTCAGGATCCAATAGCTGTTACTTTGTGAGTAAGCC) primers. The resulting PCR product was inserted into the pET-28b vector using *Nco*I and *Xho*I cloning sites and introduced into *E. coli* DH5 α cells for sequence verification. The verified plasmid was used for protein production in *E. coli* ArcticExpress (DE3) RIL Competent Cells (Agilent Technologies, CA, US).

Production of recombinant *C. perfringens* toxin Beta 2 (CPB2)

The full-length sequence of the *C. perfringens* toxin Beta 2 (CPB2) (Uniprot: Q5MQ79) without signal sequence (31 – 265) containing the N-terminal HisTag (250 aa) was obtained by PCR amplification of the whole genomic DNA isolated from a veterinary isolate of *C. perfringens* type B using forward

(GCGCCCATGGGCAGCAGCCACCACCACCACCACCACAGCAG CGGCAATGAAGTGAATAAATACCAATCTG) and reverse (GCGCCTCGAGTTAGGA TCCGGCACAATACCCTTCACCAAATACTCT) primers. The resulting PCR product was inserted into the pET-28b vector using *NcoI* and *XhoI* cloning sites and introduced into *E. coli* DH5 α cells for sequence verification. The verified plasmid was used for protein production in *E. coli* BL21 (DE3).

Production of recombinant *C. perfringens* toxin Epsilon (ETX)

The full-length sequence of the *C. perfringens* toxin Epsilon (ETX) (Uniprot: Q02307) without signal sequence and pro-peptide (46 – 328) containing the N-terminal HisTag (298 aa) was obtained by PCR amplification of the whole genomic DNA isolated from a veterinary isolate of *C. perfringens* type B using forward (GCGCCCATGGGCAGCAGCCACCACCACCACC ACCACAGCAGCGGCAAAGCTTCTTATGATAATGTAGATACATTAATTG) and reverse (TAATCTCGAGCTAGGATCCCTTTATTCCTGGTGCCTTAATATAAAGAC) primers. The resulting PCR product was inserted into the pET-28b vector using *NcoI* and *XhoI* cloning sites and introduced into *E. coli* DH5 α cells for sequence verification. The verified plasmid was used for protein production in *E. coli* BL21 (DE3).

Production of recombinant *C. difficile* toxin A (TcdA)

The C-terminal part of the **extracellular binding domain** of the *C. difficile* toxin A (Uniprot: Q189K5) (2366 – 2710) containing the N-terminal His Tag (359 aa) was obtained by PCR amplification of the whole genomic DNA isolated from a veterinary isolate of *C. difficile* using forward (GAGCCCATGGGCAGTAGCCACCACCACCACCACCACAGCAGCGGCGTAA CTGGATGGCAAACACTATCA) and reverse (TAATCTCGAGTCAGGATCCGCCATA TATCCAGGGGCTT) primers. The resulting PCR product was inserted into the pET-28b vector using *NcoI* and *XhoI* cloning sites and introduced into *E. coli* DH5 α cells for sequence verification. The verified plasmid was used for protein production in *E. coli* ArcticExpress (DE3) RIL Competent Cells.

Table 11. The protein sequences of expressed recombinant toxins

Recombinant toxin	Amino acid sequence
CPA	MGSSHHHHHHNDPSVGKNVKELVAYISTSGEKDAGTDDYMYFGIKTKDGKTQEWEMDNPOND FMTGSKDITYFKLKDENLKIDDIQNMWIRKRYTAFPDAYKPENIKLIANGKVVVDKDINEWISG NSTYNIK
CPB1	MGSSHHHHHHSSGNEVNKYQSVMVQYLEAFKNYDIDTIVDISKDSRAVTKEEYKNMLMEFKYD PNQKLKSYEITGSRKIDNGEIFSVKTEFLNGAIYNMEFTVSYIDNKLMVSNMNRISIVNEGKYIPTPS FRTQVCTWDELSQYIGDAVSFTRSSKFQYSSNTITLNFQRQYATSGRSRLKVKYSVVDHWMWGD DIRASQWVYGENPDYARQIKLYLGSGETFKNYRIKVENYTPASIKVFGEGYCAGS
CPB2	MGSSHHHHHHSSGNEVNKYQSVMVQYLEAFKNYDIDTIVDISKDSRAVTKEEYKNMLMEFKYD PNQKLKSYEITGSRKIDNGEIFSVKTEFLNGAIYNMEFTVSYIDNKLMVSNMNRISIVNEGKYIPTPS FRTQVCTWDELSQYIGDAVSFTRSSKFQYSSNTITLNFQRQYATSGRSRLKVKYSVVDHWMWGD DIRASQWVYGENPDYARQIKLYLGSGETFKNYRIKVENYTPASIKVFGEGYCAGS
ETX	MGSSHHHHHHSSGKASYDNVDTLIEKGRYNTKYNLKRMEKYYPNAMAYFDKVTINPQGNDFY INNPKVELDGPEMNYLEDVYVGKALLTNDTQQEQKLKSQSFTCKNTDVTATTHTVTGTSIQAT AKFTVPFNETGVSLTTSYSFANTNTNTNSKEITHNVPSQDILVPANTTVEVIAYLKKNVVKGNVKL VGQVSGSEWGEIPSYLAFPRDGYKFLSDDTVNKSDDLNEGTININGKGNYSAVMGDELIVKVRNL NTNNVQEVYVIPVDKKEKSNDSNIVKYRSLYIKAPGIKGS
TcdA	MGSSHHHHHHSSGVTGWQTIDGKRYFNTNTYIASTGYTIINGKHFYFNTDGMQIGVFKGPDGF EYFAPANTHNNNIEGQAILYQNKFLTLNGKKYFSGSDSKAVTGLRTIDGKKYFNTNTAVAVTG WQTINGKKYFNTNTYIASTGYTIISGKHFYFNTDGMQIGVFKGPDGFYFAPANTDANNIEGQA IRYQNRFYLDHNIYFNGNSKAAATGWATIDGNRYFEPNTAMGANGYKIDNKNFYFRNGLPQ IGVFKGPNGEYFAPANTDANNIDGQAIRYQNRFLHLLGKIYFNGNSKAVTGWQTINSKVYYFM PDTAMAAAGGLFEIDGVIYFFGVDGVKAPGIYGGs

Ribosome Display selection

Ribosome display using the ABD scaffold

A combinatorial DNA library was generated as described in Ahmad, J.N. et al., 2012. An aliquot of the generated DNA library was used for *in vitro* transcription/translation single-step reaction (EasyXpress Protein Synthesis Mini Kit, QIAGEN, Germany). The translated products were loaded into Maxisorp or Medisorp microtiter plate (NUNC, Denmark) wells pre-coated with protein for preselection at 4°C for 1 h, before transfer into wells coated with the target protein and blocked with BSA. After incubation at 4°C for 1 h, the plate wells were washed three times with TBS buffer (50 mM Tris-HCl pH 7.4, 150 mM NaCl), followed by washing with ice-cold WBT buffer (50 mM Tris-acetate, pH 7.0, 150 mM NaCl, 50 mM MgAc) with increasing concentrations of Tween 20. To release mRNA from the bound ribosome complex, elution with elution buffer (50 mM Tris-acetate, pH 7.5, 150 mM NaCl, 50 mM ethylenediaminetetraacetic acid (EDTA)) containing 50 µg/ml *Saccharomyces cerevisiae* RNA as carrier was performed. Purified RNA (Roche high pure RNA isolation kit, Roche) was transcribed into cDNA using reverse transcription with setB-rev reverse primer (TTACCTGGATCCGCGGT), annealing to the 3' end of the ABD cDNA. Double-stranded DNA was obtained by PCR using the new EWT5-ABDforN1 forward primer (TTCCTCCATGGGTATGAGAGGATCGCATCACCATCACCATCACCTGGCGGAAGCTAAAGTCTTAGCTAAC) and a reverse setB-rev primer. The final amplified DNA encoding selected ABD variants containing the T7 promoter and ribosome binding site (RBS) sequences and a truncated tolA fragment was used for the next round of RD selection. To isolate high-affinity binders, the stringency of binding and washing conditions was increased after each round of selection. DNA encoding ABD variants isolated after the final fifth round of selection was fused with the full-length tolA sequence using PCR with the new forward primer EWT5-ABDforN2

(TTCCTCCATGGGCAGCAGCCATCACCATCACCATCACCTGGCGGAAGCTAAAGTCTTAGCTAAC) and reverse primer tolA-AviTag (TTTCCGCTCGAGCTATTCGTGCCATTCGATTTTCTGAGCCTCGAAGATGTCGTTCA GGCCCGGTTTGAAGTCCAATGGCGC) containing the AviTag sequence, stop codon, and *XhoI* restriction site. The resulting DNA product was digested with *NcoI* and *XhoI* restriction enzymes, ligated into the pET28b plasmid, and transformed into *E. coli* DH5α. Individual clones producing plasmids with various ABD-TolA sequences were grown from colonies randomly picked from an agar plate. Plasmid DNA was isolated using a QIAprep® Spin Miniprep Kit (Qiagen), and then sequenced.

ABD variants selected on the recombinant His-PSP94 target within five rounds of ribosome display were named **PAB** variants. ABD variants selected on the recombinant His-KLK2 target within five rounds of ribosome display were named **KLA** variants. ABD variants selected on the recombinant His-KLK11 target within five rounds of ribosome display were named **HIP** variants. ABD variants selected on the recombinant EpCAM target within three rounds of ribosome display were named **EBA** variants. ABD variants selected on the recombinant N-cadherin target within three rounds of ribosome display were named **CAB** variants. ABD variants selected on the recombinant Stx1 B subunit target within five rounds of ribosome display were named **S1B** variants. The unique His-ABD-TolA-AviTag fusion protein variants

were produced as biotinylated proteins in the *E. coli* BL21 (DE3) BirA strain. The soluble proteins were purified from cell extracts according to the NiNTA Spin Columns protocol.

Ribosome display using the Myomedin scaffold

The sequence of the Myomedin scaffold was first optimized for expression in the *E. coli* host (GeneArt). Two models of Myomedin DNA libraries (Myomedin-Loops and Myomedin-Betasheets) were designed and synthesized using the TRIM or NNK technology, and corresponding DNA libraries were assembled (sequences not shown). The generated DNA library was used for *in vitro* transcription/translation single-step reaction. The translated products were loaded into Medisorp microtiter plate (NUNC, Denmark) wells pre-coated with protein for preselection at 4°C for 1 h, before transfer into wells coated with the target protein and blocked with BSA. After incubation at 4°C for 1 h, the plate wells were washed three times with TBS buffer, followed by washing with ice-cold WBT buffer with increasing concentrations of Tween 20. To release mRNA from the bound ribosome complex, elution with elution buffer containing 50 µg/ml *Saccharomyces cerevisiae* RNA as carrier was performed. Purified RNA was transcribed into cDNA using reverse transcription with the JOIN-R reverse primer (GAACCGACCGCGGATCCACCCTGTTTACGAATCCATTCTT), annealing to the 3' end of the Myomedin cDNA. Double-stranded DNA was obtained by PCR using the JOIN-F forward primer (CTATAGGGAGACCACAACGGTTTCCCTCTAGAAATAATTTTGTTTAACTTTAAGAAGGAGATATACATATGAAAAGCGAGCTGGCCG) and reverse JOIN-R primer. Another PCR using the T7B forward primer (ATACGAAATTAATACGACTCACTATAGGGAGACCACAACGG) and TolAk reverse primer (AGAAAGAAAGCGGCAACTGAAACCGCACACCTTACTGGTGTGCGG) was performed to obtain the DNA sequence containing the T7 promoter and ribosome binding site (RBS) sequences and a truncated *tolA* fragment. To isolate high-affinity binders, the stringency of binding and washing conditions was increased after each round of selection. DNA encoding Myomedin variants isolated after the final round of selection was digested with *NdeI* and *BamHI* restriction enzymes, ligated into the pET28b plasmid containing the C-terminal AviTag sequence and stop codon, and transformed into *E. coli* DH5α. Individual clones producing plasmids with various His-Myomedin-AviTag sequences were grown from colonies randomly picked from an agar plate. Plasmid DNA was isolated using a QIAprep® Spin Miniprep Kit (Qiagen), and then sequenced. The unique variants were produced as biotinylated proteins in the *E. coli* BL21 (DE3) BirA strain. The soluble proteins were purified from cell extracts according to the NiNTA Spin Columns protocol. His-Myomedin-AviTag variants derived from the Myomedin-loop scaffold selected on the recombinant N-cadherin target within three rounds of ribosome display were named LN variants.

Sequence analysis and clustering of selected binders

DNA constructs of selected clones expressing full-length variants were sequenced. Amino acid multiple sequence alignment of all selected clones and construction of the similarity tree were performed using the Molecular Evolutionary Genetics Analysis version 7 (MEGA7) integrated tool for conducting sequence alignment and inferring phylogenetic trees (available free of charge from <http://www.megasoftware.net>).

Binding assays using ELISA

ELISA screening of cell lysates

The binding variants with unique sequences were transformed into *E. coli* BL21 (DE3) BirA and expressed in 3 ml cultures with the addition of 1 mM IPTG and 50 μ M D-biotin for 4 hours. Bacteria were pelleted at 15,000 g for 5 min and resuspended in 0.01% PBST with 200 μ g/ml lysozyme. Cell lysis was performed with three cycles of freezing at -80 °C and thawing at 37 °C for 30 min. Cell lysate was centrifuged for 15 min and 50 μ l of supernatant was loaded to a microtiter plate, previously coated with 10 μ g/ml target protein and BSA as a negative control, and blocked with 1% BSA. After 1 h of incubation at RT, the plate was washed five times with PBST, and the bound binders were detected with HRP-conjugated streptavidin (1:5000 in 1% BSA/PBST). The color was developed by addition of 0.5 mg/ml O-phenylenediamine (OPD, Sigma-Aldrich, St. Louis, USA) and 0.01% H₂O₂ in 0.1 M citrate buffer (pH 5.0) for 5 min. The reaction was stopped by addition of 2M H₂SO₄ and absorbance was read at 492 nm. A negative background was recorded in wells loaded with 1% BSA/PBST without cell lysate.

Binding of selected variants to the immobilized target molecule

For all binding assays, a control ToLA fusion protein with the original non-mutated albumin-binding domain (ABDwt) was used as a negative control (prepared according to Kuchař, M. et al., 2013). For His-Myomedin-AviTag binders, the parental non-mutated Myomedin-wt protein was used as a negative control. A Polysorp, Maxisorp or Medisorp microtiter plate (NUNC, Denmark) was coated with different recombinant target protein variants, at 4°C overnight (coating buffer: 100 mM bicarbonate/carbonate solution, pH 9.6). The plate was washed with PBST buffer (PBS buffer with 0.05% Tween-20) and blocked with 1% BSA in PBST buffer for 2 h at room temperature. After washing, *in vitro* biotinylated binders at indicated concentrations in PBST with 1% BSA were added. The bound variants were detected by streptavidin-HRP conjugate (diluted 1:5000). The plate wells were washed repeatedly and developed in 0.1M citrate buffer, pH 5.0 containing 0.5 mg/ml O-phenylenediamine (OPD) and 0.01% H₂O₂, or alternatively with substrate solution containing tetramethylbenzidine (TMB) (TestLine Clinical Diagnostics, Czech Republic) for 5 min. The colorimetric reaction was stopped by adding 100 μ l 2M H₂SO₄ and absorbance was determined.

Binding of the target molecule to the immobilized selected variants

A microplate was coated with 1 μ g/ml recombinant streptavidin diluted in coating buffer at 4 °C overnight. The plate was washed with PBST buffer and blocked with 1% BSA in PBST buffer for 2 hours at room temperature. After washing, serially-diluted *in vivo* biotinylated binding variants were added. After washing, the recombinant target protein at concentration 10 μ g/ml was added and detected by specific antibodies and HRP conjugates. The plate wells were washed repeatedly and stained with substrate solution for 5 min. The colorimetric reaction was stopped with 100 μ l 2M H₂SO₄ and absorbance was determined.

Binding assays using flow cytometry (FACS)

Detection of PSP94

LNCaP cells were grown in an incubator at 37 ° C in 5% CO₂ according to a standard protocol in a basal medium of RPMI with 10% FBS. The disaggregated cells culture (sufficient cell density was reached on day 3 after passage) was assayed for the presence of PSP94 on the cell surface and intracellularly using fluorescence-activated cell sorting (FACS). Three different primary antibodies against PSP94 (EPR7345, sc-68920, YPSP-1) and fluorescently labeled secondary antibodies (Cy5-aR, Cy5-aM) were used for the detection of PSP94. Scraped LNCaP cells were washed with HBSS Complete buffer (10 mM HEPES, pH 7.4, 140 mM NaCl, 5 mM KCl, 1% (v/v) glucose, 2 mM CaCl₂, 2 mM MgCl₂, 1% (v/v) FCS), added to a 96-well plate (Nunc, Roskilde, Denmark) to the final number of 5x10⁵ LNCaP cells per well, centrifuged, and the buffer was removed. The cells were incubated separately with 50 µl of diluted primary antibodies against PSP94 (EPR7345, sc-68920, YPSP-1)(diluted 1:100 with HBSS Complete buffer) for 30 min at 4 °C. The cells were washed with HBSS Complete buffer and incubated with 100 µl of diluted fluorescently labeled secondary antibodies (Cy5-aR, Cy5-aM) (diluted 1:500) for 30 min at 4 °C. After washing, the cells were resuspended in 100 µl of HBSS Complete buffer and analyzed by flow cytometry in a FACS LSR II instrument (BD Biosciences, San Jose, CA) in the presence of 5 µg/ml propidium iodide. Appropriate gatings were used to exclude cell aggregates and dead cells, and binding data were deduced from the mean fluorescence intensities (MFI).

Detection of EpCAM and N-cadherin

Cells of human breast cancer cell line MCF-7, prostate cancer cell lines DU-145 and PC-3, normal skin fibroblasts CCD1070Sk (ATCC CRL 2091), and human embryonic kidney cells HEK293 were grown in DMEM medium (Biosera, Nuaille, France) supplemented with 10% fetal calf serum (FCS) (GIBCO, Grand Island, N.Y.) and antibiotic antimycotic solution (ATB) (Sigma-Aldrich, St. Louis, MO) in 5% CO₂ at 37 °C. The disaggregated cells cultures were assayed for the presence of EpCAM and N-cadherin on the cell surface using FACS. Primary antibodies against EpCAM and N-cadherin and fluorescently labeled secondary antibodies were used for the detection. Scraped cells were washed with HBSS Complete buffer, added to a 96-well plate to the final number of 5x10⁵ cells per well, centrifuged, and the buffer was removed. The cells were incubated separately with 50 µl of diluted primary antibodies against EpCAM and N-cadherin (diluted 1:100 (anti-EpCAM) or 1:20 (anti-N-cadherin) in HBSS Complete buffer) for 30 min at 4 °C. The cells were washed with HBSS Complete buffer and incubated with 50 µl of diluted fluorescently labeled secondary antibodies (diluted 1:500 (aR-APC) or 1:20 (aM-APC)) for 30 min at 4 °C. After washing, the cells were resuspended in 100 µl of HBSS Complete buffer and analyzed by flow cytometry using a BD LSRFortessa cell analyzer (BD Biosciences, San Jose, CA) in the presence of 1 µg/ml Hoechst 33258. Data were analyzed using the FlowJo software (Tree Star, Ashland, OR). Appropriate gatings were used to exclude cell aggregates and dead cells, and binding data were expressed as mean fluorescence intensity (MFI) values.

Binding of PAB clones to PSP94

The ability of *in vitro* biotinylated 6xHis-PAB-TolA-AviTag fusion products to bind to PSP94 on the surface of LNCaP cells was measured using a fluorescently labeled streptavidin

conjugate (Strep-PE). Scraped LNCaP cells were washed with HBSS Complete buffer, added to a 96-well plate to the final number of 3×10^5 LNCaP cells per well, centrifuged, and the buffer was removed. The cells were incubated with PAB clones and ABDwt diluted at 10 $\mu\text{g}/\text{ml}$ in HBSS Complete buffer for 30 min at 4°C. After washing, 50 μl of diluted Strep-PE (diluted 1:400 with HBSS Complete buffer) was added, and the cells were incubated for 30 min at 4°C. Washed cells were resuspended in 100 μl of HBSS and analyzed by FACS. The data were referenced to the relative mean fluorescence intensities (relative PAB binding).

Competition assay

N-HisTag-PSP94 diluted at different concentrations (20 $\mu\text{g}/\text{ml}$, 100 $\mu\text{g}/\text{ml}$) in HBSS Complete buffer was mixed with PAB clones and ABDwt diluted at a final concentration of 10 $\mu\text{g}/\text{ml}$ (in 100 μl), and preincubated for 15 min on ice. Scraped LNCaP cells were washed with HBSS Complete buffer, added to a 96-well plate to the final number of 3×10^5 LNCaP cells per well, centrifuged, and the buffer was removed. The cells were incubated with a prearranged mixture of PAB variants with N-HisTag-PSP94 for 30 min on ice. After washing, 50 μl of diluted Strep-PE (diluted 1:400) was added, and the cells were incubated for 30 min at 4°C. Washed cells were resuspended in 100 μl of HBSS and analyzed by FACS as described above.

Flow cytometry and whole-cell ELISA of *L. lactis* cells

For flow cytometric analyses, 10 μl of *L. lactis* suspensions were added to Tris-buffered saline (TBS) and centrifuged. Cells were resuspended in TBS with Alexa 488-labeled recombinant Stx1B (20 $\mu\text{g}/\text{m}$) prepared using an Alexa Fluor 488 Microscale Protein Labelling Kit (Thermo Fisher Scientific) and incubated at RT with constant shaking at 100 rpm. All washings, centrifugation steps, and measurements were performed as described in [89, 108].

The whole-cell ELISA was carried out according to [109] with a few modifications. *L. lactis* suspension with surface-displayed S1B variant or ABDwt was centrifuged and resuspended in PBS to an A_{600} of 1.0. Seven hundred and fifty μl of the suspensions were washed twice in PBS and incubated with 500 μl of recombinant Stx1B (20 $\mu\text{g}/\text{ml}$ in PBS) for 2 hours, followed by additional washing with PBS. The bound toxin subunit was detected by addition of 200 μl of Anti-Verotoxin I/SLT 1b (antiStx1B) primary antibody (diluted 1:20 in PBS, Abcam, Cambridge, UK) for 1 hour, followed by washing and incubation with 200 μl of (HRP)-conjugated Goat anti-mouse IgG secondary antibody (diluted 1:500 in PBS, Merck Millipore, Darmstadt, Germany). All incubations were performed at RT in a tube rotator. After incubation with secondary antibody, the cells were first washed with PBS and then with substrate buffer (150 mM Na_2HPO_4 , 50 mM citric acid, pH 6.0). Cells were finally resuspended in 1 ml of substrate buffer, and 100 μl of suspensions, or 1:5 dilutions in substrate buffer, were loaded on a microtiter plate. The color was developed by addition of 100 μl of TMB substrate and the reaction was stopped after 15 min by addition of 50 μl of 2M H_2SO_4 . Absorbances were read at 450 nm.

Microscale thermophoresis (MST)

The binding interactions between the target molecule and the binders were measured using microscale thermophoresis (MST). The purified target protein was dialyzed into a suitable buffer for subsequent fluorescent labeling, and labeled according to the attached protocol (L001™ Monolith NT.115 Protein Labeling Kit RED-NHS, NanoTemper Technologies, GmbH,

Munich, Germany). The stock solution of the labeled protein was diluted in PBS buffer at an appropriate concentration corresponding to the expected affinity. Decreasing concentrations of non-labeled purified binding variants were titrated against the labeled target protein and centrifuged for 5 min at 14,000 g to remove potential aggregates. The supernatant was soaked into standard or premium coated capillaries (NanoTemper Technologies, GmbH). Measurements were carried out at 25 °C in PBS buffer, pH 7.4, 1% (w/v) PEG1500, in a Monolith NT.115 instrument (NanoTemper Technologies GmbH, Munich, Germany) using 20% MST power. Each measurement was performed three times. Data analysis was completed with supplement NanoTemper analysis software.

Fluorescence-based thermal shift assay (TSA)

Protein samples diluted in different buffers, and 5× Sypro Orange dye (Sigma-Aldrich, St. Luis, MO) were added into 25 µl total volume. The solutions were incubated in a thermal gradient from 20°C to 80°C at increments of 0.5°C and with 30 s-hold intervals using the real-time PCR Detection System CFX96 Touch (Bio-Rad Laboratories). The degree of protein unfolding was monitored by the FRET (fluorescence resonance energy transfer) channel that captured the spectral properties of Sypro Orange unfolded protein complexes (excitation wavelength ≈ 470 nm and emission wavelength ≈ 570 nm). Data were analyzed using the CFX Manager Software and the melting temperatures were determined using the first derivative spectra.

Binding of EBA and CAB variants to MCF-7 and CCD1070Sk cells using LigandTracer Green

Diluted EBA14, EBA62, CAB043, and CAB101 *in vivo* biotinylated proteins were labeled with APC streptavidin. Two separate cell colonies of MCF-7 and CCD1070Sk cells were seeded in a single circular cell dish. This means that each fluorescently labeled ligand was incubated with the two cell colonies simultaneously. One side of the dish was kept empty for the background subtraction. The measurement was performed in 3 ml of DMEM culture media at RT. The labeled binding variants were gradually added to the medium at half-hour or one-hour intervals to the final concentration of 10 nM, 30 nM, and 90 nM. The data were obtained by direct detection of fluorescently labeled compounds by LigandTracer Green (Ridgeview Instruments AB, Vänge, Sweden) with an APC-compatible detector and analyzed using Trace Drawer 1.8 (Ridgeview Instruments AB, Vänge, Sweden).

Cleavage of the chromogenic substrate

The reaction was performed in 500 µl of Tris buffer (50 mM Tris HCl, 100 mM NaCl, pH 8) at 37°C in the presence of 0.5 mM N-benzoyl-Pro-Phe-Arg-*p*-nitroanilide hydrochloride substrate. Recombinant KLK2 protein at a concentration of 0.06 mg/ml was added to the reaction, and the reaction was stopped at different time intervals by addition of 2M H₂SO₄ and the absorbance was read at $\lambda = 405$ nm.

Determination of molecular weight of the Stx1B subunit

The molecular weight and oligomerization status of Stx1B was determined using analytical gel filtration chromatography (1.2 × 60 cm, 7 ml/h flow rate with 15 min fraction collection time) in polyacrylamide gel Bio-Gel P-100 (Bio Rad, Hercules, USA) due to Stx1B cross-reaction with the Superdex column (GE Healthcare) for size exclusion chromatography. A mixture of six proteins of 14.4-97 kDa (Amersham Low molecular weight Calibration Kit, GE Healthcare) was used as a standard.

***In vitro* binding of Stx1B to the globotriaosylceramide (Gb₃) receptor**

Binding of Stx1B to its natural receptor Gb₃ was determined by enzyme-linked immunosorbent assay (Gb₃ ELISA) as described previously [110]. Receptor Gb₃ was purchased from Matreya LLC (PA, USA) and dissolved in chloroform/methanol (2:1). One hundred µl of Gb₃ solution at concentration 10 µg/ml was used to coat Nunc PolySorp Strips (Thermo Fisher Scientific) overnight in laminar flow to evaporate chloroform/methanol. After washing with PBS containing 0.05 % Tween 20 (PBST) and blocking with 2% BSA in PBST, 100 µl of serial twofold dilutions of recombinant Stx1B in triplicate (starting with 1 µg/ml in 0.2 % BSA in PBST) were added to the wells and incubated for 1 h. Bound Stx1B-his₆ was detected with primary THETM His Tag Antibody (GenScript, NJ, USA) (dilution 1:2000 in 0.2 % BSA in PBST) and with horseradish peroxidase (HRP)-conjugated goat anti-mouse IgG secondary antibody (Merck Millipore, Darmstadt, Germany) (dilution 1:5000 in 0.2% BSA in PBST). The color was developed by addition of 100 µl substrate buffer (150 mM Na₂HPO₄, 50 mM citric acid, pH 6.0) and 100 µl 3,3',5,5'-tetramethylbenzidine (TMB) substrate (Sigma-Aldrich, MO, USA) for 15 minutes at room temperature. The reaction was terminated by addition of 50 µl 2M H₂SO₄, and absorbances were read at 450 nm using Infinite M1000 (Tecan, Salzburg, Austria). No Stx1B was added to 0.2% BSA in PBST in control wells (zero concentration), while all the other steps were performed as described above.

Internalization of recombinant Stx1B into HeLa cells

HeLa cells were grown in Dulbecco's Modified Eagle Medium (DMEM) supplemented with 10% fetal bovine serum (FBS), 1% GlutaMAX and pen-strep in 24-wells plates on coverslips. Fluorescein isothiocyanate (FITC)-labelled Stx1B (10 µg/ml in 300 µl of fresh medium) was added to the cells and incubated for 1 hour at 37 °C. Afterwards, the cells were washed with PBS, fixed with 4% paraformaldehyde in PBS for 15 min and permeabilized with 0.1% Triton X-100 in PBS for 6 min. Non-specific staining was blocked with 3% BSA in PBS for 30 min. Golgi apparatus was labeled with mouse monoclonal anti-human Golgin97 primary antibody (0.4 µg/ml in 3% BSA for 1 h, Life Technologies) and with Alexa Fluor 555-conjugated goat anti-rabbit secondary antibody (1:1000 in 3% BSA for 1 h, A-21428, Life Technologies). Coverslips were mounted with ProlongGold Antifade reagent with 4',6-diamidino-2-phenylindole (DAPI; Invitrogen). Cells were observed with a Carl Zeiss LSM 710 confocal microscope.

Surface plasmon resonance (SPR)

SPR measurements were performed with Biacore T100 (GE Healthcare) at 25 °C. In the first setup we tested binding of the S1B variants prepared in fusion with TolA spacer protein and AviTag to Stx1B captured on a Series S sensor chip CM5 (Biacore, GE Healthcare). CM5 sensor chip was activated using an Amine coupling Kit (GE Healthcare) according to

manufacturer's instructions. For immobilization of Stx1B, standard PBS buffer (137 mM NaCl, 2.7 mM KCl, 10 mM Na₂HPO₄, 1.8 mM KH₂PO₄, pH 7.4) was used as running buffer. Stx1B was diluted into 10 mM sodium acetate buffer, pH 5.0, to a final concentration of 20 µg/ml, and injected over the second flow cell. The final immobilization level was approximately 890 response units (RU). The first flow cell was empty and served as a reference cell to control the level of non-specific binding. All experiments were performed with running buffer PBS with 300 mM NaCl (300 mM NaCl, 2.7 mM KCl, 10 mM Na₂HPO₄, 1.8 mM KH₂PO₄, pH 7.4, 0.005 % P20). Each compound was injected for 2 min at a flow-rate 20 µl/min, and the dissociation was monitored for 3 min. Regeneration of the sensor surface was achieved with two 30 s pulses of 50 mM NaOH. We used the following concentrations for titration: 0, 15.625, 31.25, 62.5, 125, 250, 500, 1000, 2000 nM, and concentration 62.5 nM was repeated at the end of the concentration series.

In a reverse setup, we immobilized S1B22-TolA-Avi or S1B26-TolA-Avi variants on a sensor chip CM5. CM5 sensor chip activation and immobilization of S1B-TolA-Avi variants was performed as described above, except that two injections were needed to enrich the final immobilization level to approximately 1100 RU. All experiments were performed with running buffer PBS with 300 mM NaCl (300 mM NaCl, 2.7 mM KCl, 10 mM Na₂HPO₄, 1.8 mM KH₂PO₄, pH 7.4, 0.005 % P20). Each compound was injected for 1 min at a flow-rate of 10 µl/min, and the dissociation was monitored for 30 s. Regeneration of the sensor surface was achieved with 25 mM NaOH for 120 s. We used the following concentrations for titration: 62.5, 125, 250, 500, 1000, 2000, 4000 nM, and concentration 500 nM was repeated at the end of the concentration series. We evaluated the obtained data using the Biacore T100 Evaluation software. The sensorgrams were reference and blank subtracted and we applied the Steady State Affinity model to calculate the affinity constant.

Molecular cloning and expression of S1B-cA variants in *L. lactis*

Genes of S1B variants without tolA spacer were amplified with Phusion polymerase (New England Biolabs, Beverly, MA) using the pET28-S1Bx-TolA-Avi template and ABD-F primer and the corresponding S1B-R primer (Table 1). The gene for ABDwt was amplified using the pET28-ABDwt-TolA-Avi template and ABD-F/ABDwt-R (Table 1) primer pair, while his₆ tag was added with ABDhis₆-F/ABDwt-R primer. All PCR fragments were ligated to the pJET 1.2 cloning vector and cloned into plasmid pSDLBA3b, using *Bam*HI and *Eco*RI restriction enzymes (New England Biolabs). Plasmid DNA was isolated with a NucleoSpin plasmid kit (Macherey and Nagel, Düren, Germany), with an additional lysozyme treatment for *L. lactis*. Lactococci were transformed by electroporation using a Gene Pulser II apparatus (Bio-Rad, Hercules, CA) according to MoBiTec GmbH instructions (Goettingen, Germany). Plasmids constructed in the study are listed in Table 1. Expression of S1B-cA variants in *L. lactis* NZ9000 was performed in 10 ml cultures. Bacterial suspensions were grown to an A₆₀₀ of 0.8, followed by induction with 25 ng/ml nisin (Fluka) for 3 hours [89, 96, 111, 112]. Resulting suspensions were stored at 4 °C for flow cytometric analysis or whole-cell ELISA test.

6. References

1. Walsh, G., *Biopharmaceutical benchmarks 2014*. Nat Biotechnol, 2014. 32(10): p. 992-1000.
2. Skerra, A., *Alternative non-antibody scaffolds for molecular recognition*. Curr Opin Biotechnol, 2007. 18(4): p. 295-304.
3. Skrlec, K., B. Strukelj, and A. Berlec, *Non-immunoglobulin scaffolds: a focus on their targets*. Trends Biotechnol, 2015. 33(7): p. 408-18.
4. Lipovsek, D., *Adnectins: engineered target-binding protein therapeutics*. Protein Eng Des Sel, 2011. 24(1-2): p. 3-9.
5. Tolcher, A.W., et al., *Phase I and pharmacokinetic study of CT-322 (BMS-844203), a targeted Adnectin inhibitor of VEGFR-2 based on a domain of human fibronectin*. Clin Cancer Res, 2011. 17(2): p. 363-71.
6. Albrecht, V., et al., *Anticalins directed against the fibronectin extra domain B as diagnostic tracers for glioblastomas*. Int J Cancer, 2016. 138(5): p. 1269-80.
7. Richter, A. and A. Skerra, *Anticalins directed against vascular endothelial growth factor receptor 3 (VEGFR-3) with picomolar affinities show potential for medical therapy and in vivo imaging*. Biol Chem, 2017. 398(1): p. 39-55.
8. Schmoldt, H.U., et al., *Microbodies*. Methods Mol Biol, 2009. 535: p. 361-72.
9. Schilling, J., J. Schoppe, and A. Pluckthun, *From DARPins to LoopDARPins: novel LoopDARPin design allows the selection of low picomolar binders in a single round of ribosome display*. J Mol Biol, 2014. 426(3): p. 691-721.
10. Binz, H.K., et al., *High-affinity binders selected from designed ankyrin repeat protein libraries*. Nat Biotechnol, 2004. 22(5): p. 575-82.
11. Ebersbach, H., et al., *Affilin-novel binding molecules based on human gamma-B-crystallin, an all beta-sheet protein*. J Mol Biol, 2007. 372(1): p. 172-85.
12. Lorey, S., et al., *Novel ubiquitin-derived high affinity binding proteins with tumor targeting properties*. J Biol Chem, 2014. 289(12): p. 8493-507.
13. Hansen, S., et al., *Structures of designed armadillo repeat proteins binding to peptides fused to globular domains*. Protein Sci, 2017. 26(10): p. 1942-1952.
14. Madhurantakam, C., et al., *Structure-based optimization of designed Armadillo-repeat proteins*. Protein Sci, 2012. 21(7): p. 1015-28.
15. Altai, M., et al., *Influence of molecular design on biodistribution and targeting properties of an Affibody-fused HER2-recognising anticancer toxin*. Int J Oncol, 2016. 49(3): p. 1185-94.
16. Bass, T.Z., et al., *In vivo evaluation of a novel format of a bivalent HER3-targeting and albumin-binding therapeutic affibody construct*. Sci Rep, 2017. 7: p. 43118.
17. Eigenbrot, C., et al., *Structural basis for high-affinity HER2 receptor binding by an engineered protein*. Proc Natl Acad Sci U S A, 2010. 107(34): p. 15039-44.
18. Cantante, C., et al., *Albumin-binding domain from Streptococcus zooepidemicus protein Zag as a novel strategy to improve the half-life of therapeutic proteins*. J Biotechnol, 2017. 253: p. 23-33.
19. Nilvebrant, J. and S. Hober, *The albumin-binding domain as a scaffold for protein engineering*. Comput Struct Biotechnol J, 2013. 6: p. e201303009.
20. Johansson, M.U., et al., *Solution structure of the albumin-binding GA module: a versatile bacterial protein domain*. J Mol Biol, 1997. 266(5): p. 859-65.
21. Johansson, M.U., et al., *Structure, specificity, and mode of interaction for bacterial albumin-binding modules*. J Biol Chem, 2002. 277(10): p. 8114-20.
22. Jonsson, A., et al., *Engineering of a femtomolar affinity binding protein to human serum albumin*. Protein Eng Des Sel, 2008. 21(8): p. 515-27.
23. Ahmad, J.N., et al., *Novel high-affinity binders of human interferon gamma derived from albumin-binding domain of protein G*. Proteins, 2012. 80(3): p. 774-89.

24. Mareckova, L., et al., *Novel binders derived from an albumin-binding domain scaffold targeting human prostate secretory protein 94 (PSP94)*. Protein Cell, 2015. 6(10): p. 774-9.
25. Krizova, L., et al., *p19-targeted ABD-derived protein variants inhibit IL-23 binding and exert suppressive control over IL-23-stimulated expansion of primary human IL-17+ T-cells*. Autoimmunity, 2017. 50(2): p. 102-113.
26. Kuchar, M., et al., *Human interleukin-23 receptor antagonists derived from an albumin-binding domain scaffold inhibit IL-23-dependent ex vivo expansion of IL-17-producing T-cells*. Proteins, 2014. 82(6): p. 975-89.
27. Butz, M., P. Kast, and D. Hilvert, *Affinity maturation of a computationally designed binding protein affords a functional but disordered polypeptide*. J Struct Biol, 2014. 185(2): p. 168-77.
28. Jacobs, S.A., et al., *Fusion to a highly stable consensus albumin binding domain allows for tunable pharmacokinetics*. Protein Eng Des Sel, 2015. 28(10): p. 385-93.
29. Verma, D., G. Grigoryan, and C. Bailey-Kellogg, *Structure-based design of combinatorial mutagenesis libraries*. Protein Sci, 2015. 24(5): p. 895-908.
30. Tang, L., et al., *Construction of "small-intelligent" focused mutagenesis libraries using well-designed combinatorial degenerate primers*. Biotechniques, 2012. 52(3): p. 149-58.
31. ThermoFisherScientific. GeneArt 2018; (<https://www.thermofisher.com/cz/en/home/life-science/cloning/gene-synthesis/directed-evolution/geneart-combinatorial-libraries.html>)
32. Pluckthun, A., *Ribosome display: a perspective*. Methods Mol Biol, 2012. 805: p. 3-28.
33. Daugherty, P.S., *Protein engineering with bacterial display*. Curr Opin Struct Biol, 2007. 17(4): p. 474-80.
34. Pepper, L.R., et al., *A decade of yeast surface display technology: where are we now?* Comb Chem High Throughput Screen, 2008. 11(2): p. 127-34.
35. Bratkovic, T., *Progress in phage display: evolution of the technique and its application*. Cell Mol Life Sci, 2010. 67(5): p. 749-67.
36. McCafferty, J. and D. Schofield, *Identification of optimal protein binders through the use of large genetically encoded display libraries*. Curr Opin Chem Biol, 2015. 26: p. 16-24.
37. Zahnd, C., P. Amstutz, and A. Pluckthun, *Ribosome display: selecting and evolving proteins in vitro that specifically bind to a target*. Nat Methods, 2007. 4(3): p. 269-79.
38. Dreier, B. and A. Pluckthun, *Rapid selection of high-affinity binders using ribosome display*. Methods Mol Biol, 2012. 805: p. 261-86.
39. Gill, D.S. and N.K. Damle, *Biopharmaceutical drug discovery using novel protein scaffolds*. Curr Opin Biotechnol, 2006. 17(6): p. 653-8.
40. Barinka, C., et al., *Selection and characterization of Anticalins targeting human prostate-specific membrane antigen (PSMA)*. Protein Eng Des Sel, 2016. 29(3): p. 105-15.
41. Garousi, J., et al., *ADAPT, a Novel Scaffold Protein-Based Probe for Radionuclide Imaging of Molecular Targets That Are Expressed in Disseminated Cancers*. Cancer Res, 2015. 75(20): p. 4364-71.
42. Callahan, M.K. and J.D. Wolchok, *Clinical Activity, Toxicity, Biomarkers, and Future Development of CTLA-4 Checkpoint Antagonists*. Semin Oncol, 2015. 42(4): p. 573-86.
43. AffibodyMedicalAB. Affibody. 2018; <http://www.affibody.se/>
44. Zadavec, P., et al., *Development of Recombinant Lactococcus lactis Displaying Albumin-Binding Domain Variants against Shiga Toxin 1 B Subunit*. PLoS One, 2016. 11(9): p. e0162625.
45. PiersPharmaceuticals. Anticalins. 2018; www.pieris.com
46. Mitchell, R.E. and S.S. Chang, *Current controversies in the treatment of high-risk prostate cancer*. Curr Opin Urol, 2008. 18(3): p. 263-8.
47. Llop, E., et al., *Improvement of Prostate Cancer Diagnosis by Detecting PSA Glycosylation-Specific Changes*. Theranostics, 2016. 6(8): p. 1190-204.
48. Tang, J., et al., *Expression, crystallization, and three-dimensional structure of the catalytic domain of human plasma kallikrein*. J Biol Chem, 2005. 280(49): p. 41077-89.

49. Pan, L.H., et al., *An electrochemical biosensor to simultaneously detect VEGF and PSA for early prostate cancer diagnosis based on graphene oxide/ssDNA/PLLA nanoparticles*. *Biosens Bioelectron*, 2017. 89(Pt 1): p. 598-605.
50. Lazzeri, M., et al., *Serum index test %[-2]proPSA and Prostate Health Index are more accurate than prostate specific antigen and %fPSA in predicting a positive repeat prostate biopsy*. *The Journal of urology*, 2012. 188(4): p. 1137-43.
51. Yoo, M. and W.S. Yeo, *Determining the Ratio of Two Types of Prostate Specific Antigens with Biochips and Gold Nanoparticles for Accurate Prostate Cancer Diagnosis*. *Anal Sci*, 2016. 32(10): p. 1117-1121.
52. Shariat, S.F., et al., *New blood-based biomarkers for the diagnosis, staging and prognosis of prostate cancer*. *BJU Int*, 2008. 101(6): p. 675-83.
53. Velonas, V.M., et al., *Current status of biomarkers for prostate cancer*. *Int J Mol Sci*, 2013. 14(6): p. 11034-60.
54. Xu, H., et al., *The function of oxytocin: a potential biomarker for prostate cancer diagnosis and promoter of prostate cancer*. *Oncotarget*, 2017. 8(19): p. 31215-31226.
55. Emami, N. and E.P. Diamandis, *New insights into the functional mechanisms and clinical applications of the kallikrein-related peptidase family*. *Mol Oncol*, 2007. 1(3): p. 269-87.
56. Lovgren, J., et al., *Measurement of prostate-specific antigen and human glandular kallikrein 2 in different body fluids*. *J Androl*, 1999. 20(3): p. 348-55.
57. Guerrico, A.G., et al., *Roles of kallikrein-2 biomarkers (free-hK2 and pro-hK2) for predicting prostate cancer progression-free survival*. *J Circ Biomark*, 2017. 6: p. 1849454417720151.
58. Kwiatkowski, M.K., et al., *In prostatism patients the ratio of human glandular kallikrein to free PSA improves the discrimination between prostate cancer and benign hyperplasia within the diagnostic "gray zone" of total PSA 4 to 10 ng/mL*. *Urology*, 1998. 52(3): p. 360-5.
59. Nasser, N.J., et al., *Human tissue Kallikreins: Blood levels and response to radiotherapy in intermediate risk prostate cancer*. *Radiother Oncol*, 2017. 124(3): p. 427-432.
60. IM, S., *Prostate Cancer (PCa) Risk Variants and Risk of Fatal PCa in the National Cancer Institute Breast and Prostate Cancer Cohort Consortium*. *Eur Urol*, 2014. 65(6): p. 1069-75.
61. H, L., *Fine mapping and functional analysis of a common variant in MSMB on chromosome 10q11.2 associated with prostate cancer susceptibility*. *Proc Natl Acad Sci U S A*, 2009. 106(19): p. 7933-8.
62. Penney, K.L., et al., *Association of prostate cancer risk variants with gene expression in normal and tumor tissue*. *Cancer Epidemiol Biomarkers Prev*, 2015. 24(1): p. 255-60.
63. Whitaker, H.C., et al., *The potential value of microseminoprotein-beta as a prostate cancer biomarker and therapeutic target*. *Prostate*, 2010. 70(3): p. 333-40.
64. P, M.-P., *Reproductive tissue expression and sperm localization of porcine beta-microseminoprotein*. *Cell Tissue Res*, 2011. 344(2): p. 341-53.
65. Annabi, B., et al., *Contribution of the 37-kDa laminin receptor precursor in the anti-metastatic PSP94-derived peptide PCK3145 cell surface binding*. *Biochemical and biophysical research communications*, 2006. 346(1): p. 358-66.
66. BR, P., *Growth inhibition mediated by PSP94 or CRISP-3 is prostate cancer cell line specific*. *Asian J Androl*, 2010. 12(5): p. 677-89.
67. Kumar, A., et al., *Crystal structure of prostate secretory protein PSP94 shows an edge-to-edge association of two monomers to form a homodimer*. *J Mol Biol*, 2010. 397(4): p. 947-56.
68. Anklesaria, J.H., et al., *Prostate Secretory Protein of 94 amino acids (PSP94) binds to prostatic acid phosphatase (PAP) in human seminal plasma*. *PLoS One*, 2013. 8(3): p. e58631.
69. Shukeir, N., et al., *Prostate secretory protein PSP-94 decreases tumor growth and hypercalcemia of malignancy in a syngenic in vivo model of prostate cancer*. *Cancer Res*, 2003. 63(9): p. 2072-8.
70. Sjoblom, L., et al., *Microseminoprotein-Beta Expression in Different Stages of Prostate Cancer*. *PLoS One*, 2016. 11(3): p. e0150241.

71. Beke, L., et al., *The gene encoding the prostatic tumor suppressor PSP94 is a target for repression by the Polycomb group protein EZH2*. *Oncogene*, 2007. 26(31): p. 4590-5.
72. Riethdorf, S., et al., *Clinical applications of the CellSearch platform in cancer patients*. *Adv Drug Deliv Rev*, 2018.
73. Kolostova, K., et al., *Circulating Tumor Cells in Localized Prostate Cancer: Isolation, Cultivation In Vitro and Relationship to T-Stage and Gleason Score*. *Anticancer Res.*, 2014. 34(7): p. 3641-3646.
74. Jemal, A., et al., *Global cancer statistics*. (1542-4863 (Electronic)).
75. Wei, P., et al., *FOXM1 promotes lung adenocarcinoma invasion and metastasis by upregulating SNAIL*. *Int J Biol Sci*, 2015. 11(2): p. 186-98.
76. Gorin, M.A., et al., *Circulating tumour cells as biomarkers of prostate, bladder, and kidney cancer*. *Nat Rev Urol*, 2017. 14(2): p. 90-97.
77. Jin, X.R., et al., *Circulating tumor cells in early stage lung adenocarcinoma: a case series report and literature review*. *Oncotarget*, 2017. 8(14): p. 23130-23141.
78. van der Toom, E.E., et al., *Technical challenges in the isolation and analysis of circulating tumor cells*. *Oncotarget*, 2016. 7(38): p. 62754-62766.
79. Priyanka, B., R.K. Patil, and S. Dwarakanath, *A review on detection methods used for foodborne pathogens*. *Indian J Med Res*, 2016. 144(3): p. 327-338.
80. Sakamoto, S., et al., *Enzyme-linked immunosorbent assay for the quantitative/qualitative analysis of plant secondary metabolites*. *J Nat Med*, 2018. 72(1): p. 32-42.
81. Karabacak, N.M., et al., *Microfluidic, marker-free isolation of circulating tumor cells from blood samples*. *Nat Protoc*, 2014. 9(3): p. 694-710.
82. JanssenDiagnostics. *Cellsearch*. 2018; www.cellsearchctc.com
83. Qiagen. *AdnaTest*. 2018; www.qiagen.com
84. Maly, J., et al., *Biocompatible Size-Defined Dendrimer-Albumin Binding Protein Hybrid Materials as a Versatile Platform for Biomedical Applications*. *Macromol Biosci*, 2016. 16(4): p. 553-66.
85. Renberg, B., et al., *Affibody molecules in protein capture microarrays: evaluation of multidomain ligands and different detection formats*. *J Proteome Res*, 2007. 6(1): p. 171-9.
86. Khan, M.A., et al., *Evaluation of proprostate specific antigen for early detection of prostate cancer in men with a total prostate specific antigen range of 4.0 to 10.0 ng/ml*. *The Journal of urology*, 2003. 170(3): p. 723-6.
87. Bergan, J., et al., *Shiga toxins*. *Toxicon*, 2012. 60(6): p. 1085-107.
88. Ravnkar, M., et al., *Engineered lactic acid bacterium Lactococcus lactis capable of binding antibodies and tumor necrosis factor alpha*. *Appl Environ Microbiol*, 2010. 76(20): p. 6928-32.
89. Zadavec, P., B. Strukelj, and A. Berlec, *Improvement of LysM-mediated surface display of designed ankyrin repeat proteins (DARPs) in recombinant and nonrecombinant strains of Lactococcus lactis and Lactobacillus Species*. *Appl Environ Microbiol*, 2015. 81(6): p. 2098-106.
90. Kosler, S., B. Strukelj, and A. Berlec, *Lactic Acid Bacteria with Concomitant IL-17, IL-23 and TNFalpha- Binding Ability for the Treatment of Inflammatory Bowel Disease*. *Curr Pharm Biotechnol*, 2017. 18(4): p. 318-326.
91. Yang, J.P., et al., *Identification of binding proteins for PSP94 in human prostate adenocarcinoma cell lines LNCaP and PC-3*. *Prostate*, 1998. 35(1): p. 11-7.
92. Yang, J.P., M.A. Finkelman, and M.W. Clarke, *Detection of PSP94 and its specific binding sites in the prostate adenocarcinoma cell line LNCaP*. *The Journal of urology*, 1998. 160(6 Pt 1): p. 2240-4.
93. Lawrence, M.G., J. Lai, and J.A. Clements, *Kallikreins on steroids: structure, function, and hormonal regulation of prostate-specific antigen and the extended kallikrein locus*. *Endocr Rev*, 2010. 31(4): p. 407-46.
94. Horoszewicz, J.S., et al., *LNCaP model of human prostatic carcinoma*. *Cancer Res*, 1983. 43(4): p. 1809-18.

95. Agarkova, I. and J.C. Perriard, *The M-band: an elastic web that crosslinks thick filaments in the center of the sarcomere*. Trends Cell Biol, 2005. 15(9): p. 477-85.
96. Ravnkar, M., et al., *Engineered Lactic Acid Bacterium Lactococcus lactis Capable of Binding Antibodies and Tumor Necrosis Factor Alpha*. Applied and Environmental Microbiology, 2010. 76(20): p. 6928-6932.
97. Nagahama, M., *Vaccines against Clostridium perfringens alpha-toxin*. Curr Pharm Biotechnol, 2013. 14(10): p. 913-7.
98. Jiang, Z., et al., *Induction of potential protective immunity against enterotoxemia in calves by single or multiple recombinant Clostridium perfringens toxoids*. Microbiol Immunol, 2014. 58(11): p. 621-7.
99. Garmory, H.S., et al., *Occurrence of Clostridium perfringens beta2-toxin amongst animals, determined using genotyping and subtyping PCR assays*. Epidemiol Infect, 2000. 124(1): p. 61-7.
100. Davies, A.H., et al., *Super toxins from a super bug: structure and function of Clostridium difficile toxins*. Biochem J, 2011. 436(3): p. 517-26.
101. Pruitt, R.N. and D.B. Lacy, *Toward a structural understanding of Clostridium difficile toxins A and B*. Front Cell Infect Microbiol, 2012. 2: p. 28.
102. Wang, Y.K., et al., *A chimeric protein comprising the glucosyltransferase and cysteine proteinase domains of toxin B and the receptor binding domain of toxin A induces protective immunity against Clostridium difficile infection in mice and hamsters*. Hum Vaccin Immunother, 2015. 11(9): p. 2215-22.
103. Ashley, V.A., et al., *The Use of Biomarkers in Prostate Cancer Screening and Treatment*. Rev Urol, 2017. 19(4): p. 221-234.
104. Kalichuk, V., et al., *A novel, smaller scaffold for Affitins: Showcase with binders specific for EpCAM*. Biotechnol Bioeng, 2018. 115(2): p. 290-299.
105. Simon, M., et al., *Increasing the antitumor effect of an EpCAM-targeting fusion toxin by facile click PEGylation*. Mol Cancer Ther, 2014. 13(2): p. 375-85.
106. Rahal, E.A., et al., *Approaches to treatment of emerging Shiga toxin-producing Escherichia coli infections highlighting the O104:H4 serotype*. Front Cell Infect Microbiol, 2015. 5: p. 24.
107. Ogawa, M., et al., *Inhibition of in vitro growth of Shiga toxin-producing Escherichia coli O157:H7 by probiotic Lactobacillus strains due to production of lactic acid*. Int J Food Microbiol, 2001. 68(1-2): p. 135-40.
108. Zadavec, P., et al., *Engineering BmpA as a carrier for surface display of IgG-binding domain on Lactococcus lactis*. Protein Eng Des Sel, 2014. 27(1): p. 21-7.
109. Lindholm, A., A. Smeds, and A. Palva, *Receptor binding domain of Escherichia coli F18 fimbrial adhesin FedF can be both efficiently secreted and surface displayed in a functional form in Lactococcus lactis*. Appl Environ Microbiol, 2004. 70(4): p. 2061-71.
110. Ashkenazi, S. and T.G. Cleary, *Rapid method to detect shiga toxin and shiga-like toxin I based on binding to globotriosyl ceramide (Gb3), their natural receptor*. J Clin Microbiol, 1989. 27(6): p. 1145-50.
111. Berlec, A., et al., *Expression of a hepatitis A virus antigen in Lactococcus lactis and Escherichia coli and evaluation of its immunogenicity*. Appl Microbiol Biotechnol, 2013. 97(10): p. 4333-42.
112. Berlec, A., et al., *Identification of candidate carrier proteins for surface display on Lactococcus lactis by theoretical and experimental analyses of the surface proteome*. Appl Environ Microbiol, 2011. 77(4): p. 1292-300.

7. Enclosed publications

Publication I

Marečková L., Petroková H., Osička R., Kuchař M., Malý P. Novel binders derived from an albumin-binding domain scaffold targeting human prostate secretory protein 94 (PSP94). *Protein & Cell*, 2015, vol. 6, s. 774-779.

Publication II

Zadravec P., **Marečková L.**, Petroková H., Hodnik V., Nanut M., Anderluh G., Strukelj B., Malý P., Berlec A. Development of Recombinant *Lactococcus lactis* Displaying Albumin-Binding Domain Variants against Shiga Toxin 1 B Subunit. *PLoS ONE*, 2016, vol. 11.

Publication III

Semerádtová A., Štofík M., **Vaňková L.**, Malý P., Staněk O., Malý J. Optical microchips based on high-affinity recombinant protein binders—Human serum albumin detection in urine. *Sensors & Actuators: B. Chemical*, 2018,

Publication IV

Škrlec K., Zadravec P., Hlavničková M., Kuchař M., **Vaňková L.**, Petroková H., Křížová L., Černý J., Berlec A. and Malý P. p19-Targeting ILP Protein Blockers of IL-23/Th-17 Pro-Inflammatory Axis Displayed on Engineered Bacteria of Food Origin. *International Journal of Molecular Sciences*, 2018, vol. 19

Publication V

Hlavničková M., Kuchař M., Osička R., **Vaňková L.**, Petroková H., Malý M., Černý J., Arenberger P. and Malý P. ABD-Derived Protein Blockers of Human IL-17 Receptor A as Non-IgG Alternatives for Modulation of IL-17-Dependent Pro-Inflammatory Axis. *International Journal of Molecular Sciences*, 2018, vol. 19

